

Star-formation history and X-ray binary populations: the case of the Large Magellanic Cloud

V. Antoniou^{1*} and A. Zezas^{2,3,1}

¹Harvard-Smithsonian Center for Astrophysics, 60 Garden Street, Cambridge, MA 02138, USA

²Physics Department & Institute of Theoretical & Computational Physics, University of Crete, 71003 Heraklion, Crete, Greece

³Foundation for Research and Technology-Hellas, 71110 Heraklion, Crete, Greece

Accepted 2016 January 17. Received 2015 December 14; in original form 2015 July 31

ABSTRACT

In the present work we investigate the link between high-mass X-ray binaries (HMXBs) and star formation in the Large Magellanic Cloud (LMC), our nearest star-forming galaxy. Using optical photometric data, we identify the most likely counterpart of 44 X-ray sources. Among the 40 HMXBs classified in this work, we find 33 Be/X-ray binaries, and 4 supergiant XRBs. Using this census and the published spatially resolved star-formation history map of the LMC, we find that the HMXBs (and as expected the X-ray pulsars) are present in regions with star-formation bursts ~ 6 – 25 Myr ago, in contrast to the Small Magellanic Cloud (SMC), for which this population peaks at later ages (~ 25 – 60 Myr ago). We also estimate the HMXB production rate to be equal to 1 system per $\sim 43.5 \times 10^{-3} M_{\odot} \text{ yr}^{-1}$ or 1 system per $\sim 143 M_{\odot}$ of stars formed during the associated star-formation episode. Therefore, the formation efficiency of HMXBs in the LMC is ~ 17 times lower than that in the SMC. We attribute this difference primarily in the different ages and metallicity of the HMXB populations in the two galaxies. We also set limits on the kicks imparted on the neutron star during the supernova explosion. We find that the time elapsed since the supernova kick is ~ 3 times shorter in the LMC than the SMC. This in combination with the average offsets of the HMXBs from their nearest star clusters results in ~ 4 times faster transverse velocities for HMXBs in the LMC than in the SMC.

Key words: (galaxies:) Magellanic Clouds – X-rays: binaries – stars: formation, neutron, emission-line, Be – (stars:) pulsars: general

1 INTRODUCTION

The production rate of X-ray binaries (XRBs) is a key parameter for understanding their formation and evolution. In the last few years, numerous theoretical and observational works (e.g., Belczynski et al. 2008, Sepinsky et al. 2009, Linden et al. 2010, Fragos et al. 2013, Tzanavaris et al. 2013) have been performed, with the main focus in improving the realism in the population synthesis models as more observational constraints become available. The Magellanic Clouds are the only galactic environment so far that allow for a direct measurement of the production rate of HMXBs, systems consisting of a compact object (either a neutron star –NS– or a black hole –BH– and in few cases a white dwarf –WD) orbiting an early-type companion. The most numerous subclass of this type of objects up to now detected¹ is the so called Be/X-ray binaries

(Be-XRBs) with O- or B-type donor stars that exhibit line emission over the photospheric spectrum (for a review see Porter & Rivinius 2003).

In the Small Magellanic Cloud (SMC) several studies revealed a large number of HMXBs in low fluxes (e.g., Antoniou et al. 2009b, Antoniou et al. 2010, Haberl et al. 2012b, Sturm et al. 2013, Haberl & Sturm 2015), which allowed us to investigate the link between HMXBs and star formation (e.g., Shtykovskiy & Gilfanov 2005, Antoniou et al. 2010). We found that the Be-XRBs and the X-ray pulsars (all but one of the ~ 70 known X-ray pulsars have Oe- or Be-type companions, with the other system being a supergiant; Coe & Kirk 2015) are observed in regions with star-formation bursts ~ 25 – 60 Myr ago (strongly peaked at ~ 42 Myr). On the other hand, we found that regions with strong but more recent star formation (e.g., the Wing) are deficient in Be-XRBs, in agreement with

than the transient Be-XRBs. There may be a significant population of these sources in the Magellanic Clouds that have yet to be discovered. For example, Ducci et al. (2014) estimate the number of Galactic SFXTs at 37^{+53}_{-22} , suggesting that the SFXTs constitute a large subclass of XRBs with supergiant companions.

* E-mail: vantoniou@cfa.harvard.edu

¹ There is an increasing number of Supergiant Fast X-ray Transients (SFXTs; Negueruela et al. 2006) being discovered in the Milky Way mainly with *INTEGRAL*. SFXTs have incredibly short outburst times (rising in tens of minutes and lasting few hours), and quiescent luminosities of $\sim 10^{32}$ – 10^{34} erg s^{−1} (Chaty 2015), making them even harder to detect

the *Chandra* survey of the SMC Wing (P.I. M. Coe), which detected only 4 HMXBs in 20 observed fields² (McGowan et al. 2008) and the large *XMM-Newton* survey of the SMC (P.I. F. Haberl; Haberl et al. 2012b), where only 6 HMXBs (3 confirmed and 3 candidate) have been identified in 10 fields in the South-East part of the SMC (Sturm et al. 2013). By correlating the number of observed Be-XRBs (HMXBs) with the formation rate of their parent stellar populations (i.e., with the SFR of the regions that host these systems), Antoniou et al. (2010) derived a Be-XRB (HMXB) production rate of ~ 1 system per 3 $(2.5) \times 10^{-3} M_{\odot} \text{ yr}^{-1}$. That was the *first* direct calibration of the XRB formation rate at ~ 40 Myr by measuring the formation rate of the XRBs per unit SFR of their parent populations.

Finally, the strong spatial correlation between the Be-XRBs in the SMC and their parent stellar populations provided strong evidence for relatively small supernova (SN) kicks during the formation of the compact object. We estimated an upper limit of $\sim 15\text{--}20 \text{ km s}^{-1}$, in agreement with measured velocities of Be-XRBs in the Galaxy ($15 \pm 6 \text{ km s}^{-1}$; van den Heuvel et al. 2000) and estimated values in the SMC (Coe 2005 and Antoniou et al. 2009b).

Motivated by the above work, we investigate here the link between HMXBs and star formation in the Large Magellanic Cloud (LMC), our nearest star-forming galaxy (only at ~ 50 kpc; Macri et al. 2006). The LMC is a dwarf irregular galaxy in the Local Group. It has an extended circular shape with a prominent off-center bar, a nucleus, and irregular spiral arms (based on results from the DENIS survey; Cioni et al. 2000). It experiences intense star-formation activity with a higher star formation rate than the SMC (Cioni 2009). Despite its moderate Galactic foreground absorption ($N_{\text{H}} \simeq 6.4 \times 10^{20} \text{ cm}^{-2}$; Dickey & Lockman 1990) and closer distance, the LMC has received much less attention in the X-rays than the SMC, with most observations focusing so far on individual X-ray sources (such as LMC X-1, X-2, X-3, etc).

Another reason for selecting the LMC as a target for this study is its sub-solar metallicity ($\sim 1/2.5 Z_{\odot}$; Cole et al. 2005). Nowadays it is widely accepted that metallicity is one of the three main factors that determines the formation rate of young XRBs (the other two being the age of the parent stellar populations and the SFR). Even though the details of how metallicity affects the HMXB populations are not well understood, there is a growing body of theoretical work indicating that low metallicity is associated with higher formation efficiency of HMXBs (Dray 2006) and higher luminosity (Fragos et al. 2013). For example, Douna et al. (2015) found that galaxies with metallicities below $\sim 1/5 Z_{\odot}$, which is the typical value for the SMC (Luck et al. 1998), have on average 10 times more HMXBs per unit SFR than solar metallicity galaxies. On the other hand, Linden et al. (2010) find that for significantly sub-solar metallicity there is no dependence of the HMXB populations on the metallicity.

For such comparisons of course one needs an up-to-date tally of the number of HMXBs in this galaxy. Since Liu et al. (2005) published the list of known HMXBs in both Magellanic Clouds, several new such systems have been discovered in the LMC (mainly by the *Swift* and *INTEGRAL* satellites). As a by-product of this

² Though, as noted in this work, it is possible that a larger number of HMXBs exist in the SMC Wing, which nevertheless remain undetected due to the transient nature of the Be phase and the low probability of detecting them in outburst (for $L_X \sim 10^{38} \text{ erg s}^{-1}$ this probability is only $\sim 10\%$; Fig. 4.62 in Galache 2006). In any case, based on the lower star-formation rate (SFR) of the SMC Wing when compared to that along the SMC Bar, we expect a smaller number of Be-XRBs than those identified in the SMC Bar (Antoniou et al. 2010).

work, we compiled a list of all known HMXBs in the LMC, for which we also identified their optical counterparts. Until now, only 28 of such systems had a known counterpart in the literature. Our work provides the best candidates for spectroscopic follow-up programs that will identify the nature of the HMXBs in the LMC unambiguously.

Based on this material and the spatially-resolved star-formation history map (Harris & Zaritsky 2009; hereafter [HZ09]), we are in the position to investigate the link between HMXBs and star formation in the LMC. In Section 2 we present an up-to-date tally of the young XRB population of the LMC and in Section 3 their optical properties. In particular, in Section 3.1 we present their most likely optical counterparts along with estimations of the chance coincidence probability. The final classification of the XRBs is given in Section 3.2, while the metallicity of the young stellar populations in both Magellanic Clouds is discussed in Section 3.3. In Section 4 we investigate the global star-formation history of this galaxy, and the link between stellar and XRB populations. In Section 5 we study the properties of the HMXB population in the LMC. In particular, in Section 5.1 we discuss the star-formation history of young XRBs in the Magellanic Clouds, and in Section 5.2 the formation efficiency for the various XRB types. In Section 5.3 we present previous studies on this subject, and in Section 5.4 the spectral-type distribution of the LMC HMXBs. A discussion about the young parent stellar populations of the LMC X-ray pulsars follows in Section 5.5. The last part of this work discusses the supernova kick velocities of the LMC HMXBs (Section 5.6) and presents the "Corbet diagram" (Corbet 1984) of HMXBs in the Magellanic Clouds and the Milky Way (Section 5.7). Finally, in Section 6 we summarize the main findings of this work.

Throughout this work, we adopt a distance modulus of $(m - M)_V = 18.50 \pm 0.02 \text{ mag}$ (Alves 2004). We also use $R_V = 3.41$ (Gordon et al. 2003) in order to estimate the $E(B - V)$ ($= A_V/R_V$) reddening. A mean extinction value $\langle A_V \rangle$ for an area with a radius of $12'$ around each HMXB is derived by using the "LMC Extinction Retrieval Service" tool³ (Zaritsky et al. 2004). We estimate an average value of $\langle A_V \rangle \sim 0.50 \text{ mag}$ for early-type stars, thus resulting in $E(B - V) \sim 0.15 \text{ mag}$. Regarding the metallicity, we use the latest value of $Z_{\odot} = 0.0134$ from the review of Asplund et al. (2009), instead of the more widely-known canonical value of $Z_{\odot} = 0.02$ (Anders & Grevesse 1989).

Since the completion of this work, 2 additional sources have been reported in the literature as HMXBs, and the spin period of a known source was derived. For completeness we list them here, and in Table 1, but we do not include them in our analysis. Clark et al. (2015) identified an X-ray bright emission-line star as part of the VLT-FLAMES Tarantula Survey that could be the first HMXB identified within 30 Dor, if indeed XMMU J053833.9-691157 and CXOU J053833.4-691158 are associated with VFTS399. Swift J0549.7-6812 (reported in ATel #5286; Krimm et al. 2013a) is located at (RA, Dec.)=(05:50:06.47, -68:14:55.7) with a 90% confidence astrometric error (r_{90}) equal to $1.4''$, and a 6.2-second pulse period (ATel #5309; Krimm et al. 2013c). Although this source, also reported as LXP6.2, has a blue counterpart suggesting a neutron-star HMXB system in the hard state (ATel #5293; Krimm, Holland, & Kennea 2013b), it is not included in our analysis, because these results not been published in a refereed paper since they were reported in ATels 3 years ago, thus we are uncertain about its nature. A new X-ray pulsar that was recently detected

³ Available from <http://djuma.as.arizona.edu/~dennis/lmext.html>

in the LMC *XMM-Newton* survey is reported by Vasilopoulos et al. 2016 (to be subm.; private communication) to have a pulse period of 38.55(1) s. This source (LXP38.55) has been previously detected and it is associated with sources IGR J05007-7047 and CXOU J050046.0-704436. With the addition of the latter 2 new pulsars, the total number of known systems in the LMC is now sixteen.

2 THE HMXB POPULATION OF THE LMC

So far there has not been any complete X-ray survey of the LMC in the soft X-rays (~ 0.5 -10 keV). Shtykovskiy & Gilfanov (2005) analyzed 23 *XMM-Newton* archival observations (covering ~ 3.8 sq. degrees down to 3×10^{33} erg s $^{-1}$ at 2–8 keV) and found ~ 460 point sources. However, more than 94% of those objects have been identified as background X-ray sources observed through the LMC, and only 9 sources as candidate HMXBs (with 19 additional objects of uncertain nature). The *INTEGRAL* observatory has also surveyed the LMC, thus allowing us to study for the first time the hard (15 keV–10 MeV) X-ray emission of a handful of sources in this galaxy (Götz et al. 2006). In particular, the *INTEGRAL* survey of the LMC discovered 5 new faint high-energy sources, although only 2 of them are potentially located in this galaxy. More recently, Grebenev et al. (2013) presented the results from the ultra deep (~ 7 Ms) *INTEGRAL* survey of the LMC. They detected 7 known HMXBs, and 2 new hard X-ray sources; the nature of the latter is unknown.

Forty five LMC HMXBs are known to date (confirmed and candidate systems, however in a few cases discussed below, we question this nature based on more recent photometric surveys). Only 16 systems have been confirmed as Be-XRBs (one of these sources is most likely a WD/Be-XRB; Kahabka et al. 2006), while 5 systems have been classified as candidate Be-XRBs. In the compilation of Liu et al. (2005), one finds 2 LMC sources listed as supergiant XRBs (SG-XRBs): RX J0532.5-6551 (Haberi et al. 1995) and RX J0541.4-6936 (Sasaki et al. 2000), though in the original publications these systems are only identified as candidate SG-XRBs. Moreover, there are 2 black-hole HMXBs (LMC X-1: Hutchings et al. 1983, White & Marshall 1984; LMC X-3: Cowley et al. 1983). The remaining 20 sources are classified as NS/HMXBs based on their hard X-ray spectra, and in some cases, their association with a massive star showing H α emission. These systems have been classified in this work as either candidate Be-XRB or SG-XRBs, except for 4 cases where the classification was revised to non-HMXB systems (see below Section 3.2 and Table 5).

In Table 1 we present a list of all known HMXBs in the LMC compiled from the literature (as of Dec. 2014⁴). In Columns 1 and 2, we give the X-ray source ID and source name, respectively. In Columns 3 and 4, we list the Right Ascension and Declination (J2000.0), and in Column 5 the positional uncertainty of the X-ray source (followed by the references in parenthesis). In cases of several detections reported in the literature, the coordinates with the smallest positional uncertainty are presented. Column 6 gives the

⁴ Two additional sources published in the meantime are reported at the end of the previous section. With the exception of source IGR J05007-7047, which is already included in our HMXBs list, we do list these 2 sources in Table 1 for completeness, but we do not include them in our present work. Similarly, we added in this table the pulse period of source IGR J05007-7047, but we also do not include this source among the known LMC X-ray pulsars in our analysis (i.e., we only include it in the list of known HMXBs).

source ID from the catalog of Liu et al. (2005), which is the most recent compilation of HMXBs in the LMC prior to this work. Column 7 gives the pulse period in seconds followed by the orbital period in days (with corresponding references given in parenthesis). Finally, the spectral type of the optical counterpart and the XRB type, as presented in the literature, are given in Columns 8 and 9, respectively, with the reference list as updated as possible.

3 THE OPTICAL PROPERTIES OF THE YOUNG X-RAY SOURCE POPULATION OF THE LMC

There are two major photometric surveys of the LMC in the optical band: the Magellanic Clouds Photometric Survey (MCPS; Zaritsky et al. 2004) and the Optical Gravitational Lensing Experiment (OGLE-III; Udalski et al. 2008). The MCPS is the largest area survey of the LMC (with a pixel scale of $\sim 0.7''$ /pixel) covering $\sim 8.5^\circ \times 7.5^\circ$ with observations in the *U*, *B*, *V*, and *I* filters reaching a limiting *V*-band magnitude of 20–21 (depending on the local crowding). The final LMC photometric catalog contains over 24 million objects, the vast majority of which are stars in the LMC (Zaritsky et al. 2004). All but one (LMC X-3) of the LMC HMXBs presented in Table 1 are covered by the MCPS survey. On the other hand, the OGLE-III survey is a significant extension of the OGLE-II maps (Udalski et al. 2000) that covered only the central regions of the LMC. This survey covers ~ 40 sq. degrees of the LMC and contains *V* and *I* photometry and astrometry for about 35 million stars observed during 7 observing seasons. However, since only 27 out of the 45 X-ray sources studied here are covered even by the extended OGLE-III survey, in the present work we chose to use exclusively the MCPS catalog.

3.1 Optical counterparts of HMXBs in the LMC

As discussed in Section 1, only 28 systems had a known counterpart in the literature prior to this work (and these are clearly marked in Tables 2 – 4). In this work we perform a systematic cross correlation of the known X-ray sources in the LMC with the MCPS catalog. For consistency we extend this search to the 28 systems with known counterpart. The vast majority of the sources reported in Table 1 have been identified with X-ray telescopes with typical astrometric errors of $\sim 5''$ (e.g., *XMM-Newton*, *Swift*, *ROSAT*) or worse (e.g., *ASCA*). A few (5) sources have sub-arcsecond positions. Therefore, we adopt a search radius of $5''$, which in the case of *XMM-Newton* and *ROSAT* also includes the boresight error (e.g., Brusa et al. 2007, K \acute{u} urster & Hasinger 1993, respectively).

The resulting matches are presented in Table 2. In Column 1, we give the X-ray source ID (same as in Column 1 of Table 1). In Columns 2 and 3, we give the Right Ascension and Declination (J2000.0) of the MCPS counterparts, while their photometric data are listed in Columns 4–13 (these data are taken directly from the original catalogs without applying any reddening correction): apparent magnitudes in the *U*, *B*, *V*, and *I* bands (Columns 4, 6, 8, and 10), the *B* – *V* color (Column 12), and their errors (Columns 5, 7, 9, 11 and 13, respectively). The distance (in arcseconds) of the counterpart to the X-ray source is given in Column 14, while in Column 15 "n" indicates a newly identified counterpart from this work, "k" a known counterpart in the literature, and "A" those counterparts that are discussed in the Appendix A. There are only 10 X-ray sources with unique optical matches within $5''$, while there is one more source without any match at this radius. For completeness, we also repeated this exercise for larger radii. This is partic-

ularly important for sources detected with *ROSAT* PSPC or *ASCA*, which have error circles larger than $5''$ (see Table 1). The resulting matches are presented in Tables 3 and 4, which follow the structure of Table 2. However, we emphasize that in the case of sources with sub-arcsecond positional uncertainties, we do not identify any counterpart at distances larger than $\sim 1.7''$ (consistent with *Chandra*'s off-axis averaged astrometric error following the prescription of Hong et al. 2005).

Based on thorough Monte Carlo simulations presented in Section 3.1.1, we propose here as the most likely counterpart of sources with more than one optical matches within the search radius, the brightest one (and among sources of similar brightness the bluest one), which is indicated in bold in Table 2. Following Section 3.1.1 we give preference to sources with $M_{V_o} < -2$ and $(B-V)_o \leq 0.25$ or $M_{V_o} < -3$ and $(B-V)_o > 0.25$; these are referred to as "unambiguous" matches because of their very low chance coincidence. For only 26 out of the 44 X-ray sources with MCPS coverage there is an unambiguous counterpart within $5''$, i.e. within the 1σ search radius. For other 6 X-ray sources, this unambiguous match is a bright source ($V \lesssim 20$ mag and $B-V \lesssim 0.2$ mag) that lies within the $5''$ to $10''$ annulus (presented at Table 3), while 2 additional X-ray sources have an unambiguous match at a distance larger than $10''$ (these sources have large X-ray positional uncertainties; Table 4).

In Fig. 1 we show a $V, B-V$ color-magnitude diagram constructed from 500,000 randomly selected MCPS stars (black contours) listed in the catalog of Zaritsky et al. (2004). Shown with dark yellow and red filled circles are the Be and B[e] III-V stars, respectively, from the spectroscopic study of Reid & Parker (2012). The O and B stars from the census of Bonanos et al. (2009) are shown in green and blue circles, respectively, with luminosity class III-V objects shown with filled symbols, and luminosity class I-II objects shown with open symbols. Since Reid & Parker (2012) do not list the MCPS photometry of their objects, we cross-correlated their coordinates with the MCPS catalog using a search radius of $1''$. All these different datasets constitute the background of this color-magnitude diagram, while in the foreground we show the identified optical counterparts to the X-ray sources marked by the X-ray source ID (Column 1 of Table 1). Magenta symbols indicate unambiguous matches (i.e. the counterpart of each source that falls in the area of lowest chance coincidence probability; c.f. Section 3.1.1). All the remaining sources are shown with cyan symbols, and the most likely matches among those are marked with black diamonds (if possible to select one; see detailed discussion in the Appendix A). We also overplot the Geneva isochrones (Lejeune & Schaerer 2001) for metallicity $Z=0.008$ and for various ages ranging from 1 Myr to ~ 490 Myr.

From the comparison of the $V, B-V$ color-magnitude diagram in the LMC (Fig. 1), and the SMC (Fig. 2 of Antoniou et al. 2009b), we see that the counterparts of HMXBs in the LMC are bluer than those in the SMC. Most of the matches in the LMC are clustered around $(B-V)_o \sim -0.2$ mag (corrected for reddening), while in the SMC they are found around $(B-V)_o \sim -0.1$ mag. Similarly, from the overlaid Geneva isochrones (Lejeune & Schaerer 2001), we find counterparts as young as ~ 3 Myr in the LMC with their majority being younger than $\sim 45-55$ Myr, while in contrast in the SMC their estimated age is $\sim 15-85$ Myr (Antoniou et al. 2009b).

3.1.1 Chance coincidence probability

In order to estimate the chance coincidence probability of identifying spurious matches from the MCPS catalog as the optical counterparts of the HMXBs, we performed extensive Monte Carlo sim-

ulations showing that the brightest match is the most likely optical counterpart.

Following the same procedure as in Antoniou et al. (2009b), we looked for matches of the X-ray sources after applying a random positional offset in Right Ascension and Declination. In particular, we created 1,000 random such samples with offsets drawn from a uniform distribution, taking care that the new position is outside the search radius of each source, and then we cross-correlated each of these samples with the MCPS catalog in the same way as the observed data. The chance coincidence probability was estimated for 2 different search radii ($5''$ and $10''$, corresponding to 1 and 2 times our typical search radius, respectively). In order to account for the varying density of stars in different regions of the color-magnitude diagram, we performed the cross correlations for a grid of magnitudes and colors, in regions of the $V, B-V$ color-magnitude diagram that have a range of 1 mag in the V band and 0.2 mag in the $B-V$ color, in all but the cases where the stellar density of these regions was small. In these cases, we increased this range accordingly so as to obtain meaningful results from the cross correlations. The results are given in Fig. 2. It is clear from this figure that for X-ray sources with more than one optical matches, the brightest one has the lowest probability of being a spurious match, while for equally bright matches, the one with the smallest chance coincidence probability is the bluest source. For sources with fainter optical counterparts the chance coincidence increases significantly (see also Antoniou et al. 2009b).

We also studied the chance coincidence probability as a function of search radius for stars in the locus of OB spectral types ($M_{V_o} \leq -0.75$ and $(B-V)_o \leq 0.20$). These results indicate that for a search radius of $5''$, about $21 \pm 10\%$ of the bright blue ($V \lesssim 18.25$ mag and $(B-V) \lesssim 0.35$ mag) matches are spurious associations (this probability increases to $\sim 29 \pm 9\%$ and $\sim 40 \pm 9\%$ for search radii of $7.5''$ and $10''$, respectively). By comparing these results with Fig. 2, we conclude that this relatively large chance coincidence probability is mainly driven by the fainter, more numerous stars in the OB-star locus. Instead for the earlier spectral types the chance coincidence probability is considerably lower. In Fig. 3 we present the normalized chance coincidence probability for OB stars as a function of the search radius.

3.2 Final source classification

In Table 5 we present the final classification of the X-ray sources listed in Table 1. In particular, we list the X-ray source ID, name and XRB classification found in the literature, followed by the classification from this work (Columns 1 to 4, respectively⁵). In Column 5 we give additional notes for each source. In summary, we classify the X-ray sources listed in the literature as HMXBs based on the photometric properties of their optical counterparts identified in this work. In total we revise the classification of 4 systems from being a member of the HMXB class to being an X-ray source with a late-type companion (their most likely counterpart falls on or above the Red Giant Branch on the $V, B-V$ color-magnitude diagram). For other 12 X-ray sources, which are listed as confirmed or candidate HXMBs in the list of Liu et al. (2005) and for which we revise their classification, we propose a candidate Be-XRB nature, while for one additional source we are able to only classify it as an HMXB. Most importantly, we classify 2 sources (identified until

⁵ Columns 1, 2, and 3 of Table 5 are identical to Columns 1, 2, and 9 of Table 1.

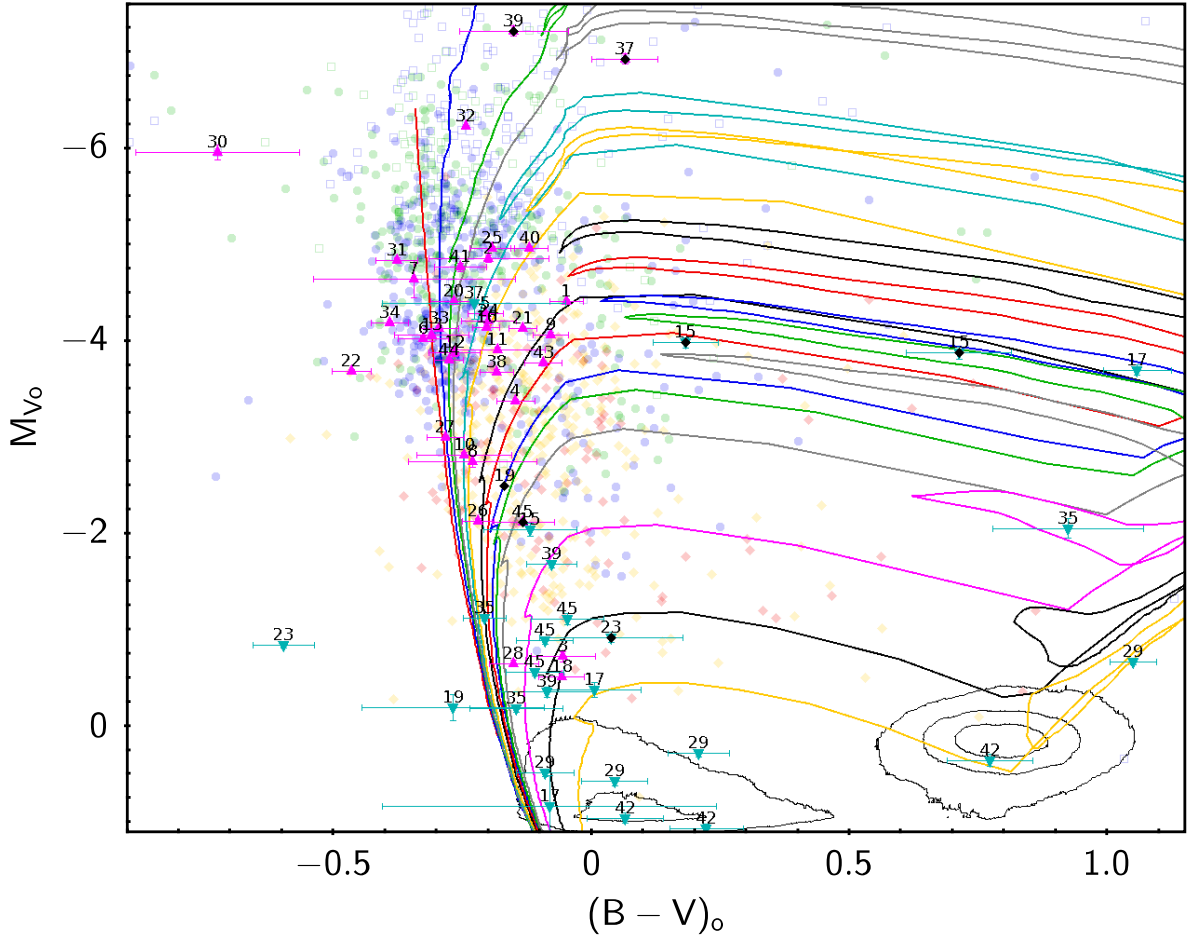


Figure 1. A reddening-corrected $V, B-V$ color-magnitude diagram (presented as the absolute V -magnitude M_{V_o} versus the $(B-V)_o$ color) of the optical counterparts of the LMC HMXBs (marked with their IDs; Column 1 of Table 1). Only the matches shown in bold in Tables 2–4 are presented. The counterpart of LXP 8.04 (source ID # 14) is not shown in this figure due its very blue $B-V$ color (see discussion in Appendix A2). For sources with more than one optical match, we select as the most likely counterpart the one that is located in the region of least chance coincidence probability (c.f. Section 3.1.1). Magenta symbols indicate unambiguous matches and cyan symbols show the remaining sources for which such a choice is not feasible (in few cases, and based on arguments discussed in Appendix A, we mark with black diamonds the most likely matches among similarly likely associations). We also show (i) 500,000 randomly selected MCPS stars (listed in the catalog of Zaritsky et al. (2004); shown with black contours); (ii) the Be and B[e] III-V stars from the spectroscopic study of Reid & Parker (2012) (shown in dark yellow and red filled circles, respectively); (iii) the O and B III-V stars (shown in green and blue filled circles, respectively) and O and B I-II stars (shown in green and blue open circles, respectively) from the census of Bonanos et al. (2009); (iv) the isochrones from the Geneva database (Lejeune & Schaerer 2001) for $Z=0.008$ and ages ranging from 1 Myr to ~ 490 Myr – from top to bottom: 1 Myr (red), 5 Myr (blue), 10 Myr (green), 12.3 Myr (gray), 20 Myr (cyan), 25 Myr (yellow), 44.7 Myr (black), 56.2 Myr (red), 69.2 Myr (blue), 79.4 Myr (green), 100 Myr (gray), 177.8 Myr (magenta), 316.2 Myr (black), 489.8 Myr (yellow).

now only as HMXBs) as supergiant XRBs (SG-XRBs), bringing the total number of known SG-XRBs in the LMC to four (i.e. doubling the currently known number), which makes them significant enough as a class to be studied further on their own. These sources are discussed in detail in Appendix A. In Table 6 (Column 1) we summarize our results by presenting the number of sources in the LMC for the different XRB types (Be-, SG-, pulsar-, e.t.c.), found in the literature and revised in the present work (Columns 2 and 3, respectively).

3.3 The metallicity of young stellar populations in the Magellanic Clouds

Metallicity is a key parameter that determines the evolution and physical parameters of stars and binary stellar systems (e.g., Belczynski et al. 2008, Linden et al. 2010, Fragos et al. 2013). The generally used values of the Magellanic Clouds’ metallicities are $Z_{\text{LMC}} \sim 1/2.5 Z_{\odot}$ and $Z_{\text{SMC}} \sim 1/5 Z_{\odot}$. For $Z_{\odot} = 0.0134$ (Asplund et al. 2009), these correspond to $Z_{\text{LMC}} \sim 0.005$ and $Z_{\text{SMC}} \sim 0.003$ (while assuming $Z_{\odot} = 0.02$, they would be $Z_{\text{LMC}} \sim 0.008$ and $Z_{\text{SMC}} \sim 0.004$).

As a by-product of this work, we compiled a list of metallicities

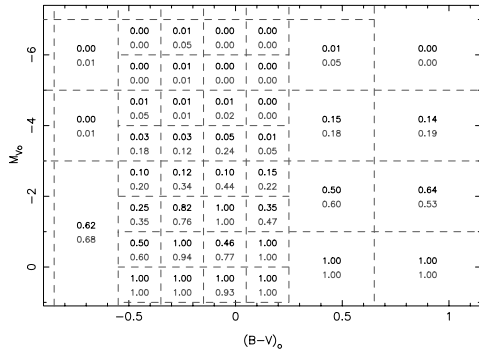


Figure 2. Chance coincidence probability (optical matches per X-ray source) in different regions of the reddening-corrected $V, B - V$ color-magnitude diagram. In each of these regions (i.e. cells identified by the grid shown with dashed lines) we present the probability of detecting one or more spurious matches for a source, for 2 different search radii ($5''$ shown in black at the top part of each cell, and $10''$ shown in grey at the bottom part of each cell). For example, for sources with $-4 < M_{V_0} \leq -3$ magnitudes and $-0.55 < (B - V)_0 \leq -0.35$ colors (corresponding to $15 < V \leq 16$ and $-0.4 < B - V \leq -0.2$, respectively) there is a 3% chance coincidence probability for the matches found within $5''$ from the X-ray source position, while this probability increases to 18% when found within $10''$.

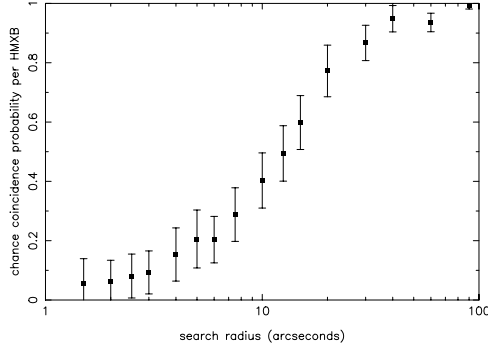


Figure 3. Chance coincidence probability for optical sources in the locus of OB stars as a function of the search radius (for a comparison with the SMC refer to Fig. 4 of Antoniou et al. 2009b).

ties for young stars in the Magellanic Clouds. We first examined the metallicity of B-type stars⁶ (i.e. stars with ages up to ~ 50 Myr), and then we investigated the metallicity of young (< 100 Myr) clusters.

In Table 7 we present the Fe abundances found in the literature for B-type stars in the LMC, compared to those for the same type of objects in the SMC, SMC Wing, and the Magellanic Bridge areas (Column 1). To the best of our knowledge, the studies used here are the most comprehensive ones in which an Fe abundance is presented for these spectral-types. Systems for which there were no available Fe abundances are excluded from Table 7. In Column

⁶ Ideally, of course, we would like to have information about the metallicity of the particular companion stars – in other words, of the known counterparts of the studied HMXBs – or of regions as close as possible to their location. However, the vast majority of the companions are Be-stars, which as broad-line stars are not used in metallicity studies.

2 we list the name of the B-type star studied, in Columns 3 and 4 its Right Ascension and Declination (J2000.0), and in Columns 5 and 6 its spectral type and $[\text{Fe}/\text{H}]$ abundance (followed by the corresponding references in parenthesis), respectively. The Z/Z_\odot and Z values are derived using $Z/Z_\odot = 10^{[\text{Fe}/\text{H}]}$ (e.g., Russell & Dopita 1992) and $Z_\odot = 0.0134$ (Asplund et al. 2009) (Columns 7 and 8, respectively). The estimated mean Z values are: $\sim 0.007 \pm 0.003$ for the LMC, $\sim 0.003 \pm 0.002$ for the SMC, ~ 0.001 for the SMC Wing, and $\sim 10^{-4}$ for the Magellanic Bridge. We note though the following caveats that apply to this compilation: (a) these are measurements for B-type stars, i.e. non Be-stars⁶, (b) most of them are supergiant stars (for example, in the LMC only 3 out of 17 stars presented in Table 7 are III-V luminosity class stars), in contrast to the majority of the companions of the HMXBs in the Magellanic Clouds which are main-sequence stars (see Table 6), and (c) most of them are stars in clusters of particularly young ages (only few Myr old), while the formation of the HMXBs, in the SMC at least, shows its peak at ages as old as $\sim 25 - 60$ Myr (this is less of a concern for the LMC; see Section 4.1).

In order to obtain a more complete picture of stellar metallicities in a broader age range, in Table 8 we present the ages and Fe abundances of young (< 100 Myr) star clusters in the Magellanic Clouds compiled from an extensive literature search. Since there are multiple, often contradictory, values for the age and metallicity of star clusters in the Magellanic Clouds reported in the literature, mainly due to the different methods used for their derivation, we opted to use the metallicity and age of the clusters listed only in [HZ09], which is the largest homogeneous compilation of cluster parameters (only the data for the NGC2100 and NGC1818 clusters are taken from different works). This list contains 85 star clusters, which is an adequate number for a comparison of the average metallicities of young stellar populations in the Magellanic Clouds. In Columns 1 and 2 we list the galaxy and star cluster names (24 in total for the LMC and 9 in the SMC). The age, $[\text{Fe}/\text{H}]$, Z/Z_\odot and Z values are given in Columns 3, 5, 7, and 9, respectively (followed by their errors in Columns 4, 6, 8, and 10, respectively). The reference from where most data are taken is given in Column 11. When the Z/Z_\odot (and/or Z) values were not available in the literature, we used the $Z/Z_\odot = 10^{[\text{Fe}/\text{H}]}$ relation and $Z_\odot = 0.0134$ (Asplund et al. 2009). From the data of Table 8 we estimate mean Z values of: $\sim 0.006 \pm 0.002$ for the LMC, and ~ 0.003 (with < 0.001 standard deviation) for the SMC, in good agreement within the errors with the values derived from the B-type stars above.

4 THE STAR-FORMATION HISTORY OF THE LMC

[HZ09] presented the detailed spatially resolved star-formation history map of the whole galaxy ($8.5^\circ \times 7.5^\circ$) in $24' \times 24'$ cells (each cell was further subdivided into a 2×2 grid of subregions with $> 25,000$ stars) by utilizing the MCPS survey (Zaritsky et al. 2004). This study focused on the structure of the LMC, and on the recent episodes of enhanced star-formation activity (younger than ~ 100 Myr). More recently, also Indu & Subramaniam (2011) studied the recent star-formation history of both Magellanic Clouds, and found peaks in the star-formation activity of the LMC at 0–10 Myr and 90–100 Myr, and at 0–10 Myr and 50–60 Myr in the SMC, in broad agreement with [HZ09] and [HZ04], respectively. At ~ 40 Myr ago, which is the age of the regions in the SMC that host the largest number of HMXBs (Antoniou et al. 2010), the SFR for the entire LMC is $\sim 0.25^{+0.15}_{-0.10} M_\odot \text{ yr}^{-1}$ (derived from its integrated star-formation history as presented in Fig. 11 of [HZ09]). At the same epoch the

SFR of the SMC is $\sim 0.30^{+0.55}_{-0.15} M_{\odot} \text{ yr}^{-1}$ (Fig. 19 in [HZ09]; note that based on this figure, the maximum SFR value in the SMC is at least $0.85 M_{\odot} \text{ yr}^{-1}$). In order to derive the star-formation history of the Magellanic Clouds, [HZ09] and [HZ04] have fitted the color-magnitude diagrams with stellar populations of 4 and 3 different metallicities for the LMC and the SMC, respectively. Throughout this work we are using the star-formation history for the highest metallicity populations ($Z = 0.008$), which is the most relevant for the young stellar populations, and in agreement with the average metallicity of LMC stars discussed in the previous section. Since the above SFRs in the two Magellanic Clouds are comparable (within the errors), one would expect to find not too different numbers for the same types of XRBs in the two galaxies.

4.1 Star-formation history and young XRB populations in the LMC

In order to investigate the link between stellar and XRB populations, we follow the procedure described in [Antoniou et al. \(2010\)](#): we calculate the average star-formation history for the MCPS regions ($\sim 12' \times 12'$; [HZ09]) that host the 15 confirmed Be-XRBs⁷ listed in Table 5. Since the HMXBs presented in this work have been identified by many different X-ray observatories (from *ROSAT* to *XMM-Newton*, *Swift* and *INTEGRAL*), without any of them having performed a complete survey of the whole galaxy so far, we opted to derive the star-formation history only for the MCPS region that contains each HMXB, and not for the whole field of view of each X-ray satellite in each case. The SFR errors are derived based on the upper and lower confidence intervals given by [HZ09], while when more than one HMXBs fall in the same MCPS region, we weight the SFR by the number of encompassed X-ray sources in each region.

We repeat this exercise for regions in the LMC hosting each of the following source classes: 14 X-ray pulsars, 4 SG-XRBs, 1 BH-HMXB (the only known within the area covered by MCPS), 40 HMXBs, 17 candidate Be-XRBs, and 1 WD/Be-XRB that have been so far identified (Table 5). For comparison, we also derive the star-formation history of the MCPS region in the SMC (which also has a $\sim 12' \times 12'$ size; [HZ04]) that hosts the 1 candidate WD/Be-XRB.

In Fig. 4 we present the average star-formation history of regions in the LMC with: confirmed Be-XRBs (*top left*); X-ray pulsars (*bottom left*); SG-XRBs (*top right*); and LMC X-1 (the only BH-HMXB with MCPS coverage; *bottom right*). Similarly, in Fig. 5 we present the average star-formation history of regions in the LMC with: all HMXBs (*top left*); candidate Be-XRBs (i.e. based on photometric properties, but still lacking an optical spectroscopic identification; *bottom left*); candidate WD/Be-XRBs in the LMC and SMC (*top and bottom right panels, respectively*).

We find that the star-formation history in regions associated with the different XRB types is strongly peaked at the following ages:

(a) ~ 6.3 Myr for all known HMXBs, HMXBs without a BH or WD compact object, the candidate Be-XRBs, the SG-XRBs, and

⁷ We chose to show the star-formation history of this XRB population – and not that of all LMC HMXBs for example – for a direct comparison with the SMC ([Antoniou et al. 2010](#)). As a reminder, the SMC has an HMXB population consisting almost exclusively of NS/Be-XRBs, while the LMC has also 2 BH-HMXBs and 4 SG-XRBs among the 40 HMXBs studied in this work.

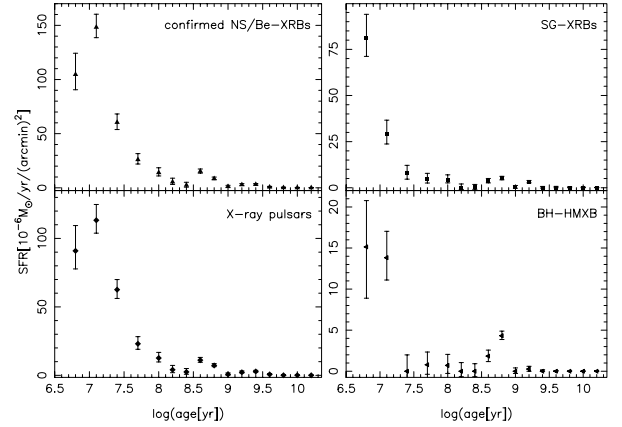


Figure 4. Average star-formation history (using data from [HZ09]) of regions in the LMC with: confirmed NS/Be-XRBs (*top left*); X-ray pulsars (*bottom left*); SG-XRBs (*top right*); and LMC X-1, the only BH-HMXB with MCPS coverage (*bottom right*). For a comparison with the SMC, refer to Fig. 1 of [Antoniou et al. \(2010\)](#).

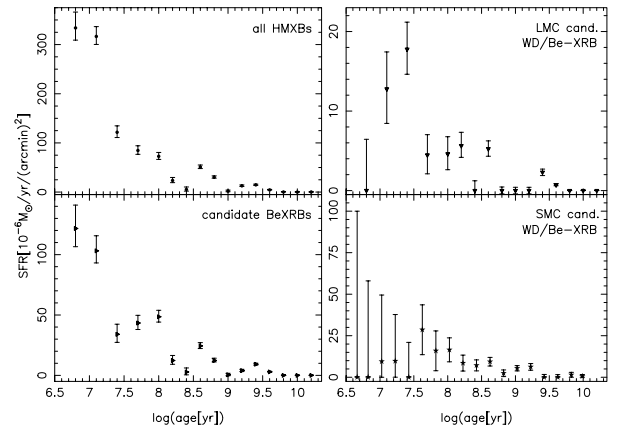


Figure 5. Average star-formation history (using data from [HZ09]) of regions in the LMC with: all HMXBs (*top left*); candidate Be-XRBs, i.e. systems without an optical spectroscopic identification (*bottom left*); candidate WD/Be-XRBs in the LMC and SMC (*top and bottom right, respectively*). For a comparison with the SMC, refer to Fig. 1 of [Antoniou et al. \(2010\)](#).

the BH-HMXB;

(b) ~ 12.6 Myr for all the confirmed Be-XRBs, the confirmed Be-XRBs with a NS compact object, and the X-ray pulsars; and

(c) ~ 25.1 Myr for the candidate WD/Be-XRB in the LMC.

In contrast the candidate WD/Be-XRB in the SMC lies in a region with a star-formation peak at ~ 42.2 Myr.

A comparison of the total SFR for the Magellanic Clouds at the above ages shows that at ~ 10 Myr the SFRs are $\sim 0.43^{+0.30}_{-0.15} M_{\odot} \text{ yr}^{-1}$ and $\sim 0.33^{+0.52}_{-0.18} M_{\odot} \text{ yr}^{-1}$ for the LMC and SMC, respectively, while at ~ 25 Myr they become $\sim 0.30^{+0.18}_{-0.12} M_{\odot} \text{ yr}^{-1}$ and $\sim 0.15^{+0.70}_{-0.10} M_{\odot} \text{ yr}^{-1}$, respectively. Although the upper bound of the SMC SFR at both ages is very large (i.e. the maximum SFR value is at least $0.85 M_{\odot} \text{ yr}^{-1}$), we see that at ~ 10

Myr and ~ 25 Myr the SFR is higher in the LMC, while for older star-formation episodes (~ 40 Myr) it is higher in the SMC.

5 DISCUSSION

In the previous sections we presented a comprehensive compilation of all known X-ray binaries associated in the LMC. By comparing them with stellar catalogs of the LMC we updated and completed their optical classifications. Based on these results we identified the main star-formation episodes in the history of the LMC that are associated with its HMXB populations. In this section we discuss these results in the context of the formation efficiency of HMXBs, and their nature in comparison with the SMC and our Galaxy.

5.1 Star-formation history of young XRBs in the Magellanic Clouds

Below we discuss the major findings of this work and we compare them with the results for the young XRBs in the SMC (c.f. [Antonou et al. 2010](#)):

(a) In contrast to the SMC, the confirmed Be-XRBs and (as expected) XRB pulsars in the LMC are related to a major star-formation burst $\sim 6 - 25$ Myr ago (as a reminder, the SMC Be-XRBs are present in regions with star-formation bursts at $\sim 25 - 60$ Myr ago), indicating younger Be-star populations in the LMC than in the SMC regions (also obvious from the position of the counterparts on the $V, B - V$ color-magnitude diagram as discussed earlier in Section 3.1).

(b) The SFR of the major burst associated with the confirmed Be-XRBs and the X-ray pulsars in the LMC is almost 3 and 2 times, respectively, higher than that in the SMC.

(c) the candidate Be-XRBs show a star-formation episode that started earlier than 12.6 Myr ago, which is similar to the star-formation episode for the confirmed Be-XRBs (although the latter is more centered around ~ 12 Myr). The fact that the peak of the star-formation episode associated with the candidate Be-XRBs is at ~ 6 Myr suggests that this population may include misclassified SG-XRBs, since the latter are expected to be abundant at these young ages due to their massive companions. This is the first hint for a significant SG-XRB population in the LMC (we already know 4 such systems), at least in comparison to the SMC where only two systems are known to date: SMC X-1 ([Webster et al. 1972](#)) that is not covered by the MCPS survey, and source CXOU J005409.57-724143.5 ([Maravelias et al. 2014](#); although the nature of this source is debated; [Clark et al. 2013](#)). From Fig. 5 we also see that there is another star-formation episode ~ 100 Myr ago at the regions associated with candidate Be-XRBs. However, the association of this peak with the observed XRB populations is ruled out by the location of their optical counterparts in the OB locus of the color-magnitude diagram (Fig. 1), since the least massive B-type stars have a main-sequence lifetime of less than 100 Myr.

(d) the five regions that host the 4 known SG-XRB and LMC X-1 (the one BH-HMXB in the LMC with MCPS coverage) show a peak in their star-formation history at even younger ages ($\lesssim 10$ Myr), as expected based on the more massive companions (i.e. shorter lifetimes) of these XRB types. This is also supported by the location of their counterparts on the color-magnitude diagram (Fig. 1); they are systematically younger than $\lesssim 10$ Myr). As a note, no BH-HMXB has been found in the SMC yet.

(e) We also examined the star-formation history of the regions in which two of the most promising detections of WD/Be-XRBs

have been made. For the LMC WD/Be-XRB (source XMMU J052016.0-692505 with $L_X > 10^{36}$ erg s $^{-1}$; [Kahabka et al. 2006](#)), the peak in its star-formation history is shifted to older ages ($\sim 11 - 40$ Myr) with respect to the NS/Be-XRB population in this galaxy. We observe a similar trend in the SMC (source XMMU J010147.5-715550 with $L_X \sim 3 \times 10^{34}$ erg s $^{-1}$; [Sturm et al. 2012a](#)), though the star-formation burst in this case is wide (it appears at $\sim 32 - 141$ Myr ago). We note that in this analysis we have not included the second discovered WD/Be-XRB in the SMC (MAXI J0158-744; [Li et al. 2012](#)), since this system is located in the SMC Wing, which is not covered by the MCPS survey, thus there is no information on its star-formation history.

5.2 Formation efficiency for the various XRB types

In order to measure the formation efficiency of XRBs we need first to associate them with an individual star-formation episode. The location of the optical counterparts of the X-ray sources on the color-magnitude diagram clearly links them with stellar populations younger than ~ 50 Myr, which associates them with the star-formation episode peaking at $\sim 10 - 30$ Myr, depending on the exact star-formation history at the location of different XRB populations (Figs. 4 and 5). In the case of SG-XRBs in particular, we see from Fig. 1 that they are associated with even younger stellar populations, which clearly links them with an earlier star-formation episode ($\lesssim 10$ Myr; Fig. 4).

The number of systems in each class of XRBs is given in Table 9: Column 1 lists the XRB types considered in each calculation, while Column 2 gives the number of objects. Column 3 lists the age of the peak of their maximum SFR⁸, while Column 4 presents its estimated duration (in this we take into account that the star-formation episodes started before reaching their maximum intensity at the time given in Column 3), and Column 5 gives the SFR at the peak of each episode. In Column 6 we list the number of MCPS subregions (each $12' \times 12'$ [HZ09]) used for the derivation of the average star-formation history of regions with different XRB types (as these are given in Columns 1 and 2). In the same table, we also list the formation efficiency for each class of objects with respect to the SFR at the peak of the star-formation episode they are associated with. In particular, in Column 7 we list the number of systems we observe today per unit SFR at the peak of the SF episode, and in Column 8 the required SFR for the production of 1 system for each class. We note that we derive a formation efficiency only for those XRB populations for which we can establish a strong correlation with a particular star-formation episode. In addition, we estimate the number of XRBs normalized by the stellar mass M_* formed during the star-formation episode that produced them. We calculate the total M_* by integrating the binned star-formation histories shown in Figs. 4, 5. The formation rate of XRBs per unit stellar mass formed during their respective SF episode is given in Column 9. The errors in this quantity reflect the upper and lower limits of the SFR in Figs. 4, 5. For the SMC we have found that we need a SFR of $\sim 3 (2.5) \times 10^{-3} M_\odot \text{ yr}^{-1}$ for the production of one Be-XRB (HMXB) at ~ 40 Myr after a star-formation episode ([Antonou et al. 2010](#)). In the present work we find that:

⁸ For the cases with a significant secondary star-formation burst, e.g., for all known HMXBs, the HMXBs without a BH or WD compact object, and the candidate Be-XRBs listed in Table 5, we also provide the same information for this secondary episode, although it is not associated with the production of the XRBs under consideration (Section 5.1).

(a) the production of NS/Be-XRBs and HMXBs in the LMC ($\sim 21.4 \times 10^{-3} M_{\odot} \text{ yr}^{-1}$ and $\sim 43.5 \times 10^{-3} M_{\odot} \text{ yr}^{-1}$, respectively; Table 9) is ~ 7 and ~ 17 times less efficient than the production of the same populations in the SMC (with respect to their parent star-formation episodes, i.e. at ~ 12.6 Myr and ~ 42.2 Myr, respectively).

(b) based on the SFR of the SMC at the age of ~ 10 Myr ($\sim 0.33^{+0.52}_{-0.18} M_{\odot} \text{ yr}^{-1}$; Section 4.1) and the formation efficiency of LMC SG-XRBs at this age ($\sim 85.3^{+44.7}_{-44.0}$ systems/(M_{\odot}/yr); Table 9), we estimate a large number of 28^{+47}_{-21} SG-XRBs in the SMC (or equivalently, about 7 to 75 such systems). This large number is in stark contrast with the only 2 known SG-XRBs in the SMC (Section 5.1). On the other hand, recently, we have identified the elusive population of SG-XRBs in our Galaxy: (a) the heavily obscured SG-XRBs (a small known population exhibiting low luminosities, e.g., IG J16318-4848; Matt & Guainazzi 2003, Barragán et al. 2009; CI Cam; Belloni et al. 1999, Bartlett et al. 2013; GX301-2; Ricker et al. 1973, Islam & Paul 2014), and (b) the SFXTs, which have short (less than few hrs long) outbursts and low-level quiescent X-ray emission ($L_X \sim 10^{32} - 10^{34} \text{ erg s}^{-1}$; Section 1). However, this population is not expected to be easily detectable in *Chandra* and *XMM-Newton* surveys of the Magellanic Clouds. Given that this calculation is based on rescaling the numbers of SG-XRBs detected in the LMC to the SMC, both of which have been surveyed with similar strategies, we would not expect that the discrepancy between observed and estimated number of SG-XRBs in the SMC is the result of selection effects or missing populations as these would influence the SMC and the LMC in similar ways. Therefore, we consider that this discrepancy could be the result of a strong metallicity dependence of the XRB formation efficiency at least in the case of SG-XRBs.

(c) Based on the same argument, the SFR of the SMC at 25 Myr ($\sim 0.15^{+0.70}_{-0.10} M_{\odot} \text{ yr}^{-1}$; Section 4.1), and the formation efficiency of the LMC WD/Be-XRBs at this age (390.3 systems/(M_{\odot}/yr); Table 9), we predict ~ 59 SMC WD/Be-XRBs. However, thus far only one system has been identified as a candidate WD/Be-XRB in the LMC (Section 4.1), also pointing to a strong metallicity dependence.

5.3 Previous studies

Two other works discuss in some detail the link between young X-ray source populations and recent star formation:

- Shtykovskiy & Gilfanov (2005) used archival *XMM-Newton* data to study the X-ray source population of the LMC. They found significant field-to-field variations of the HMXBs in the LMC, which are not correlated with differences in their FIR or H_{α} emission, hence they suggest that these differences are due to the age dependence of the HMXB population. This is in good agreement with our work, which also shows differences in the types of XRBs and their formation efficiency as a function of age. Furthermore, they estimated that the number of HMXBs per total stellar mass to less than $10^{-4} M_{\odot}^{-1}$ at ages $\sim 1-2$ Myr, and $(1.00 \pm 0.45) \times 10^{-4} M_{\odot}^{-1}$ at $\sim 10-12$ Myr. This is a factor of ~ 70 lower than the formation efficiency listed in Table 9. This difference however is the result of the more complete census of HMXBs used in the present work, and the different assumptions in the calculation of the total stellar mass in the two works.

- On the other hand, Williams et al. (2013) found that the preferred age of HMXBs in NGC 300 and NGC 2403 is 40–55 Myr, which is the *same* age in which HMXBs are observed in the SMC. Although these galaxies have metallicities higher than that of the

SMC, the remarkable similarity of the ages of the stellar populations in which the HMXBs are observed in the SMC, NGC 300 and NGC 2403, make the argument for increased HMXB formation efficiency at an age of ~ 40 Myr even stronger.

5.4 Spectral-type distribution of LMC HMXBs

Moreover, we investigated differences in the spectral-type distribution of Be-XRBs, HMXBs with OB companions (i.e. non-Be stars), and Be stars and OB stars not associated with XRBs in the LMC. In Fig. 6 we show this distribution for Be starts (filled dark yellow histogram; Reid & Parker 2012), and O- and B-type stars (green and blue solid lines, respectively; Bonanos et al. 2009), all of luminosity class III-V. The HMXBs associated with Oe or Be stars are shown with a black solid line, while those with O- or B-type optical counterparts are presented with a magenta dashed line (all data are taken from Table 1). In this figure, spectral type IDs from 0 to 9 correspond to O-type stars, and IDs from 10 to 19 correspond to B-type stars. We find that the peak of the spectral-type distribution of the LMC Be-XRBs is around B0 and that of LMC Be stars around B1, in agreement with previous studies which have used smaller sample sizes (e.g., Neugeruela & Coe 2002, Antoniou et al. 2009a).

For completeness, we note here that the peak of the spectral-type distribution of the SMC Be-XRBs is instead around B1, but based on the two-sample Kolmogorov-Smirnov (K-S) test, it is not possible to definitely say if the SMC Be-XRBs follow a different spectral-type distribution from Galactic and LMC Be-XRBs (Antonou et al. 2009a). This is consistent with McBride et al. (2008), who note that there is indication for similar distributions in the SMC and the Milky Way. They find a spectral distribution cutoff for the SMC Be-XRBs around B2, but Maravelias et al. (2014) find that the spectral-type distribution is skewed towards later spectral types (actually, they identify several systems within the B2 to B5 spectral-type range). On the other hand, the SMC Be-star population peaks at earlier spectral types (i.e. at B0), in contrast to the LMC, where it peaks at later spectral types ($\sim B1$) than the Be-XRBs ($\sim B0$). The main caveats in these comparisons are the (large in many cases) uncertainties in the spectral-type classification, the small size of the LMC samples, and a possible selection effect towards brighter targets in the optical, thus earlier spectral types.

5.5 The young parent stellar populations of the LMC X-ray pulsars

From the above analysis, perhaps one would find surprising that the LMC X-ray pulsars are associated with a star-formation episode at such a young age, i.e. at only ~ 12.6 Myr (if not younger; see Fig. 4 and Table 9). The obvious question then is: could an X-ray pulsar form in such a short period? The answer to this question is not straightforward. Nevertheless, we approach this based on simple arguments regarding the age of the optical companions of these systems. Out of the 14 X-ray pulsars, 9 have known spectral types (Table 1). Of those, 8 have a late-type Oe or early-type Be star companion (only LMC X-4 with a pulse period of 13.5 s has an O7III-V/O8III counterpart, i.e. it has not shown H_{α} in emission). On the other hand, we know that the LMC HMXBs with Be-star companions show a peak in their spectral-type distribution at B0 (Fig. 6), and that the main-sequence lifetime can be simply estimated as:

$$t_{\text{MS}}/t_{\odot} = (M/M_{\odot})^{-2.5} \quad (1)$$

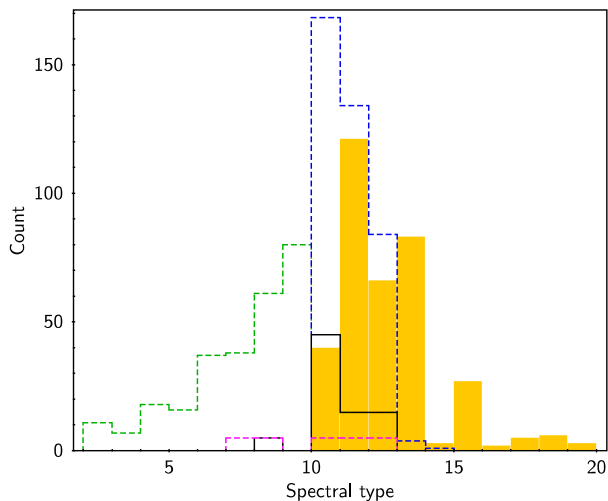


Figure 6. Spectral-type distribution for (a) Be field starts (filled dark yellow histogram); (b) O-type field stars (green dashed line); (c) B-type field stars (blue dashed line); (d) HMXBs with Oe or Be stars as the optical counterparts (black solid line); and (e) HMXBs with O- or B-type stars as the optical counterparts (magenta dashed line). The x-axis shows the spectral type, starting from O2 stars (corresponding to number 2) up to A0 stars (corresponding to 20), in steps of one spectral subtype. All sources have III-V luminosity classes and are taken from (a) the spectroscopic study of Reid & Parker (2012), (b,c) the census of Bonanos et al. (2009), and (d,e) the literature (see Table 1), respectively. Due to the small number of known HMXBs, the distributions (d,e) have been rescaled by a factor of 5.

using $t_{\odot} \sim 10$ Gyr. Thus, a B0 V star (having a mass of $14.6 M_{\odot}$; see Table 10) has $t_{MS} \sim 12.3$ Myr, while the lifetime of a blue supergiant is $\lesssim 1$ Myr (Table 4.1 from the PhD thesis of Chiřă 2011). This main-sequence lifetime of 12.3 Myr is very similar to the age of the peak of the star-formation history of the stellar populations associated with Be-XRBs and the X-ray pulsars in the LMC (see Figs. 4 and 5).

We note that the Be stars can appear at ages even younger than $\lesssim 10$ Myr. They have been observed in Magellanic Clouds clusters –NGC 346 and NGC 371 in the SMC and LH 72 and NGC 1858 in the LMC– with ages as young as ~ 5 –8 Myr (Wisniewski et al. 2007). Thus, although one would expect to mainly find SG-XRBs or BH-XRBs at that young ages based simply on their more massive companions⁹, there is evidence that the Be-XRB pulsars in the LMC can be as young as ~ 10 Myr.

Belczynski et al. (2008) find that a NS forms from stars with zero-age main sequence (ZAMS) masses between $\sim 7.5 M_{\odot}$ and $\sim 21 M_{\odot}$ (though we note that these estimations are based on single stellar evolution and solar metallicity). From Table 10 we see that this mass range corresponds to a main-sequence lifetime of ~ 5 Myr to ~ 100 Myr. Therefore, XRB pulsars can indeed form at such young ages.

⁹ This is true for the 4 SG-XRBs and the one BH-HMXB in the LMC, for which we can derive their star-formation histories (Fig. 4, right panels).

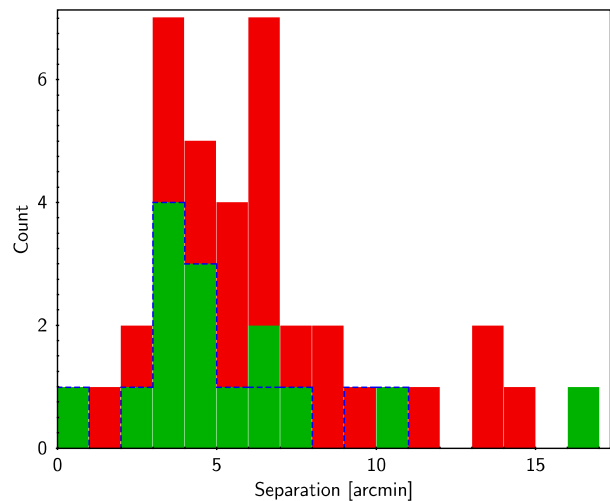


Figure 7. Distribution of the distance (in arcminutes) between XRBs in the LMC and their nearest star cluster from the catalog of Werchan & Zaritsky (2011). The 38 HMXBs without BH or WD compact objects are shown with a red solid histogram, the 15 confirmed NS/Be-XRBs are shown with a green solid histogram, and the 14 X-ray pulsars are shown with a blue dashed histogram.

5.6 Supernova kick velocities of LMC HMXBs

In order to estimate the kick velocity imparted onto the compact object at the time of its formation as a result of an asymmetry in the SN explosion, we follow the approach of Coe (2005) that was applied to the HMXB population of the SMC. We first derive the traveled distance of the HMXBs since their birth by using the mean offset between each X-ray source from Table 1 and its nearest star cluster. The catalog of Werchan & Zaritsky (2011) (hereafter [WZ11]) contains 1,066 clusters from the MCPS survey. All known LMC HMXBs but LMC X-3 are also covered by this survey. For the 38 non-BH or -WD HMXBs of this work (see Table 5), we find a mean offset of $6.4' \pm 3.6'$ ($\sim 92.0 \pm 52.4$ pc assuming a distance to the LMC equal to ~ 50 kpc; Macri et al. 2006), with the minimum distance equal to $1'$ and the maximum equal to $16.7'$ (in the cases of HMXBs and HMXBs with neutron stars exclusively these distributions are bimodal; Fig. 7). All reported error values are the standard deviations of the distribution of offsets. On the other hand, the 15 confirmed Be-XRBs and the 14 confirmed X-ray pulsars have a mean offset of $5.5' \pm 3.7'$ and $5.0' \pm 2.5'$, respectively (we consider the two classes separately since not all Be-XRBs have been identified as pulsars, and not all pulsars have been associated with spectroscopically confirmed Be stars).

From these offsets we can calculate the kick velocities imparted on the neutron star if we have an estimate of the travel time (e.g., Zezas & Fabbiano 2002; Coe 2005). The travel time is equal to the time since the supernova explosion. The spectral-type distribution of our stars peaks at B0 (Section 5.4), which corresponds to a star with a mass of $14.6 M_{\odot}$ and thus a main-sequence lifetime of ~ 12.3 Myr (Table 10; Williams 2011). The earliest time that pulsars are produced is given by the most massive stars that can produce compact objects with masses $\lesssim 3 M_{\odot}$. These are $\sim 21 M_{\odot}$ stars (Belczynski et al. 2008), which have a main-sequence lifetime of ~ 5 Myr (Section 5.5). Therefore, the minimum travel time

is ~ 7.3 Myr. Here we take into account the fact that the Be phenomenon appears towards the end of the main-sequence lifetime of a B-type star (e.g., Fabregat 2003). If Be stars are younger, then the estimated velocities are even larger. Combining this with the mean offset of $6.4' \pm 3.6'$ found above, we estimate a transverse velocity of $\sim 12.4 \pm 7.0$ km s $^{-1}$ (or a space velocity $\sqrt{2}$ times larger) for the HMXBs in the LMC (excluding the BH or WD systems). The confirmed NS/Be-XRB population in particular travels distances equal to $5.5' \pm 3.7'$ at the same time, resulting in a transverse velocity of $\sim 10.8 \pm 7.3$ km s $^{-1}$. Similarly, the LMC X-ray pulsars travel $5.0' \pm 2.5'$ with a transverse velocity of $\sim 9.7 \pm 4.9$ km s $^{-1}$.

We also investigate whether the positions of HMXBs in the LMC are significantly different from a uniform distribution. For this reason, we have estimated the minimum distance between 100,000 random points drawn from a uniform distribution in R.A., Dec., and in each case, the nearest star cluster (similarly to Coe 2005). The mean value was found to be equal to $4.4' \pm 1.4'$. Then we used the Kolmogorov-Smirnov (K-S) test to quantify the probability that the distributions of the offsets between the HMXBs and the real clusters in one case, and the random positions in the LMC and the clusters in the second case are different. We find that the two distributions are different at $>99.95\%$ confidence level. However, for the smaller samples (X-ray pulsars and Be-XRBs) the results from the K-S test are inconclusive.

In order to compare these results with those for the SMC, we follow the same approach. Coe (2005) has estimated a mean distance of $3.85'$ between the HMXBs in the SMC and their nearest clusters, and assumed a maximum lifetime of the Be star after the formation of the neutron star of ~ 5 Myr. We thus estimate a transverse velocity of ~ 13.1 km s $^{-1}$ (by using that $1'$ corresponds to 17.4 pc at the 60 kpc distance to the SMC; Hilditch, Howarth, & Harries 2005). On the other hand, if we take into account the fact that the peak of the spectral-type distribution of the companions of SMC HMXBs appears at B1 type that corresponds to an $11 M_{\odot}$ mass and a main-sequence lifetime of ~ 24.9 Myr, we estimate a minimum travel time of ~ 19.9 Myr. In this case, the SMC HMXBs have a transverse velocity of 3.3 km s $^{-1}$, or equivalently the LMC HMXBs travel with up to ~ 4 times larger velocities than their SMC counterparts.

On the other hand, the Milky Way Be-XRBs have low run-away velocities (mean peculiar tangential velocity equal to 15 ± 6 km s $^{-1}$), indicating low masses ejected into the supernovae that formed the neutron stars ($\lesssim 1-2 M_{\odot}$) and kick velocities received by their neutron stars at birth in the range of $60 - 250$ km s $^{-1}$ (van den Heuvel et al. 2000). These velocities are in broad agreement with the transverse velocities for the LMC neutron star accreting binaries estimated above. However, the SMC systems seem to have even smaller velocities, which is consistent with enhanced fraction of electron-capture supernovae that impart very small kicks, as predicted by Linden et al. (2009) for the SMC metallicity.

Furthermore, we also examine the mean offset of the identified HMXBs from the nearest young star cluster as a function of the cluster's age. In this comparison we used the catalog of Baumgardt et al. (2013) (hereafter [B13]), which provides age information for a large number of star clusters in the LMC. About one third of the 320 clusters in the [B13] catalog has ages younger than or equal to 100 Myr (with a mean age of 52 ± 28 Myr). If we focus on these 99 young clusters, we find that the 38 non-BH or -WD HMXBs have a mean offset of $16.8' \pm 13.9'$, which is more than double the distance derived using the [WZ11] catalog. The large standard deviation is the result of few systems having very large offsets (which is expected since this catalog is sparser than [WZ11]). The other two

subsets, the confirmed NS/Be-XRBs and the X-ray pulsars, have offsets of $16.6' \pm 17.5'$ and $12.8' \pm 15.3'$, respectively. In Fig. 8(a) we present the mean separation (in arcminutes) of all HMXBs (excluding those systems with BH or WD compact objects), the confirmed NS/Be-XRBs and only the X-ray pulsars (red circles, blue squares, and green triangles, respectively) from the nearest young star cluster (with an age ≤ 100 Myr) listed in [B13] catalog as a function of the cluster's age. The size of each data point is proportional to the relative error on the number of the identified matches in each age bin, while the x-axis error-bars are equal to half the age bin. Similarly, in Fig. 8(b) we give the number of the identified matches as a function of the age of the cluster, following the color scheme of Fig. 8(a). In this case, the data points have sizes proportional to the relative error on the separation. We find that the majority of the X-ray sources reside nearby a cluster with age (20, 40] Myr ($\sim 61\%$, $\sim 67\%$ and $\sim 79\%$, for the HMXBs without BH or WD compact objects, the confirmed NS/Be-XRBs and the X-ray pulsars, respectively). Although the star-formation history of the regions associated with X-ray pulsars shows its peak at younger ages (~ 12.6 Myr; see Table 9) than the 30 Myr peak in Fig. 8, the major star-formation burst has a duration of ~ 32 Myr, well within the (20,40] Myr age range. The mean separation of the aforementioned 3 populations at the (20,40] Myr age range is $15.5' \pm 12.2'$, $10.1' \pm 9.8'$, and $10.4' \pm 9.4'$, respectively.

5.7 Corbet diagram

An updated version of the "Corbet diagram" (Corbet 1984), i.e. a log-log plot of the spin period versus the orbital period, of X-ray pulsars with Be and SG stars donors is shown in Fig. 9. The position of sources in this diagram depends on the accretion torques exerted into the NS, resulting in the division of the sources in 3 groups corresponding to 3 different mass-transfer mechanisms (Corbet et al. 2009). When the primary is a Be star, the accretion occurs through the star's decretion disk, but when it is a SG star, the accretion can happen either through stellar winds (wind-fed systems) or through Roche-Lobe overflow (RLOF) if the star fills its Roche Lobe. The 8 LMC, 38 SMC and 20 Milky Way Be-XRBs with known P_{spin} and P_{orb} values are shown in red, green and blue circles, respectively, while the 10 Milky Way wind-fed SG-XRBs in yellow triangles. There are also 3 RLOF systems (Cen X-3, LMC X-4, and SMC X-1) shown in black squares. The data for the LMC are taken from the references listed in Table 1, while those for the SMC and the Milky Way from the compilations of Klus et al. (2014) and Townsend et al. (2011), respectively. We see that all but one of the LMC Be-XRBs have orbital periods of less than ~ 30 days. Only LXP96.1 (source RX J0544.1-7100) has a much larger orbital period of 286 days. Similarly, all but one of the LMC Be-XRBs have spin periods longer than ~ 4 sec. Only LXP0.07 (source RX J0535.6-6651) is known to have a 70 millisecond spin period (in the Milky Way there are 2 systems with such short spin periods). Although the number of known LMC Be-XRB systems is small, all identified members fall within the locus of the SMC and Milky Way Be-XRBs. In the same plot we also show the location of the apparent dips in the bimodal $\log(P_{\text{spin}})$ and $\log(P_{\text{orb}})$ distributions of Be-XRBs (dashed lines), as identified by Knigge et al. (2011), and subsequently confirmed by Coe & Kirk (2015). These authors associate those sub-populations (also distinct in the $\log(P_{\text{spin}})$ -eccentricity plane) with 2 types of supernovae: electron-capture supernovae systems are thought to produce short spin and orbital periods and low eccentricity (imparting smaller kick velocities to the neutron stars), while iron core-collapse supernovae are thought to be responsible

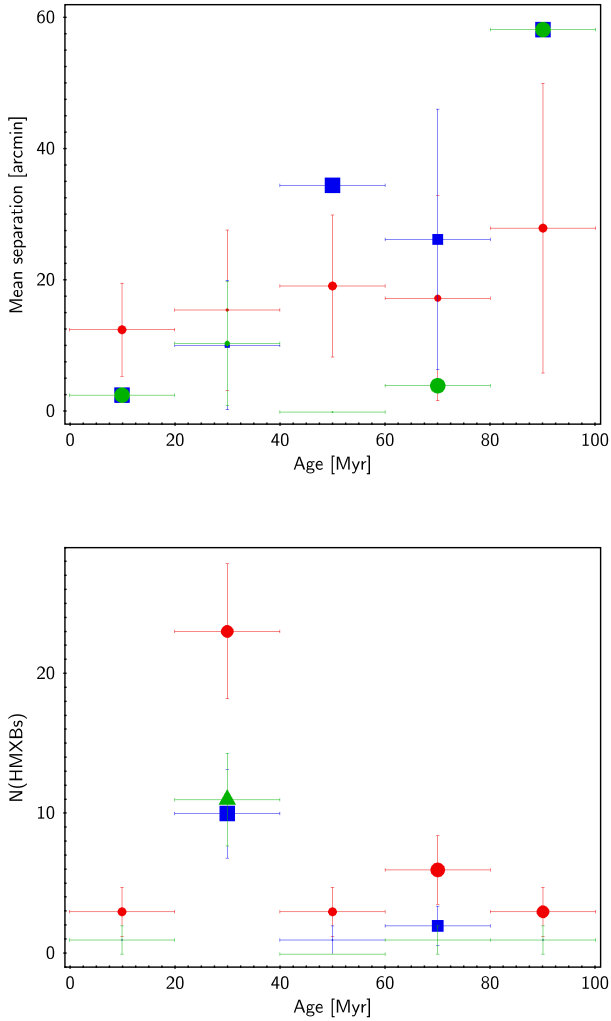


Figure 8. (a) Mean separation (in arcminutes) of all non-BH or -WD HMXBs (red circles), only confirmed NS/HMXBs (blue squares) and X-ray pulsars (green triangles; color scheme similar to Fig. 7) from the nearest young star cluster (with an age ≤ 100 Myr) listed in Baumgardt et al. (2013) as a function of age. The data have been binned in the following age ranges: (0, 20] Myr, (20, 40] Myr, (40, 60] Myr, (60, 80] Myr, (80, 100] Myr, which are shown as error bars in the x-axis. The size of the data points is proportional to the relative error on the number of X-ray sources with matches in the cluster catalog within each age bin. The y-axis error bar shows the standard deviation of the mean separation distribution of sources within each age bin. (b) Similar to panel (a) but this time in the y-axis is the number of X-ray sources with matches in the cluster catalog within each age bin, while the size of the data points is proportional to the relative error on the separation (in arcminutes). The y-axis error bar corresponds to \sqrt{N} , where N is the number of sources in each bin.

for higher eccentricity systems with slightly higher neutron star masses. We find that most of the known LMC Be-XRBs fall on the bottom left part of this diagram, i.e. pointing to electron-capture supernovae, in agreement with the small estimated center of the mass velocities for these systems. However, the lack of LMC X-ray pulsars at the top right part of the "Corbet diagram" could be the result of a selection effect: it is easier to detect orbital periods of a few weeks than several months or years, and spin periods of a few seconds than ~ 100 sec.

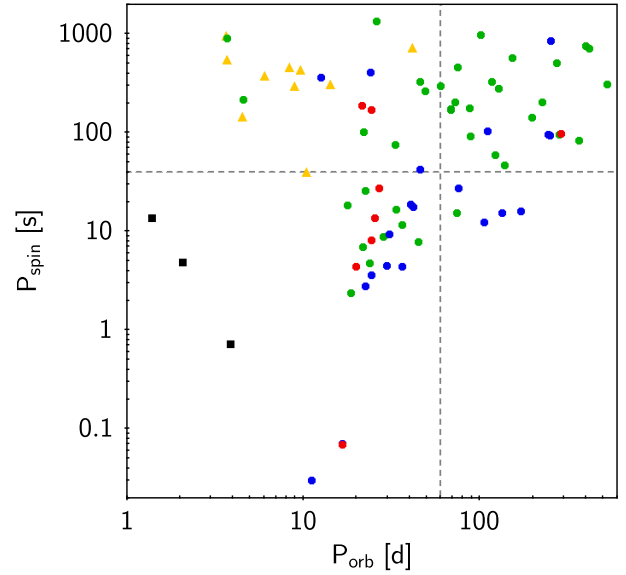


Figure 9. Spin period versus orbital period –the so called "Corbet diagram"– for LMC, SMC and Milky Way NS/Be-XRBs (shown in red, green and blue filled circles, respectively). We also show the Galactic wind-fed SG-XRBs (in yellow triangles) and 3 RLOF SG-XRB systems (Cen X-3, LMC X-4, and SMC X-1 shown in black squares).

In contrast, Linden et al. (2009) have found that electron-capture supernovae are highly associated with the production of Be-XRBs for the SMC metallicity, so if the argument of Knigge et al. (2011) holds then one would expect to find the majority of the SMC Be-XRBs on the lower-left quadrant of the "Corbet diagram". Instead, Fig. 9 shows that less than half of the systems are located in the lower-left quadrant with respect to long spin and orbital period systems. On the other hand, Cheng, Shao, & Li (2014) proposed that the bimodal P_{spin} distribution is most likely due to the difference in the accretion modes of the NSs in the Be-XRB systems. They also note that the two types of supernovae can affect the spin evolution of the NS through the configuration of the decretion disk of the Be star. Recently, Haberl & Sturm (2015) used the most complete census of HMXBs in the SMC to investigate which mechanism is responsible for the bimodal P_{spin} distribution. They found larger long-term X-ray variability for sources with short spin periods, thus favoring the accretion model of Cheng, Shao, & Li (2014) as an explanation of the bimodal P_{spin} distribution of Be-XRBs.

6 SUMMARY

In this work, we present an up-to-date list of HMXBs in the LMC. Using the MCPS survey (Zaritsky et al. 2004) and extensive Monte Carlo simulations, we identify the most likely counterpart of X-ray sources identified in previous X-ray surveys of the LMC and estimate their chance coincidence probability. In particular, we classify 40 such systems, further divided in 33 Be-XRBs, 4 SG-XRBs and 3 sources for which we could only assign a broad HMXB class. In addition, we revise the classification of 4 X-ray sources listed in the literature as (candidate) HMXBs to non-HMXB systems. As a by-product of this work, we compiled a list of metallicities available for young OB-type stars in the Magellanic Clouds.

Using the spatially resolved star-formation history map of the

LMC by [HZ09], we investigate the link of star formation and young XRBs. We find that the star-formation history is strongly peaked at ~ 6.3 Myr for regions hosting HMXBs, SG-XRBs, and the one BH-HMXB (LMC X-1) with MCPS coverage; at ~ 12.6 Myr for the NS/Be-XRBs and X-ray pulsars; and at ~ 25.1 Myr for the candidate WD/Be-XRB. We find that the age of the stellar populations in regions associated with pulsars in the LMC is much younger than the age of the same population in the SMC (25 – 60 Myr; Antoniou et al. 2010). Similarly, the age of the stellar populations associated with the only WD/Be-XRB in the LMC is younger than the age of the same population in the SMC (~ 42.2 Myr). Thus, this study (in combination with previous works; e.g., Shtykovskiy & Gilfanov 2005, Antoniou et al. 2010, Williams et al. 2013) reinforces the idea that the HMXBs are associated with young stellar populations of ages ~ 10 –40 Myr.

Comparing the SFR at the peak of the star-formation episode associated with the NS/Be-XRBs (HMXBs) sources in the LMC and the SMC, we find that their production rate in the LMC is almost 7 (17) times lower than that in the SMC. In particular, we find a production rate of 1 system per $\sim 21.4 \times 10^{-3} M_{\odot} \text{ yr}^{-1}$ and $\sim 43.5 \times 10^{-3} M_{\odot} \text{ yr}^{-1}$ for the NS/Be-XRBs and HMXBs in the LMC, respectively, or 1 system per $\sim 333 M_{\odot}$ ($\sim 143 M_{\odot}$) of stars formed during the star-formation episode that is associated with the Be-XRBs (HMXBs). On the other hand, based on the SFR of the SMC at the age of ~ 10 Myr ($\sim 0.33^{+0.52}_{-0.18} M_{\odot} \text{ yr}^{-1}$; Section 4.1) and the formation efficiency of LMC SG-XRBs at this age ($\sim 85.3^{+44.7}_{-44.0}$ systems/(M_{\odot} /yr); Table 9), we estimate a large number of 28^{+47}_{-21} SG-XRBs in the SMC, which is in stark contrast with the only 2 known such systems in the SMC. Based on similar arguments, the SFR of the SMC ($\sim 0.15^{+0.70}_{-0.10} M_{\odot} \text{ yr}^{-1}$; Section 4.1), and the formation efficiency of the LMC WD/Be-XRBs (390.3 systems/(M_{\odot} /yr); Table 9), both at the age of ~ 25 Myr, we predict ~ 59 SMC WD/Be-XRBs. Although the fact that nowadays we know only one candidate WD/Be-XRB in the LMC points to a strong metallicity dependence, in order to investigate the formation channels of the WD/Be-XRB systems and to constrain their evolutionary models, many more such systems need to be identified first.

Furthermore, we find a peak at the spectral-type distribution of the LMC Be-XRBs at around B0, in agreement with previous studies (e.g., Negueruela & Coe 2002, Antoniou et al. 2009a), which have used smaller sample sizes.

We have also examined the mean offset of the identified HMXBs from the nearest young star cluster as a function of the cluster's age (using the [B13] catalog; Baumgardt et al. 2013). We find that the majority of the (a) HMXBs without BH or WD compact objects, (b) the confirmed NS/Be-XRBs and (c) the X-ray pulsars reside near a cluster with age between 20 – 40 Myr, while we find almost equal numbers of X-ray pulsars in the 20 – 30 Myr and 30 – 40 Myr age bins.

In addition, using the [WZ11] catalog (Werchan & Zaritsky 2011), we find that the 15 confirmed NS/Be-XRBs (14 confirmed X-ray pulsars) have a mean offset of $5.5' \pm 3.7'$ ($5.0' \pm 2.5'$) from their nearest cluster, respectively. Assuming a minimum pulsar birth timescale of ~ 5 Myr after the burst and an elapsed time of ~ 7.3 Myr since the kick imparted onto the neutron star during the supernova explosion for a B0 star, we estimate a transverse velocity of $\sim 10.8 \pm 7.3 \text{ km s}^{-1}$ ($\sim 9.7 \pm 4.9 \text{ km s}^{-1}$) for the NS/Be-XRBs (X-ray pulsars) in the LMC. In addition, the 38 HMXBs without BH or WD compact objects have a mean offset of $6.4' \pm 3.6'$, thus resulting in transverse velocities of $\sim 12.4 \pm 7.0 \text{ km s}^{-1}$. Following the same approach in the case of the SMC, we find that SMC bi-

naries have up to ~ 4 times smaller transverse velocities (estimated assuming an elapsed time of ~ 19.9 Myr for a B1 star and the same minimum pulsar birth timescale).

ACKNOWLEDGEMENTS

We thank the anonymous referee and Georgios Vasilopoulos for their insightful comments, which have improved the paper. This material is based upon work supported by the National Aeronautics and Space Administration under Grant No. NNX10AH47G issued through the Astrophysics Data Analysis Program. VA also acknowledges financial support from NASA/Chandra grants GO3-14051X and AR4-15003X. AZ acknowledges financial support from NASA/ADAP grant NNX12AN05G and funding from the European Research Council under the European Union's Seventh Framework Programme (FP/2007-2013)/ERC Grant Agreement n. 617001. This research has made use of the NASA/IPAC Extragalactic Database (NED) which is operated by the Jet Propulsion Laboratory, California Institute of Technology, under contract with the National Aeronautics and Space Administration; the Vizier catalogue access tool, CDS, Strasbourg, France; the SIMBAD database, operated at CDS, Strasbourg, France; NASA's Astrophysics Data System; the Tool for OPERations on Catalogues And Tables (TOPCAT) software package (Taylor 2005).

REFERENCES

- Alves, D. R. 2004, *New Astron. Rev.*, 48, 659
 Anders, E., & Grevesse, N. 1989, *Geochim. Cosmochim. Acta*, 53, 197
 Antoniou, V., Hatzidimitriou, D., Zezas, A., & Reig, P. 2009a, *ApJ*, 707, 1080
 Antoniou, V., Zezas, A., Hatzidimitriou, D., & McDowell, J. C. 2009b, *ApJ*, 697, 1695
 Antoniou, V., Zezas, A., Hatzidimitriou, D., & Kalogera, V. 2010, *ApJ*, 716, L140
 Ardeberg, A., & Maurice, E. 1977, *A&AS*, 30, 261
 Asplund, M., Grevesse, N., Sauval, A. J., & Scott, P. 2009, *ARA&A*, 47, 481
 Ayres, T. R. 2010, *ApJS*, 187, 149
 Barragán L., Wilms J., Pottschmidt K., Nowak M. A., Kreykenbohm I., Walter R., Tomsick J. A., 2009, *A&A*, 508, 1275
 Bartlett E. S., Clark J. S., Coe M. J., Garcia M. R., Uttley P., 2013, *MNRAS*, 429, 1213
 Baumgardt, H., Parmentier, G., Anders, P., & Grebel, E. K. 2013, *MNRAS*, 430, 676
 Beardmore, A. P., Coe, M. J., Markwardt, C., Osborne, J. P., Baumgartner, W. H., Tueller, J., & Gehrels, N. 2009, *The Astronomer's Telegram*, 1901, 1
 Belczynski K., Kalogera V., Rasio F. A., Taam R. E., Zezas A., Bulik T., Maccarone T. J., Ivanova N., 2008, *ApJS*, 174, 223
 Belloni T., et al., 1999, *ApJ*, 527, 345
 Bica, E., Bonatto, C., Dutra, C. M., & Santos, J. F. C. 2008, *MNRAS*, 389, 678
 Blair, W. P., Oliveira, C., Lamassa, S., et al. 2009, *PASP*, 121, 634
 Blanco, V. M., & Hiltner, W. A. 1977, *IAU Circ.*, 3039, 3
 Bodaghee, A., et al. 2007, *A&A*, 467, 585
 Bonanos, A. Z., Massa, D. L., Sewilo, M., et al. 2009, *AJ*, 138, 1003
 Brunet, J. P., Imbert, M., Martin, N., et al. 1975, *A&AS*, 21, 109
 Brusa, M., Zamorani, G., Comastri, A., et al. 2007, *ApJS*, 172, 353
 Chaty S., 2015, arXiv, arXiv:1510.07681
 Charles, P. A., et al. 1983, *MNRAS*, 202, 657
 Cheng Z.-Q., Shao Y., Li X.-D. 2014, *ApJ*, 786, 128
 Chevalier, C., & Ilovaisky, S. A. 1977, *A&A*, 59, L9

- Chiosi, C., Vallenari, A., Bressan, A., Deng, L., & Ortolani, S. 1995, *A&A*, 293, 710
- Chiosi, E., Vallenari, A., Held, E. V., Rizzi, L., & Moretti, A. 2006, *A&A*, 452, 179
- Chişă, S. M. 2011, PhD Thesis, Utrecht University, ISBN 978-90-393-5249-6
- Chu, Y.-H., Kim, S., Points, S. D., Petre, R., & Snowden, S. L. 2000, *AJ*, 119, 2242
- Cioni, M.-R. L., Habing, H. J., & Israel, F. P. 2000, *A&A*, 358, L9
- Cioni, M.-R. L. 2009, *A&A*, 506, 1137
- Clark J. S., Bartlett E. S., Coe M. J., Dorda R., Haberl F., Lamb J. B., Negueruela I., Udalski A., 2013, *A&A*, 560, A10
- Clark J. S., et al., 2015, *A&A*, 579, A131
- Coe, M. J. 2005, *MNRAS*, 358, 1379
- Coe M. J., Finger M., Bartlett E. S., Udalski A., 2015, *MNRAS*, 447, 1630
- Coe M. J., & Kirk J. 2015, *MNRAS*, 452, 969
- Coe, M. J., Negueruela, I., Buckley, D. A. H., Haigh, N. J., & Laycock, S. G. T. 2001, *MNRAS*, 324, 623
- Cole A. A., Tolstoy E., Gallagher J. S., III, Smecker-Hane T. A., 2005, *AJ*, 129, 1465
- Colucci, J. E., Bernstein, R. A., Cameron, S. A., & McWilliam, A. 2011, *ApJ*, 735, 55
- Corbet, R. H. D., Coe, M. J., McGowan, K. E., et al. 2009, *IAU Symposium*, 256, 361
- Corbet, R. H. D. 1984, *A&A*, 141, 91
- Corbet, R. H. D., Mason, K. O., Branduardi-Raymont, G., Cordova, F. A., & Parmar, A. N. 1985, *MNRAS*, 212, 565
- Cowley, A. P., Crampton, D., Hutchings, J. B., Helfand, D. J., Hamilton, T. T., Thorstensen, J. R., & Charles, P. A. 1984, *ApJ*, 286, 196
- Cowley, A. P., Crampton, D., Hutchings, J. B., Remillard, R., & Penfold, J. E. 1983, *ApJ*, 272, 118
- Cowley A. P., Schmidtke P. C., Anderson A. L., McGrath T. K., 1995, *PASP*, 107, 145
- Cowley, A. P., Schmidtke, P. C., McGrath, T. K., Ponder, A. L., Fertig, M. R., Hutchings, J. B., & Crampton, D. 1997, *PASP*, 109, 21
- Crampton, D., Cowley, A. P., Thompson, I. B., & Hutchings, J. B. 1985, *AJ*, 90, 43
- Crampton, D., & Greasley, J. 1982, *PASP*, 94, 31
- Cui, W., Feng, Y. X., Zhang, S. N., et al. 2002, *ApJ*, 576, 357
- Cusumano, G., Israel, G. L., Mannucci, F., Masetti, N., Mineo, T., & Nicasastro, L. 1998, *A&A*, 337, 772
- Da Costa, G. S., & Hatzidimitriou, D. 1998, *AJ*, 115, 1934
- D'Ai A., La Parola V., Cusumano G., Segreto A., Romano P., Vercellone S., Robba N. R., 2011, *A&A*, 529, A30
- Dennerl, K., Haberl, F., & Pietsch, W. 1995, *IAU Circ.*, 6184, 2
- Dickey J. M., Lockman F. J., 1990, *ARA&A*, 28, 215
- Dirsch, B., Richtler, T., Gieren, W. P., & Hilker, M. 2000, *A&A*, 360, 133
- Douna V. M., Pellizza L. J., Mirabel I. F., Pedrosa S. E., 2015, *A&A*, 579, A44
- Dray, L. M. 2006, *MNRAS*, 370, 2079
- Ducci L., Doroshenko V., Romano P., Santangelo A., Sasaki M., 2014, *A&A*, 568, A76
- Dufton, P. L., Ryans, R. S. I., Thompson, H. M. A., & Street, R. A. 2008, *MNRAS*, 385, 2261
- Ebisawa, K., Bourban, G., Bodaghee, A., Mowlavi, N., & Courvoisier, T. J.-L. 2003, *A&A*, 411, L59
- Edge, W. R. T., Coe, M. J., Galache, J. L., & Hill, A. B. 2004, *MNRAS*, 349, 1361
- Elson, R. A. W. 1991, *ApJS*, 76, 185
- Evans, C. J., Lennon, D. J., Smartt, S. J., & Trundle, C. 2006, *A&A*, 456, 623
- Fabregat J., 2003, *ASPC*, 292, 65
- Fariña, C., Bosch, G. L., Morrell, N. I., Barbá, R. H., & Walborn, N. R. 2009, *AJ*, 138, 510
- Fragos T., et al., 2013, *ApJ*, 764, 41
- Fuhrmeister, B., & Schmitt, J. H. M. M. 2003, *A&A*, 403, 247
- Galache, J. L. 2006, PhD Thesis, University of Southampton
- Gilmozzi, R., Kinney, E. K., Ewald, S. P., Panagia, N., & Romaniello, M. 1994, *ApJ*, 435, L43
- Glatt, K., Grebel, E. K., & Koch, A. 2010, *A&A*, 517, A50
- Gordon, K. D., Clayton, G. C., Misselt, K. A., Landolt, A. U., & Wolff, M. J. 2003, *ApJ*, 594, 279
- Götz, D., Mereghetti, S., Merlini, D., Sidoli, L., & Belloni, T. 2006, *A&A*, 448, 873
- Grebenev, S. A., & Lutovinov, A. A. 2010, *The Astronomer's Telegram*, 2695, 1
- Grebenev, S. A., Lutovinov, A. A., Tsygankov, S. S., & Mereminskiy, I. A. 2013, *MNRAS*, 428, 50
- Haberl, F., Dennerl, K., & Pietsch, W. 1995a, *A&A*, 302, L1
- Haberl, F., Dennerl, K., & Pietsch, W. 2003, *A&A*, 406, 471
- Haberl, F., Dennerl, K., Pietsch, W., & Reinsch, K. 1997, *A&A*, 318, 490
- Haberl, F., & Pietsch, W. 1999a, *A&AS*, 139, 277
- Haberl, F., & Pietsch, W. 1999b, *A&A*, 344, 521
- Haberl, F., Pietsch, W., & Dennerl, K. 1995b, *A&A*, 303, L49
- Haberl F., & Sturm R. 2015, arXiv:1511.00445, *A&A* accepted
- Haberl, F., Sturm, R., Ballet, J., et al. 2012b, *A&A*, 545, A128
- Haberl, F., Sturm, R., Filipović, M. D., Pietsch, W., & Crawford, E. J. 2012, *A&A*, 537, L1
- Harris, J., & Zaritsky, D. 2004, *AJ*, 127, 1531
- Harris, J., & Zaritsky, D. 2009, *AJ*, 138, 1243
- Hilditch R. W., Howarth I. D., Harries T. J., 2005, *MNRAS*, 357, 304
- Hilker, M., Richtler, T., & Gieren, W. 1995, *A&A*, 294, 648
- Hill, R. S., Cheng, K.-P., Bohlin, R. C., et al. 1995, *ApJ*, 446, 622
- Hill, V. 1999, *A&A*, 345, 430
- Hong J., van den Berg M., Schlegel E. M., Grindlay J. E., Koenig X., Laycock S., Zhao P., 2005, *ApJ*, 635, 907
- Hunter, D. A., Shaya, E. J., Holtzman, J. A., et al. 1995, *ApJ*, 448, 179
- Hutchings, J. B., Crampton, D., & Cowley, A. P. 1978, *ApJ*, 225, 548
- Hutchings, J. B., Crampton, D., & Cowley, A. P. 1983, *ApJ*, 275, L43
- Hutchings, J. B., Crampton, D., Cowley, A. P., Bianchi, L., & Thompson, I. B. 1987, *AJ*, 94, 340
- Johnston, M. D., Bradt, H. V., Doxsey, R. E., Griffiths, R. E., Schwartz, D. A., & Schwarz, J. 1979, *ApJ*, 230, L11
- Jasniewicz, G., & Thevenin, F. 1994, *A&A*, 282, 717
- Jaxon, E. G., Guerrero, M. A., Howk, J. C., Walborn, N. R., Chu, Y.-H., & Wakker, B. P. 2001, *PASP*, 113, 1130
- Johnston, M. D., Griffiths, R. E., & Ward, M. J. 1980, *Nature*, 285, 26
- Joss P. C., Rappaport S. A., 1984, *ARA&A*, 22, 537
- Ilovaisky, S. A., Chevalier, C., Motch, C., Pakull, M., van Paradijs, J., & Lub, J. 1984, *A&A*, 140, 251
- Inam, S. Ç., Townsend, L. J., McBride, V. A., et al. 2009, *MNRAS*, 395, 1662
- Indu, G., & Subramaniam, A. 2011, *A&A*, 535, A115
- Irwin, M. J., Demers, S., & Kunkel, W. E. 1990, *AJ*, 99, 191
- Islam N., Paul B., 2014, *MNRAS*, 441, 2539
- Kahabka, P. 2002, *A&A*, 388, 100
- Kahabka, P., Haberl, F., Payne, J. L., & Filipović, M. D. 2006, *A&A*, 458, 285
- Keller, S. C., Bessell, M. S., Cook, K. H., Geha, M., & Syphers, D. 2002, *AJ*, 124, 2039
- Kelley, R. L., Jernigan, J. G., Levine, A., Petro, L. D., & Rappaport, S. 1983, *ApJ*, 264, 568
- Klus, H., Bartlett, E. S., Bird, A. J., et al. 2013, *MNRAS*, 428, 3607
- Klus, H., Ho, W. C. G., Coe, M. J., Corbet, R. H. D., & Townsend, L. J. 2014, *MNRAS*, 437, 3863
- Knigge, C., Coe, M. J., & Podsiadlowski, P. 2011, *Nature*, 479, 372
- Korn, A. J., Becker, S. R., Gummersbach, C. A., & Wolf, B. 2000, *A&A*, 353, 655
- Krimm, H. A., et al. 2009, *The Astronomer's Telegram*, 2011, 1
- Krimm H. A., et al., 2013a, *ATel*, 5286, 1
- Krimm H. A., Holland S. T., Kennea J. A., 2013b, *ATel*, 5293, 1
- Krimm H. A., Gelbord J. M., Holland S. T., Kennea J. A., 2013c, *ATel*, 5309, 1
- Kürster, M., & Hasinger, G. 1993, *ROSAT AMCS Status Report - Bore-sighting re-analysis*, MPE Technical Note TN-ROS-ME-ZA00/30,

- Max-Planck-Institut für Extraterrestrische Physik, D 85740 Garching near Munich, Germany
- Lehner, N. 2002, *ApJ*, 578, 126
- Lehner, N., Howk, J. C., Keenan, F. P., & Smoker, J. V. 2008, *ApJ*, 678, 219
- Lejeune, T., & Schaerer, D. 2001, *A&A*, 366, 538
- Li, K. L., Kong, A. K. H., Charles, P. A., et al. 2012, *ApJ*, 761, 99
- Linden, T., Kalogera, V., Sepinsky, J. F., et al. 2010, *ApJ*, 725, 1984
- Linden T., Sepinsky J. F., Kalogera V., Belczynski K., 2009, *ApJ*, 699, 1573
- Liu, Q., de Grijs, R., Deng, L. C., Hu, Y., Baraffe, I., & Beaulieu, S. F. 2009, *MNRAS*, 396, 1665
- Liu, Q. Z., van Paradijs, J., & van den Heuvel, E. P. J. 2005, *A&A*, 442, 1135
- Luck, R. E., Moffett, T. J., Barnes, T. G., III, & Gieren, W. P. 1998, *AJ*, 115, 605
- Macri, L. M., Stanek, K. Z., Bersier, D., Greenhill, L. J., & Reid, M. J. 2006, *ApJ*, 652, 1133
- Maggi, P., Haberl, F., Sturm, R., et al. 2013, *A&A*, 554, A1
- Maravelias, G., Zezas, A., Antoniou, V., & Hatzidimitriou, D. 2014, *MNRAS*, 438, 2005
- Masetti, N., et al. 2006b, *A&A*, 459, 21
- Massey, P. 2002, *ApJS*, 141, 81
- Massey, P., Parker, J. W., & Garmany, C. D. 1989, *AJ*, 98, 1305
- Matt G., Guainazzi M., 2003, *MNRAS*, 341, L13
- McBride V. A., Coe M. J., Negueruela I., Schurch M. P. E., McGowan K. E., 2008, *MNRAS*, 388, 1198
- McGowan, K. E., Coe, M. J., Schurch, M. P. E., et al. 2008, *MNRAS*, 383, 330
- Negueruela, I., & Coe, M. J. 2002, *A&A*, 385, 517
- Negueruela I., Smith D. M., Reig P., Chaty S., Torrejón J. M., 2006, *ESASP*, 604, 165
- Oey, M. S., & Massey, P. 1995, *ApJ*, 452, 210
- Olsen, K. A. G., Hodge, P. W., Wilcots, E. M., & Pastwick, L. 1997, *ApJ*, 475, 545
- Pakull M. W., Olander, 1976, *IAUC*, 3017, 3
- Reid, N., Glass, I. S., & Catchpole, R. M. 1988, *MNRAS*, 232, 53
- Reid, W. A., & Parker, Q. A. 2012, *MNRAS*, 425, 355
- Russell, S. C., & Dopita, M. A. 1992, *ApJ*, 384, 508
- Parker, J. W., Garmany, C. D., Massey, P., & Walborn, N. R. 1992, *AJ*, 103, 1205
- Peters, G. J., & Adelman, S. J. 2006, *Astrophysics in the Far Ultraviolet: Five Years of Discovery with FUSE*, 348, 136
- Piatti, A. E., Geisler, D., Bica, E., & Clariá, J. J. 2003, *MNRAS*, 343, 851
- Piatti, A. E., Santos, J. F. C., Jr., Clariá, J. J., et al. 2005, *A&A*, 440, 111
- Piatti, A. E., Sarajedini, A., Geisler, D., Clark, D., & Seguel, J. 2007, *MNRAS*, 377, 300
- Piatti, A. E., Geisler, D., Sarajedini, A., Gallart, C., & Wischnjewsky, M. 2008, *MNRAS*, 389, 429
- Pietrzynski, G., & Udalski, A. 1999, *Acta Astron.*, 49, 157
- Pietrzynski, G., & Udalski, A. 2000a, *Acta Astron.*, 50, 337
- Porter, J. M., & Rivinius, T. 2003, *PASP*, 115, 1153
- Ricker G. R., McClintock J. E., Gerassimenko M., Lewin W. H. G., 1973, *ApJ*, 184, 237
- Rolleston, W. R. J. 1995, *Irish Astronomical Journal*, 22, 17
- Rolleston, W. R. J., Dufton, P. L., Fitzsimmons, A., Howarth, I. D., & Irwin, M. J. 1993, *A&A*, 277, 10
- Rolleston, W. R. J., Dufton, P. L., McErlean, N. D., & Venn, K. A. 1999, *A&A*, 348, 728
- Rolleston, W. R. J., Trundle, C., & Dufton, P. L. 2002, *A&A*, 396, 53
- Rousseau, J., Martin, N., Prévot, L., et al. 1978, *A&AS*, 31, 243
- Sabogal, B. E., Mennickent, R. E., Pietrzyński, G., & Gieren, W. 2005, *MNRAS*, 361, 1055
- Sagar, R., & Richtler, T. 1991, *A&A*, 250, 324
- Samus, N. N., Durlевич, O. V., & et al. 2009, *VizieR Online Data Catalog*, 1, 2025
- Sasaki, M., Haberl, F., & Pietsch, W. 2000, *A&AS*, 143, 391
- Sazonov, S., Churazov, E., Revnivtsev, M., Vikhlinin, A., & Sunyaev, R. 2005, *A&A*, 444, L37
- Schmidtke, P. C., & Cowley, A. P. 2009, *The Astronomer's Telegram*, 2012, 1
- Schmidtke, P. C., & Cowley, A. P. 2010, *The Astronomer's Telegram*, 2601, 1
- Schmidtke, P. C., Cowley, A. P., McGrath, T. K., & Anderson, A. L. 1995, *PASP*, 107, 450
- Schmidtke, P. C., Cowley, A. P., Frattare, L. M., et al. 1994, *PASP*, 106, 843
- Sepinsky J. F., Willems B., Kalogera V., Rasio F. A., 2009, *ApJ*, 702, 1387
- Shtykovskiy P., Gilfanov M., 2005, *MNRAS*, 362, 879
- Shtykovskiy, P., & Gilfanov, M. 2005, *A&A*, 431, 597
- Sirianni, M., Nota, A., De Marchi, G., Leitherer, C., & Clampin, M. 2002, *ApJ*, 579, 275
- Skinner, G. K. 1980, *Nature*, 288, 141
- Skinner, G. K., Bedford, D. K., Elsner, R. F., Leahy, D., Weisskopf, M. C., & Grindlay, J. 1982, *Nature*, 297, 568
- Skrutskie, M. F., et al. 2006, *AJ*, 131, 1163
- Stevens, J. B., Coe, M. J., & Buckley, D. A. H. 1999, *MNRAS*, 309, 421
- Sturm, R., Haberl, F., Pietsch, W., et al. 2012a, *A&A*, 537, A76
- Sturm, R., Haberl, F., Pietsch, W., Immler, S., & Udalski, A. 2012c, *The Astronomer's Telegram*, 3993, 1
- Sturm, R., Haberl, F., Rau, A., et al. 2012b, *A&A*, 542, A109
- Sturm, R., Haberl, F., Pietsch, W., et al. 2013, *A&A*, 558, A3
- Taylor M. B. 2005, *ASPC*, 347, 29
- Tendulkar S. P., et al., 2014, *ApJ*, 795, 154
- Torrejón, J. M., Schulz, N. S., Nowak, M. A., & Kallman, T. R. 2010, *ApJ*, 715, 947
- Townsend, L. J., Coe, M. J., Corbet, R. H. D., & Hill, A. B. 2011, *MNRAS*, 416, 1556
- Townsley L. K., Broos P. S., Feigelson E. D., Garmire G. P., Getman K. V., 2006, *AJ*, 131, 2164
- Trundle, C., Dufton, P. L., Hunter, I., et al. 2007, *A&A*, 471, 625
- Tzanavaris P., et al., 2013, *ApJ*, 774, 136
- Udalski, A., et al. 2008, *Acta Astron.*, 58, 89
- Udalski, A., Szymanski, M., Kubiak, M., Pietrzynski, G., Soszynski, I., Wozniak, P., & Zebur, K. 2000, *Acta Astron.*, 50, 307
- Ulaczyk, K., Szymański, M. K., Udalski, A., et al. 2012, *Acta Astron.*, 62, 247
- Vallenari, A., Aparicio, A., Fagotto, F., et al. 1994, *A&A*, 284, 447
- van den Heuvel, E. P. J., Portegies Zwart, S. F., Bhattacharya, D., & Kaper, L. 2000, *A&A*, 364, 563
- van der Klis, M., Tuohy, I., Elso, J., van Paradijs, J., Charles, P. A., & Thorstensen, J. R. 1983, *MNRAS*, 203, 279
- Vasilopoulos, G., Haberl, F., Sturm, R., Maggi, P., & Udalski, A. 2014, *A&A*, 567, A129
- Vasilopoulos, G., Maggi, P., Haberl, F., et al. 2013a, *A&A*, 558, A74
- Vasilopoulos, G., Maggi, P., Sturm, R., et al. 2013b, *The Astronomer's Telegram*, 4748, 1
- Vasilopoulos, G., Sturm, R., Haberl, F., Maggi, P., & Udalski, A. 2013c, *The Astronomer's Telegram*, 5540, 1
- Vasilopoulos, G., Sturm, R., Maggi, P., & Haberl, F. 2013d, *The Astronomer's Telegram*, 5673, 1
- Véron-Cetty, M.-P., & Véron, P. 2010, *A&A*, 518, A10
- Webster, B. L., Martin, W. L., Feast, M. W., & Andrews, P. J. 1972, *Nature Physical Science*, 240, 183
- Werchan, F., & Zaritsky, D. 2011, *AJ*, 142, 48
- White, N. E., & Marshall, F. E. 1984, *ApJ*, 281, 354
- Williams, B. F., Binder, B. A., Dalcanton, J. J., Eracleous, M., & Dolphin, A. 2013, *ApJ*, 772, 12
- Williams, Stephen J. 2011, PhD thesis, Georgia State University
- Will, J.-M., Bomans, D. J., Vallenari, A., Schmidt, J. H. K., & de Boer, K. S. 1996, *A&A*, 315, 125
- Wisniewski, J. P., Bjorkman, K. S., Magalhães, A. M., et al. 2007, *ApJ*, 671, 2040
- Zaritsky, D., Harris, J., Thompson, I. B., & Grebel, E. K. 2004, *AJ*, 128, 1606
- Zezas A., Fabbiano G., 2002, *ApJ*, 577, 726

Table 1. Compilation of LMC HMXBs^a

ID [1]	X-ray Source Name [2]	R.A. (J2000.0) [3]	Dec. [4]	Pos. Unc. ($''$) [5]	Lut's ID [6]	P _{pulse} /P _{orb} [7]	Spectral [8]	Type	XRB ^b [9]
1	Swift J045106.8-694803, LXP187	04 51 06.8 04 51 07.0	-69 48 03.2 -69 48 03.1	3.5 (10) 3.6 (70)	...	187.07±0.04 (70) / 21.631±0.005 (70)	B0-1 III-Ve (70)	HMXB/Bc-XRB? (10), Bc-XRB (70)	
2	Swift J045558.9-702001	04 55 58.9	-70 20 01	2.2 (72) / ...	B1-2e (72)	Bc-XRB (72)	
3*	RX J0456.9-6824	04 56 54.1	-68 24 35.0	11.1 (38)	93	... /	HMXB? (37,38)	
4*	RX J0457.2-6612	04 57 12.4	-66 12 10.0	14.5 (38)	94	... /	HMXB? (37,38)	
5	IGR J05007-7047, CXOU J050046.0-704436 (20)	05 00 46.08	-70 44 36.0	0.6 (20)	...	38.55±0.01 < (44) / 30.77±0.01 (11)	B2 III (39), Be? (24)	HMXB (39), Bc-XRB? (24)	
6	RX J0501.6-7034, CAL 9, 2E 0501.8-7038, 1E 0501.8-7036	05 01 23.9	-70 33 33.0	2.9 (2)	95	... / ...	B0 Ve (1), O8e (42), B0e (43)	Bc-XRB (62)	
7	RX J0502.9-6626, CAL E, LXP4.10	05 02 51.6	-66 26 25.0	1.2 (2)	96	4.0635 (35) / ...	O9.5-B0 IIIe / B0 Ve (1), O9 V (42), B0 III(e) (43)	Bc-XRB (62)	
8*	RX J0507.6-6847, RX J050736-6847.8	05 07 37.9	-68 47 49.0	7.1 (38)	97	... /	HMXB/Bc-XRB? (36)	
9	LXP169, XMMU J050755.4-682505	05 07 55.38	-68 25 04.6	0.17 (73)	...	168.777±0.006 (73) / 24.329±0.008 (73)	...	eclipsing Bc-XRB (73)	
10*	RX J0512.6-6717	05 12 41.8	-67 17 23.0	4.0 (49)	98	... /	HMXB? (38)	
11	Swift J0513.4-6547 (12), LXP27.3	05 13 28.05	-65 47 20.0	1.9 (12)	...	27.28 (9) / 27.405 (9)	...	HMXB (12), Bc-XRB (9)	
12	RX J0516.0-6916	05 16 00.1	-69 16 09.0	7.3 (2)	99	... / ...	~B1 V (25)	HMXB? (25)	
13	XMMU J052016.0-692505	05 20 16.0	-69 25 05.8	3 (8) / ...	B0-3 IIIe (8)	likely WD/Bc-XRB (8)	
14	RX J0520.5-6932, LXP8.04	05 20 29.8	-69 31 55	2.9 (74)	100	8.03533±0.00003 (75) / 24.4 (4) 8.032375±0.000005 (14) / 24.4302±0.0026 (59) 8.032932±0.000005 (14) / ...	O8e (62), O9 Ve (4)	Bc-XRB (4)	
15*	RX J0523.2-7004	05 23 14.9	-70 04 12.0	9.9 (38)	101	... /	HMXB (38)	
16*	RX J0524.2-6620	05 24 12.7	-66 20 50.0	7.0 (38)	102	... /	HMXB (38)	
17*, •	RX J0527.1-7005	05 27 07.9	-70 05 00.0	11.9 (38)	103	... /	HMXB (38)	
18*	RX J0527.3-6552	05 27 23.7	-65 52 35.0	15.9 (38)	104	... /	HMXB? (37,38)	
19*	RX J0529.4-6952	05 29 25.9	-69 52 11.0	9.8 (38)	105	... /	HMXB (37,38)	
20	XMMU J052947.4-655639 (6), LXP69.2, RX J0529.8-6556 (5), RX J0529.7-6556	05 29 47.4	-65 56 39	3-4 (6)	106	69.232±0.002 (6) / ...	B0.5 Ve (1), B2e (5)	Bc-XRB (5)	

Table 1 – continued

ID	Name	X-ray Source	R.A. (J2000.0)	Dec. ($^{\circ}$)	Pos.Unc. ($''$)	Liu's ID	$P_{\text{pulse}}/P_{\text{orb}}$	Spectral Type	XRB †
[1]	[2]		[3]	[4]	[5]	[6]	[7]	[8]	[9]
21	XMMU J053011.2-65122, LXP272, RX J0530.1-6551		05 30 10.6	-65 51 27.0	2.8 (38)	107	271.97±0.05 (6) /	Be-XRB? (6)
22	Swift J053041.9-665426, LXP28.8		05 30 42.17	-66 54 31.0	0.5 (26)	...	28.77521 ± 0.00010 (26) / ...	B0-1.5Ve (26)	Be-XRB (26)
23*	RX J0530.7-6606		05 30 47.4	-66 06 15.0	11.4 (38)	108	... /	HMXB (38)
24	RX J0531.2-6607, EXO 0531.1-6609, LXP13.7, XMMU J053113.3-660705, EXO 053109-6609.2 (46), XMMU J053113.1-660707, IRXS J05311.0-660657 (19), IGR J05305-6559 (69)		05 31 13.8	-66 07 03.0	2.2 (38)	109	13.7 (7) / 25.4 (7)	B0.7 Ve (1)	Be-XRB (47)
25	XMMU J053115.4-705350		05 31 15.4	-70 53 50.0	~4 (48)	110	... / ...	B0 Ie (71)	HMXB (48, 71)
26*	XMMU J053118.2-660730		05 31 18.2	-66 07 30	~4 (48) /	HMXB? (48)
27	RX J0531.5-6518, IRXS J053137.1-651759 (19)		05 31 36.1	-65 18 16.0	18.8 (49)	111	... / ...	B2 V(e?) (1)	HMXB (49), Be-XRB? (1)
28*	RX J0532.3-7107, CAL 50 (19), IRXS J053219.5-710806 (19)		05 32 22.7	-71 07 32.0	24.3 (38)	112	... /	HMXB? (37,38)
29*,•	RX J0532.4-6535, IRXS J053226.0-653505 (19)		05 32 25.3	-65 35 09.0	17.4 (49)	113	... /	HMXB? (49)
30	RX J0532.5-6551, XMMU J053232.4-655139, IRXS J053224.1-655112 (19)		05 32 32.0	-65 51 41	8 (51)	114	... / ...	B0.5 II (50), B0 II (1)	SG-XRB (51)
31	2A 0532-664, LMC X-4, LXP13.5, RX J0532.8-6622 (19), CAL 49, IRXS J053246.1-662203 (38), 4U 0532-66 (57), RASS 232 (49)		05 32 49.79	-66 22 13.8	1.02 (68)	115	13.5 (30) / 1.408±0.002 (31)	O8 III (1), O7 III-V (32)	HMXB (58)
32	Swift J053321.3-684121 (66)		05 33 21.3	-68 41 21	5.5 (66) / ...	B3 I (65)	HMXB? (66)
33	RX J0535.0-6700		05 35 05.9	-67 00 15.0	4 (49)	116	... / 241.0 (34)	B0 Ve (1)	Be-XRB (1)
34	1A 0535-668, RX J0535.6-6651, LXP0.07, CAL G (19), IRXS J053539.0-665158 (19)		05 35 41.2	-66 51 52.0	2 (63)	117≡118	0.069 (28) / 16.668±0.002 (29)	B2 IIIe (27), B0.5-1 II-III (2)	Be-XRB (52)
35*,•	RX J0535.8-6530, IRXS J053555.0-653039 (19)		05 35 53.8	-65 30 34.0	13 (49)	119	... /	HMXB? (49)

Table 1 – continued

ID	Name	X-ray Source	R.A. (J2000.0)	Dec. (J2000.0)	Pos. Unc. (\prime)	Liu's ID	Pulse/ P_{orb}	Spectral Type	XRB [†]
36	IH 0538-641, LMC X-3, XMMU J053856.7-640503 (19), IRXS J053855.6-640457 (19), IRXS J053855.5-640457 (19), RX J0538.9-6405, CAL 70 (19), 3A 0539-641, 4U 0538-64 (19),		05 38 56.63	-64 05 03.29	0.05, 0.08 \pm (67)	120	... / 1.705 (18)	~B2.5 V pec. (1), B3 V (18)	BH-HMXB (18)
37	3A 0540-697, LMC X-1, IRXS J053938.8-694515 (19)		05 39 38.85	-69 44 35.71	0.02, 0.02 \pm (67)	121	... / 4.2288 \pm 0.0006 (33)	O8 III-V (1), O8 (fp) (16)	BH-HMXB (53,54)
38	IGR J05414-6858 (13), LXP4-42		05 41 26.62	-69 01 23.0	0.52 (61)	...	4.4208 (61) / 19.9 (61)	B0-I IIIe (61)	Be-XRB (61)
39	RX J0541.4-6936		05 41 22.2	-69 36 29.0	6.6 (2)	122	... / ...	B2 SG (2) B4 III-1 (16)	SG-XRB? (2)
40	XMMU J054134.7-682550, LXP60.8		05 41 34.7	-68 25 50.0	4 (48)	123	60.77 \pm (2.59 $\times 10^{-5}$) (60) /	HMXB? (48), Be-XRB? (60)
41	RX J0541.5-6833, RX J0541.6-6832 (40)		05 41 37.1	-68 32 32.0	4.5 (64)	124	... / ...	B0 III (17)	HMXB? (2)
42* \bullet	RX J0543.9-6539 (38)		05 43 58.0	-65 39 52.0	8.6 (38)	125	... /	HMXB? (37)
43	ISAX J0544.1-7100, LXP96.1, RX J0544.1-7100 (38), AX J0548-704, AX J0544.1-7100 (40), IWGA J0544.1-7100		05 44 06.3	-71 00 50.0	3.3 (49)	126	96.08 \pm 0.06 (3) / 286.0 (4)	B0 Ve (4)	Be-XRB (4)
44	H 0544-665 \ddagger (41)		05 44 15.5 \blacklozenge	-66 33 50.0 \blacklozenge	30 (56)	127	... / ...	B0 Ve (55,1)	Be-XRB (55,56)
45*	RX J0546.8-6851, RX J0547.0-6852 (38), 2E 0547.2-6852, IRXS J054655.3-685142		05 46 48.3	-68 51 47.0	48.7 (38)	128	... /	HMXB? (38)
Additional sources reported in the literature after the completion of this work, thus not taken into account in the present analysis (see Section 1)									
A	XMMU J053833.9-691157 (48), CXOU J053833.4-691158 (45)		05 38 33.46	-69 11 58.7	0.4 \square (45) / ...	O9 IIIe (23)	HMXB (23)
B	Swift J0549.7-6812 (15), LXP6.2 (21)		05 50 06.47	-68 14 55.7	1.4 (21)	...	6.2 (21) /	HMXB (22)

Notes – The Right Ascension is given in h m s, the Declination in $^{\circ}$ \prime $''$, the pulse period P_{pulse} in seconds, and the orbital period P_{orb} in days. References are given in parenthesis and are listed below.

Δ Based on the literature as of Dec. 2014.

\dagger This is the classification presented in the literature. In this work, we re-classify some of these sources and the final classification is given in Table 5.

\star New counterparts for these X-ray sources are identified in this study.

\triangleleft This pulse period is not taken into account in the present work; see comments on last paragraph of Introduction and footnote #4.

\bullet These sources have been re-classified as non-HMXB systems.

\triangleright Positional uncertainty in Right Ascension, followed by that in Declination.

\ddagger We believe this source was erroneously related to IRXS J054450.0-663445 (Ebisawa et al. 2003). The same correlation appears in the Simbad database too. In particular, this ROSAT All Sky Survey Faint Source is approximately located at 4.1' and 3.6' from the X-ray (R.A., Decl.)_{B1950.0}=(05:44:11.5, -66:35:24.0) with 60" positional uncertainty) and optical (R.A., Decl.)_{B1950.0}=(05:44:15.6, -66:34:59.0) with a 3" positional uncertainty of the optical match) positions, respectively, thus we propose that these are 2 different sources. Stevens et al. (1999) give this source as (R.A., Decl.)_{2000.0}=(05:44:15.5, -66:33:50.0) with a 30" positional uncertainty (at a 90% confidence level).

\blacklozenge Transformed from (R.A., Decl.)_{B1950.0}=(05:44:15.6, -66:34:59.0) using NASA/IPAC Extragalactic Database (NED): <https://ned.ipac.caltech.edu/forms/calculator.html>). We note that in

Liu et al. (2005) the B1950.0 coordinates were erroneously listed as 12000.0.

\square Formal 1σ radial positional error.

- References:** (1) Negueruela & Coe (2002); (2) Sasaki et al. (2000); (3) Cusumano et al. (1998); (4) Coe et al. (2001); (5) Haberl et al. (1997); (6) Haberl et al. (2003); (7) Dennerl et al. (1995); (8) Kahabka et al. (2006); (9) Coe et al. (2015); (10) Beardmore et al. (2009); (11) D’Ai et al. (2011); (12) Krimm et al. (2009); (13) Grebenev & Lutovinov (2010); (14) Tendulkar et al. (2014); (15) Krimm et al. 2013a; (16) Fariña et al. (2009); (17) Massey (2002); (18) Cowley et al. (1983); (19) SIMBAD: Identifier query; (20) Sazonov et al. (2005); (21) Krimm et al. (2013c); (22) Krimm, Holland, & Kennea (2013b); (23) Clark et al. (2015); (24) Schmidtke & Cowley (2010); (25) Cowley et al. (1997); (26) Vasilopoulos et al. (2013a); (27) Corbet et al. (1985); (28) Skinner et al. (1982); (29) Skinner (1980); (30) Kelley et al. (1983); (31) Chevalier & Ilovaisky (1977); (32) Hutchings et al. (1978); (33) Hutchings et al. (1987); (34) Reid et al. (1988); (35) Schmidtke et al. (1995); (36) Chu et al. (2000); (37) Kahabka (2002); (38) Haberl & Pietsch (1999a); (39) Masetti et al. (2006b); (40) Ebisawa et al. (2003); (41) Johnston et al. (1979); (42) Cowley et al. (1984); (43) Crampton et al. (1985); (44) Vasilopoulos et al. (2016, to be subm.; private communication); (45) Townsley et al. (2006); (46) Bodaghee et al. (2007); (47) Haberl et al. (1995); (48) Shytkovskiy & Gilfanov (2005); (49) Haberl & Pietsch (1999b); (50) Jaxon et al. (2001); (51) Haberl et al. (1995); (52) Charles et al. (1983); (53) Hutchings et al. (1983); (54) White & Marshall (1984); (55) van der Klis et al. (1983); (56) Stevens et al. (1999); (57) Torrejón et al. (2010); (58) Joss & Rappaport (1984); (59) Vasilopoulos et al. (2014); (60) Inam et al. (2009); (61) Sturm et al. (2012b); (62) Schmidtke et al. (1994); (63) Johnston et al. (1980); (64) Brunet et al. (1975); (65) Rousseau et al. (1978); (66) Sturm et al. (2012c); (67) Cui et al. (2002); (68) Fuhrmeister & Schmitt (2003); (69) Grebenev et al. (2013); (70) Klus et al. (2013); (71) Reid & Parker (2012); (72) Vasilopoulos et al. (2013c); (73) Maggi et al. (2013); (74) Vasilopoulos et al. (2013b); (75) Vasilopoulos et al. (2013d).

Table 2. Optical properties of HMXBs

Src ID	R.A. (h m s)	Decl. ($^{\circ}$ ' ")	U	errU	B	errB	V	errV	I	errI	B-V	err(B-V)	Offset (")	C/part
[1]	[2]	[3]	[4]	[5]	[6]	[7]	[8]	[9]	[10]	[11]	[12]	[13]	[14]	[15]
1	04 51 06.10 04 51 06.30 04 51 06.89	-69 48 01.0 -69 48 04.9 -69 48 02.4	20.676 19.932 13.736	0.262 0.192 0.038	21.408 20.368 14.702	0.143 0.082 0.024	20.767 19.084 14.600	0.116 0.048 0.023	0.641 1.284 0.102	0.184 0.095 0.033	4.23 3.10 0.91	...
2	04 55 58.89	-70 19 59.8	13.179	0.044	14.104	0.108	14.153	0.042	14.072	0.051	-0.049	0.116	1.19	k
3	04 56 53.88 04 56 54.14 04 56 54.72 04 56 54.75	-68 24 33.0 -68 24 38.9 -68 24 37.5 -68 24 32.8	20.376 22.354 21.341 21.659	0.102 0.390 0.141 0.200	20.604 21.147 20.904 20.826	0.119 0.143 0.220 0.119	18.839 21.553 ... 20.600	0.083 0.438 ... 0.189	-0.228 1.207 0.437 0.833	0.157 0.415 0.261 0.233	2.32 3.89 4.28 4.23	...
4	04 57 12.89	-66 12 10.0	22.221	0.203	21.391	0.133	19.541	0.070	0.830	0.243	2.95	...
5	05 00 46.08	-70 44 35.8	16.676	0.091	14.672	0.028	14.727	0.021	14.622	0.030	-0.055	0.035	0.33	k
6	05 01 23.73 05 01 23.85 05 01 24.23	-70 33 29.4 -70 33 33.6 -70 33 34.3	20.351 13.839 ...	0.176 0.038 ...	20.088 14.806 17.913	0.094 0.042 0.053	18.187 14.982 16.528	0.143 0.026 0.040	17.587 15.209 15.062	0.102 0.091 0.042	1.901 -0.176 1.385	0.171 0.049 0.066	3.66 0.60 2.09	...
7	05 02 51.82 05 02 51.96	-66 26 26.8 -66 26 20.8	13.051 19.198	0.012 0.151	14.171 20.637	0.026 0.103	14.364 19.983	0.193 0.088	13.988 19.454	0.035 0.112	-0.193 0.654	0.195 0.135	2.22 4.77	k
8	05 07 37.68 05 07 37.82 05 07 38.18 05 07 38.23 05 07 38.25	-68 47 51.9 -68 47 48.6 -68 47 47.8 -68 47 45.3 -68 47 52.3	17.636 18.545 15.869 16.065 17.598	0.070 0.093 0.050 0.052 0.080	17.008 17.176 16.180 16.323 18.084	0.098 0.179 0.110 0.114 0.050	17.577 17.139 16.260 16.427 18.046	0.052 0.125 0.060 0.067 0.044	17.706 16.584 16.448 16.601 18.248	0.062 0.054 0.099 0.046 0.053	-0.569 0.037 -0.080 -0.104 0.038	0.111 0.218 0.125 0.132 0.067	3.10 0.62 1.93 4.12 3.85	...
9	05 07 55.49 05 07 55.80	-68 25 04.8 -68 25 08.0	14.018 20.317	0.080 0.175	15.016 18.513	0.022 0.061	14.945 17.046	0.026 0.035	14.894 15.672	0.038 0.186	0.071 1.467	0.034 0.070	0.64 4.08	k
10	05 12 41.26 05 12 41.33 05 12 41.49 05 12 42.31	-67 17 26.8 -67 17 23.4 -67 17 18.4 -67 17 23.1	20.222 15.369 18.959 16.618	0.181 0.024 0.100 0.042	18.707 16.090 19.425 17.205	0.038 0.089 0.064 0.03	17.327 16.187 19.409 17.254	0.028 0.024 0.052 0.027	15.764 16.394 19.213 17.407	0.025 0.054 0.055 0.045	1.380 -0.097 0.016 -0.049	0.047 0.092 0.082 0.040	4.89 2.74 4.93 2.94	...
11	05 13 27.60 05 13 28.01	-65 47 16.2 -65 47 24.1	... 20.405	... 0.169	21.210 20.389	0.116 0.070	20.537 20.039	0.111 0.074	... 20.112	... 0.119	0.673 0.350	0.161 0.102	4.72 4.08	...

Table 2 – continued

Src ID	R.A. (h m s)	Decl. (° ' ")	U	errU	B	errB	V	errV (mag)	I	errI	B-V	err(B-V)	Offset (")	C/part
[1]	[2]	[3]	[4]	[5]	[6]	[7]	[8]	[9]	[10]	[11]	[12]	[13]	[14]	[15]
	05 13 28.26	-65 47 18.4	14.122	0.036	15.067	0.088	15.098	0.027	15.328	0.039	-0.031	0.092	2.06	k
12	05 15 59.58	-69 16 05.7	20.489	0.316	20.013	0.189	19.186	0.269	18.485	0.284	0.827	0.329	4.32	...
	05 15 59.67	-69 16 11.0	19.056	0.069	17.603	0.100	16.533	0.089	1.453	0.121	3.01	...
	05 15 59.92	-69 16 07.6	14.228	0.031	15.011	0.029	15.126	0.041	14.99	0.049	-0.115	0.050	1.66	k,A
	05 16 00.39	-69 16 06.0	18.645	0.088	18.954	0.071	18.928	0.152	17.93	0.092	0.026	0.168	3.42	...
	05 16 00.79	-69 16 09.6	18.254	0.062	16.783	0.067	15.449	0.051	1.471	0.091	3.70	...
13	05 20 15.33	-69 25 02.5	19.563	0.147	18.531	0.071	17.202	0.074	16.377	0.043	1.329	0.103	4.33	...
	05 20 16.15	-69 25 05.3	13.905	0.031	14.785	0.031	14.944	0.065	14.665	0.073	-0.159	0.072	0.86	k
	05 20 16.83	-69 25 07.0	20.297	0.129	18.587	0.136	19.366	0.148	1.710	0.187	4.80	...
14♠	05 20 29.70	-69 31 55.24	14.312	0.087	16.004	0.471	-1.692	0.479	0.60	k,A
	05 20 29.91	-69 31 51.35	18.306	0.095	18.442	0.114	17.612	0.153	18.429	0.137	0.830	0.191	3.70	...
15	05 23 14.02	-70 04 13.9	19.003	0.170	18.795	0.120	19.437	0.119	0.208	0.208	4.85	...
	05 23 14.29	-70 04 13.2	19.023	0.125	18.599	0.077	0.424	0.147	3.32	...
	05 23 14.62	-70 04 07.4	20.876	0.260	20.111	0.191	20.250	0.224	0.765	0.323	4.82	...
	05 23 14.71	-70 04 15.0	18.631	0.085	18.729	0.074	18.095	0.158	18.345	0.089	0.634	0.174	3.14	...
	05 23 15.05	-70 04 11.7	19.594	0.137	19.745	0.153	18.555	0.120	18.088	0.084	1.190	0.194	0.85	...
	05 23 15.58	-70 04 11.1	16.573	0.052	15.991	0.080	15.129	0.063	14.094	0.073	0.862	0.102	3.62	n,A
16	05 24 12.46	-66 20 50.4	19.032	0.082	19.093	0.035	19.190	0.073	19.120	0.056	-0.097	0.081	1.49	...
17	05 27 06.99	-70 04 58.4	17.373	0.047	16.516	0.043	15.308	0.050	13.713	0.051	1.208	0.066	4.91	n,A
	05 27 08.00	-70 05 03.6	21.121	0.427	21.455	0.263	20.790	0.285	0.665	0.388	3.59	...
	05 27 08.17	-70 05 00.3	20.754	0.272	19.899	0.095	19.83	0.31	0.069	0.324	1.40	n,A
	05 27 08.25	-70 04 58.1	20.998	0.360	20.380	0.132	19.994	0.191	0.386	0.232	2.59	...
18	05 27 23.14	-65 52 38.0	20.643	0.152	20.603	0.066	20.407	0.051	20.198	0.126	0.196	0.083	4.53	...
	05 27 23.26	-65 52 35.8	22.513	0.304	21.787	0.150	0.726	0.339	2.92	...
	05 27 23.54	-65 52 32.0	21.723	0.335	21.671	0.128	21.192	0.126	20.662	0.166	0.479	0.180	3.15	...
	05 27 24.18	-65 52 31.0	21.467	0.339	22.292	0.211	21.146	0.126	1.146	0.246	4.98	...
	05 27 24.21	-65 52 36.6	22.361	0.192	22.029	0.216	0.332	0.289	3.54	...
19	05 29 25.47	-69 52 06.7	21.021	0.266	20.185	0.115	19.542	0.082	18.668	0.093	0.643	0.141	4.84	...
	05 29 26.10	-69 52 13.3	21.217	0.512	20.531	0.177	19.804	0.137	18.779	0.172	0.727	0.224	2.47	...

Table 2 – *continued*

Src ID	R.A. (h m s)	Decl. (° ' ")	U	errU	B	errB	V	errV	I	errI	B-V	err(B-V)	Offset (")	C/part
[1]	[2]	[3]	[4]	[5]	[6]	[7]	[8]	[9]	[10]	[11]	[12]	[13]	[14]	[15]
05 29 26.22	-69 52 10.3	19.757	0.126	20.085	0.145	-0.328	0.192	1.78	...
05 29 26.48	-69 52 08.0	20.385	0.166	20.142	0.170	0.243	0.238	4.22	...
05 29 48.10	-65 56 55.2	20.949	0.213	21.333	0.091	20.951	0.097	20.734	0.170	0.382	0.133	4.60
05 29 48.45	-65 56 50.5	20.985	0.082	20.772	0.106	20.615	0.178	0.213	0.134	0.58
05 29 48.66	-65 56 46.5	22.094	0.172	20.711	0.125	1.383	0.213	4.73
21
22	05 30 41.39	-66 54 26.7	21.529	0.470	21.665	0.179	22.032	0.240	20.662	0.235	-0.367	0.299	3.80	...
05 30 42.13	-66 54 30.1	14.312	0.022	15.007	0.033	15.321	0.018	15.586	0.023	-0.314	0.038	1.71	k	...
23	05 30 47.25	-66 06 15.0	21.734	0.283	20.852	0.084	20.684	0.108	0.168	0.137	0.93	...
05 30 47.84	-66 06 17.6	21.174	0.248	21.485	0.121	21.576	0.200	-0.091	0.234	3.74
05 30 47.92	-66 06 16.3	22.493	0.217	22.127	0.345	0.366	0.408	3.42
24	05 31 13.61	-66 07 04.5	20.479	0.155	20.070	0.103	20.288	0.110	-0.218	0.151	1.89	...
25	05 31 15.53	-70 53 48.5	13.158	0.038	14.009	0.035	14.051	0.025	13.799	0.028	-0.042	0.043	1.64	k,A
26	05 31 18.10	-66 07 31.6	20.965	0.210	20.390	0.065	20.097	0.145	19.769	0.294	0.293	0.159	1.69	...
05 31 18.12	-66 07 28.9	18.078	0.046	18.160	0.075	18.157	0.035	18.117	0.073	0.003	0.083	1.18
05 31 18.66	-66 07 31.6	16.471	0.034	16.804	0.021	16.873	0.023	-0.069	0.031	3.21	n,A	...
27	05 31 36.20	-65 18 17.5	21.921	0.163	21.731	0.239	0.190	0.289	1.61	...
05 31 36.81	-65 18 16.1	15.401	0.031	15.875	0.029	16.007	0.021	16.226	0.153	-0.132	0.036	4.48	k	...
28	05 32 21.72	-71 07 31.4	20.456	0.202	20.580	0.091	20.179	0.061	19.879	0.105	0.401	0.110	4.77	...
05 32 22.92	-71 07 30.7	21.411	0.150	21.024	0.116	0.387	0.190	1.71
05 32 23.39	-71 07 33.6	20.855	0.111	21.053	0.133	-0.198	0.173	3.73
05 32 23.45	-71 07 31.5	20.348	0.275	20.769	0.129	19.437	0.067	18.471	0.052	1.332	0.145	3.69
29	05 32 24.93	-65 35 05.5	22.509	0.217	22.432	0.298	20.852	0.28	0.077	0.369	4.20	...
05 32 25.44	-65 35 07.9	19.613	0.112	20.525	0.054	19.983	0.059	19.008	0.066	0.542	0.080	1.38
30	05 32 32.62	-65 51 40.2	12.212	0.038	12.474	0.138	13.048	0.076	13.162	0.146	-0.574	0.158	3.85	k,A
31	05 32 49.54	-66 22 12.9	15.449	0.070	13.940	0.029	14.167	0.029	-0.227	0.041	1.72	k,A
32	05 33 20.80	-68 41 23.2	11.673	...	12.684	...	12.776	...	12.239	0.142	-0.092	...	3.50	k
05 33 21.65	-68 41 19.3	20.801	0.422	19.571	0.304	1.230	0.520	2.55
33	05 35 05.99	-67 00 15.4	13.941	0.026	14.728	0.029	14.873	0.023	14.910	0.032	-0.145	0.037	0.65	k

Table 2 – continued

Src ID	R.A. (h m s)	Decl. (° ′ ″)	U	errU	B	errB	V	errV	I	errI	B-V	err(B-V)	Offset (″)	C/part
[1]	[2]	[3]	[4]	[5]	[6]	[7]	[8]	[9]	[10]	[11]	[12]	[13]	[14]	[15]
	05 35 06.07	-67 00 13.6	18.726	0.126	18.842	0.167	18.905	0.159	-0.116	0.209	1.74	...
34	05 35 41.01	-66 51 53.1	13.828	0.025	14.584	0.029	14.824	0.022	15.281	0.358	-0.240	0.036	1.58	k
	05 35 41.20	-66 51 51.9	17.939	0.230	18.412	0.161	18.311	0.087	17.745	0.134	0.101	0.183	0.06	...
	05 35 41.66	-66 51 48.6	17.606	0.041	18.363	0.137	17.926	0.045	-0.757	0.143	4.38	...
35	05 35 53.40	-65 30 31.9	19.892	0.166	19.948	0.128	19.031	0.037	18.207	0.055	0.917	0.133	3.21	...
	05 35 53.48	-65 30 34.8	22.330	0.226	21.327	0.155	1.003	0.274	2.16	...
	05 35 53.62	-65 30 38.3	20.031	0.167	19.775	0.064	18.847	0.055	17.868	0.067	0.928	0.084	4.44	...
	05 35 54.12	-65 30 29.8	21.152	0.113	20.406	0.084	19.668	0.093	0.746	0.141	4.64	...
36★
37	05 39 38.73	-69 44 40.1	16.945	0.256	18.094	0.257	17.234	0.204	0.860	0.328	4.46	...
	05 39 38.84	-69 44 35.6	13.819	0.087	14.535	0.050	14.612	0.171	13.886	0.093	-0.077	0.178	0.10	k
	05 39 39.39	-69 44 38.0	17.928	0.136	16.596	0.151	1.332	0.203	3.67	...
38	05 41 26.64	-69 01 21.3	19.183	0.238	19.042	0.103	17.997	0.057	16.731	0.477	1.045	0.118	1.75	...
	05 41 26.67	-69 01 23.3	14.463	0.024	15.296	0.022	15.329	0.024	15.527	0.025	-0.033	0.033	0.43	k
	05 41 27.29	-69 01 23.0	21.772	0.479	19.755	0.110	20.087	0.110	19.516	0.133	-0.332	0.156	3.60	...
39	05 41 21.84	-69 36 30.1	20.999	0.315	20.644	0.197	20.183	0.128	0.355	0.372	2.18	...
	05 41 21.89	-69 36 28.4	19.565	0.132	19.271	0.130	19.067	0.095	18.999	0.082	0.204	0.161	1.75	...
	05 41 22.19	-69 36 25.3	19.991	0.181	19.964	0.096	19.085	0.099	18.342	0.08	0.879	0.138	3.66	...
	05 41 22.33	-69 36 31.0	19.898	0.114	19.509	0.058	18.945	0.051	18.151	0.076	0.564	0.077	2.14	...
	05 41 22.60	-69 36 25.3	19.413	0.154	19.406	0.055	18.414	0.064	17.437	0.059	0.992	0.084	4.23	...
	05 41 22.98	-69 36 30.0	18.711	0.081	18.714	0.074	18.650	0.054	18.539	0.136	0.064	0.092	4.21	A
40	05 41 34.34	-68 25 48.3	13.138	0.031	14.072	0.030	14.043	0.019	13.911	0.040	0.029	0.036	2.59	k
	05 41 35.30	-68 25 49.4	20.152	0.213	20.903	0.160	-0.751	0.266	3.38	...
	05 41 35.30	-68 25 51.8	19.499	0.166	20.177	0.127	19.112	0.074	18.097	0.053	1.065	0.147	3.78	...
41	05 41 36.74	-68 32 36.4	21.817	0.138	20.915	0.125	20.900	0.245	0.902	0.186	4.81	...
	05 41 37.54	-68 32 33.3	13.121	0.030	14.136	0.026	14.240	0.044	14.356	0.022	-0.104	0.051	2.73	k,A
42	05 43 57.76	-65 39 52.2	21.801	0.113	21.438	0.109	20.644	0.165	0.363	0.157	1.52	...
	05 43 58.43	-65 39 53.6	20.138	0.165	20.436	0.052	20.063	0.049	19.018	0.065	0.373	0.071	3.12	n,A
	05 43 58.43	-65 39 55.8	23.239	0.493	23.409	0.524	-0.170	0.719	4.68	...

Table 2 – *continued*

Src ID	R.A. (h m s)	Decl. (° ' ")	U	errU	B	errB	V	errV (mag)	I	errI	B-V	err(B-V)	Offset (")	C/part
[1]	[2]	[3]	[4]	[5]	[6]	[7]	[8]	[9]	[10]	[11]	[12]	[13]	[14]	[15]
43	05 44 06.34	-71 00 45.5	19.802	0.134	18.426	0.028	17.356	0.131	1.376	0.137	4.54	...
	05 44 06.66	-71 00 49.1	20.317	0.220	20.552	0.120	20.009	0.076	19.946	0.142	0.543	0.142	1.95	...
	05 44 06.80	-71 00 51.2	20.560	0.140	19.469	0.061	18.336	0.055	1.091	0.153	2.70	...
44	05 44 15.77	-66 33 47.1	14.127	0.036	15.075	0.018	15.201	0.021	15.202	0.078	-0.126	0.028	3.33	k
45	05 46 48.87	-68 51 50.2	20.362	0.225	20.537	0.091	19.803	0.061	19.042	0.098	0.734	0.110	4.46	...

Notes – Three dots indicate that an entry was not available in the MCPS catalog. The most likely counterpart of each X-ray source is indicated in bold. For sources without a match shown in bold in this table, its most likely counterpart is presented either in the 1σ < search radius < 2σ area or even at larger than $10''$ distances (Tables 3 and 4, respectively). An input "n" in Column 15 indicates a newly identified counterpart from this work, a "k" a known in the literature counterpart, and an "A" those counterparts that are discussed in Appendix A.

Additional identifications and notes for the sources follow below, which however by no means consist a complete list.

- Src 1:** [Massey2002]9775 (blue star) at 0.85" from X-ray source; 2MASS J04510685-6948032 at 0.32" from X-ray source; [MACHO]44.1741.17
- Src 5:** [MACHO]23.3300.10 (24); [Massey2002]48644 (blue star) at 0.14" from X-ray source; 2MASS J05004604-7044360=USNO-B1.0192-00057570 (19)
- Src 6:** [MACHO]23.3424.11 blue variable star (Keller et al. 2002) and [Massey2002]51265 source at 1.17" and 1.04" from X-ray position, respectively
- Src 7:** [MACHO]53.3727.19 blue variable star (Keller et al. 2002) at 3.18" from X-ray position
- Src 8:** 1.1" from the MCPS star cluster LMC0540 (R.A., Decl.)_{J2000.0}=(05:07:38, -68:47:50), log(age)~8, and V=13.45 mag; Glatt et al. 2010); 5.9" from the cluster OGLE-CL LMC 129 (R.A., Decl.)_{J2000.0}=(05:07:38.63, -68:47:45.9), apparent radius ~20", and log(age)~7.9; Pietrzyński & Udalski 2000a); [Massey2002]73045 and 2MASS J05073783-6847492 at 4.29" and 0.44" from the X-ray source, respectively
- Src 11:** 2MASS J05132826-6547187 source at 1.82" from X-ray source (12); [MACHO]59.5431.442 with < R > ~ 15.6 and V - R ~ 0.05 (Schmidtke & Cowley 2009)
- Src 12:** [Massey2002]101869 at 4.83" from X-ray source
- Src 13:** [Massey2002]118611 (blue star) at 1.33" from X-ray source; [OGLE-II]05201625-6925053 with (R.A., Decl.)_{J2000.0}=(05:20:16.25,-69:25:05.3) is a Type-4 object (i.e. light curve similar to Galactic Be stars; Sabogal et al. 2005) at 1.35" from X-ray source
- Src 15:** [MACHO]6.6940.6123 at 1.25" from X-ray position
- Src 16:** 2MASS J05241180-6620512 at 5.05" from X-ray position
- Src 18:** 2MASS J05272496-6552385 at 8.53" from X-ray position
- Src 20:** 2MASS J05294785-6556437 (at 8") ≡ UCAC2 2849264 (19)
- Src 21:** 2MASS J05301136-6551240 at 5.54" from the X-ray source (19)
- Src 24:** 2MASS J05311318-6607092 at 7.27" from the X-ray source (19)
- Src 25:** 2MASS J05311556-7053485 at 1.66" from the X-ray source (19) and LMC V3134 variable source with (R.A., Decl.)_{J2000.0}=(05:31:15.66,-70:53:49.9) at 1.29"
- Src 27:** 2MASS J05313676-6518162 at 4.18" from the X-ray source
- Src 28:** 2MASS J05322417-7107336 at 7.35" from the X-ray source and [MACHO]14.8376.548 (38) match
- Src 29:** 2MASS J05322587-6535012 at 8.54" from the X-ray source
- Src 30:** USNO-A2.0 0225-02109716 (19)

- Src 31:** Source 316 in [Habert & Pletsch \(1999b\)](#) is 2MASS J05324953-6622132 with $J = 14.586 \pm 0.037$ mag, $H = 14.780 \pm 0.075$ mag, and $K = 14.750 \pm 0.115$ mag; Variable star LMC V3213 (from the Extragalactic Variable Stars Catalogue Vol. V of [Samus et al. 2009](#)) at $2.18''$ from X-ray position, classified as an X-ray pulsar
- Src 33:** 2MASS J05350598-6700157 at $0.56''$ from the X-ray source; Mira (Omicron) Ceti-type variable star LMC V3394 at $0.8''$ from the X-ray source (from the Extragalactic Variable Stars Catalogue Vol. V of [Samus et al. 2009](#)). These are long-period variable giants with characteristic late-type emission spectra (Me, Ce, Se) and light amplitudes from 2.5 to 11 mag in V. Their periodicity is well pronounced, and the periods lie in the range between 80 and 1000 days. Infrared amplitudes are usually less than in the visible and may be <2.5 mag. For example, in the K band they usually do not exceed 0.9 mag. [Habert & Pletsch \(1999b\)](#) classified this system as a Be-XRB (instead of a Mira variable).
- Src 34:** 2MASS J05354101-6651535 at $1.88''$ from X-ray position
- Src 35:** 2MASS J05355458-6530382 at $6.45''$ from X-ray position, and [2MASX]05355466-6530384 (from the 2MASS Extended Source Catalog of) at $6.97''$
- Src 36:** Variable star LMC V3758 (from the Extragalactic Variable Stars Catalogue Vol. V of [Samus et al. 2009](#)) at $1.83''$ from X-ray position, classified as a rotating ellipsoidal variable and a close binary system that is a source of strong, variable X-ray emission.
- Src 37:** extended objects SNR0540-69.7 (Supernova remnant) and LMC-N159F (Nebula w/probable embedded cluster) at $4.0''$ and $4.8''$, respectively ([Bica et al. 2008](#)); 2MASS objects J05393883-6944356, J05394007-6944337, and J05393990-6944413 at $3.69''$, $4.42''$, and $4.86''$, respectively from X-ray position
- Src 38:** [Massey2002]176277 and 2MASS J05412663-6901224 at $1.58''$ and $2.54''$ from the X-ray position (with $3.0''$ positional accuracy), respectively
- Src 39:** 2MASS J05412014-6936229 ($9.12''$ from X-ray source)≡SSTISAGEMC J054120.18-693622.9 (19)
- Src 40:** [Massey2002]176466 (blue star) and 2MASS J05413431-6825484 at $2.30''$ and $2.64''$ from the X-ray source, respectively
- Src 41:** [Massey2002]176538 (blue star) and 2MASS J05413431-6825484 at $2.84''$ and $2.64''$ from the X-ray source, respectively
- Src 43:** 2MASS J05440640-7100454 at $4.55''$ from X-ray source (19)
- ◆ None of the matches listed within $5''$ from the X-ray source position has been presented anywhere in the literature. Although the coordinates of the sources are somehow compatible, their magnitudes are totally different (especially the $B - V$ color). We believe that these works blend together multiple point sources, resulting in erroneous B and/or V magnitudes. For more details, see notes in Appendix A2.
- ★ There is no coverage by either the OGLE-II ([Udalski et al. 2000](#)), OGLE-III ([Udalski et al. 2004](#)) or MCPS ([Zaritsky et al. 2004](#)) surveys. [Negueruela & Coe \(2002\)](#) list the following magnitudes: $B = 16.85$, $V = 16.74$, $R = 16.89$ with 0.05 errors, and they mention that the optical counterpart of LMC X-3 is very variable (varying between $V = 16.5$ mag and $V = 17.3$ mag).

Table 3. Bright optical counterparts of HMXBs within $1\sigma <$ search radius $< 2\sigma$

Src ID	R.A. (h m s)	Decl. ($^{\circ}$ ' ")	U	errU	B	errB	V	errV (mag)	I	errI	B-V	err(B-V)	Offset (")	C/part
[1]	[2]	[3]	[4]	[5]	[6]	[7]	[8]	[9]	[10]	[11]	[12]	[13]	[14]	[15]
2	04 55 57.31	-70 19 56.8	19.927	0.073	18.896	0.084	18.156	0.054	1.031	0.111	9.05	...
	04 55 57.69	-70 19 57.0	19.977	0.188	20.962	0.133	20.537	0.127	0.425	0.184	7.30	...
	04 55 57.97	-70 19 56.5	20.788	0.098	20.112	0.142	19.986	0.190	0.676	0.173	6.52	...
	04 55 58.88	-70 20 08.4	21.542	0.119	21.055	0.144	20.617	0.202	0.487	0.187	7.45	...
	04 55 59.49	-70 19 52.0	21.280	0.122	20.611	0.145	0.669	0.189	9.45	...
	04 55 59.72	-70 20 04.7	20.952	0.306	21.841	0.183	20.772	0.174	1.069	0.253	5.54	...
	04 56 00.41	-70 20 03.9	20.909	0.242	21.589	0.108	20.993	0.112	20.170	0.133	0.596	0.156	8.16	...
	04 56 00.66	-70 19 58.5	19.918	0.146	19.425	0.084	18.481	0.103	17.787	0.055	0.944	0.133	9.22	...
	04 56 00.85	-70 20 01.3	19.438	0.083	19.530	0.058	19.470	0.077	19.433	0.078	0.060	0.096	9.85	...
3	04 56 53.35	-68 24 40.4	19.991	0.179	19.845	0.050	19.895	0.075	19.675	0.130	-0.050	0.090	6.84	...
	04 56 53.65	-68 24 26.6	18.795	0.124	19.777	0.053	19.580	0.043	19.672	0.095	0.197	0.068	8.76	...
	04 56 55.07	-68 24 27.6	18.092	0.078	18.378	0.035	18.283	0.051	18.287	0.063	0.095	0.062	9.10	n
4	04 57 11.55	-66 12 08.0	20.412	0.183	20.090	0.064	19.956	0.059	19.745	0.102	0.134	0.087	5.55	...
6	05 01 25.12	-70 33 32.1	18.590	0.061	18.931	0.052	18.851	0.072	19.074	0.153	0.080	0.089	6.14	...
7	05 02 51.49	-66 26 19.4	19.548	0.128	19.271	0.046	19.200	0.053	18.933	0.091	0.071	0.070	5.68	...
	05 02 51.57	-66 26 34.8	19.785	0.140	19.663	0.090	19.504	0.086	19.040	0.181	0.159	0.124	9.80	...
	05 02 52.77	-66 26 26.9	20.199	0.219	20.195	0.096	19.996	0.071	20.160	0.210	0.199	0.119	7.25	...
8	05 07 36.87	-68 47 49.9	17.481	0.057	17.967	0.047	17.959	0.045	17.963	0.046	0.008	0.065	5.64	...
	05 07 36.97	-68 47 45.4	15.752	0.051	16.172	0.031	16.024	0.067	16.269	0.039	0.148	0.074	6.20	...
	05 07 37.30	-68 47 52.8	17.828	0.065	17.873	0.110	17.835	0.042	17.948	0.050	0.038	0.118	5.01	...
	05 07 37.53	-68 47 43.2	17.664	0.064	17.596	0.087	17.771	0.063	17.238	0.095	-0.175	0.107	6.14	...
	05 07 37.95	-68 47 55.6	19.733	0.152	19.613	0.094	0.120	0.179	6.56	...
	05 07 38.70	-68 47 45.2	15.932	0.054	16.440	0.169	16.363	0.038	16.375	0.061	0.077	0.173	5.81	...
	05 07 38.71	-68 47 53.1	20.107	0.091	19.974	0.065	19.570	0.108	0.133	0.112	5.99	...
	05 07 38.80	-68 47 56.2	19.095	0.158	18.868	0.156	18.871	0.088	-0.003	0.179	8.69	...
	05 07 38.88	-68 47 43.0	17.472	0.123	17.326	0.193	17.718	0.073	18.032	0.127	-0.392	0.206	8.03	...
	05 07 38.93	-68 47 48.7	16.286	0.061	16.499	0.055	16.591	0.033	16.717	0.042	-0.092	0.064	5.61	...
	05 07 39.04	-68 47 45.7	18.581	0.325	18.655	0.121	-0.074	0.347	7.04	...

Table 3 – continued

Src ID	R.A. (h m s)	Decl. (° ′ ″)	U	errU	B	errB	V	errV (mag)	I	errI	B-V	err(B-V)	Offset (″)	C/part
[1]	[2]	[3]	[4]	[5]	[6]	[7]	[8]	[9]	[10]	[11]	[12]	[13]	[14]	[15]
	05 07 39.32	-68 47 48.6	16.608	0.091	16.940	0.057	17.025	0.035	17.259	0.056	-0.085	0.067	7.72	...
	05 07 39.34	-68 47 50.7	18.385	0.122	18.439	0.084	18.396	0.094	-0.054	0.148	7.99	...
10	05 12 40.29	-67 17 22.9	19.947	0.190	19.707	0.088	19.741	0.072	19.532	0.276	-0.034	0.114	8.72	...
	05 12 40.41	-67 17 18.1	19.721	0.099	19.815	0.056	19.765	0.092	19.528	0.102	0.050	0.108	9.39	...
12	05 15 59.40	-69 16 14.9	17.895	0.051	18.068	0.041	18.105	0.185	17.808	0.118	-0.037	0.189	6.99	...
	05 16 00.03	-69 16 14.4	17.608	0.048	17.862	0.044	17.885	0.053	17.712	0.077	-0.023	0.069	5.42	...
	05 16 00.79	-69 16 04.4	19.959	0.120	19.803	0.083	19.613	0.273	19.554	0.278	0.190	0.285	5.89	...
	05 16 01.22	-69 16 12.4	17.650	0.047	18.090	0.058	18.035	0.082	18.113	0.112	0.055	0.100	6.82	...
13	05 20 17.33	-69 25 02.4	18.496	0.073	18.638	0.067	19.028	0.501	18.412	0.204	-0.390	0.505	7.47	...
14	05 20 29.01	-69 31 52.03	19.575	0.128	19.299	0.072	18.161	0.172	1.138	0.186	5.09	...
	05 20 29.31	-69 31 59.84	19.167	0.130	19.349	0.094	17.431	0.124	17.196	0.110	1.918	0.156	5.48	...
15	05 23 14.22	-70 04 15.8	16.533	0.049	16.997	0.062	16.965	0.065	17.151	0.097	0.032	0.090	5.18	n,A
16	05 24 11.83	-66 20 50.9	13.837	0.024	14.813	0.014	14.867	0.022	14.866	0.021	-0.054	0.026	5.31	n
18	05 27 22.51	-65 52 40.5	18.266	0.058	18.586	0.034	18.494	0.030	18.552	0.047	0.092	0.045	9.10	n
	05 27 23.81	-65 52 26.1	20.131	0.113	20.084	0.045	19.956	0.061	19.806	0.107	0.128	0.076	8.95	...
19	05 29 24.23	-69 52 10.3	20.100	0.149	19.362	0.079	19.381	0.073	19.122	0.083	-0.019	0.108	8.64	...
	05 29 24.60	-69 52 09.9	19.703	0.078	18.804	0.052	17.641	0.134	0.899	0.094	6.79	...
	05 29 27.24	-69 52 14.6	20.45	0.205	19.686	0.098	18.808	0.075	17.523	0.096	0.878	0.123	7.81	...
	05 29 25.17	-69 52 15.8	18.782	0.127	18.693	0.110	18.811	0.139	18.853	0.156	-0.118	0.177	6.12	n,A
	05 29 26.36	-69 52 17.8	20.671	0.233	20.002	0.118	19.757	0.145	18.903	0.136	0.245	0.187	7.24	...
	05 29 27.14	-69 52 03.6	19.838	0.164	19.382	0.114	19.530	0.228	19.369	0.168	-0.148	0.255	9.76	...
	05 29 27.33	-69 52 07.6	21.127	0.343	19.865	0.149	19.599	0.175	18.662	0.143	0.266	0.230	8.12	...
20	05 29 47.82	-65 56 43.4	13.761	0.029	14.477	0.038	14.594	0.022	14.741	0.106	-0.117	0.044	8.36	k
21	05 30 11.37	-65 51 23.5	13.933	0.034	14.894	0.016	14.877	0.022	14.691	0.023	0.017	0.027	5.89	k
22	05 30 42.27	-66 54 38.6	18.238	0.055	18.360	0.060	18.556	0.056	18.680	0.067	-0.196	0.082	9.80	...
23	05 30 46.70	-66 06 18.3	20.617	0.168	20.358	0.039	20.061	0.067	19.815	0.106	0.297	0.078	5.36	...
24	05 31 13.08	-66 07 06.7	13.862	0.029	14.749	0.014	14.798	0.051	14.763	0.039	-0.049	0.053	5.71	k,A
	05 31 13.14	-66 07 09.3	16.131	0.041	16.157	0.029	15.740	0.123	15.080	0.038	0.417	0.126	7.44	...
	05 31 15.20	-66 07 05.0	17.496	0.038	17.714	0.018	17.741	0.026	-0.027	0.032	8.76	...

Table 3 – *continued*

Src ID	R.A. (h m s)	Decl. (° ' ")	U	errU	B	errB	V	errV	I	errI	B-V	err(B-V)	Offset (")	C/part
[1]	[2]	[3]	[4]	[5]	[6]	[7]	[8]	[9]	[10]	[11]	[12]	[13]	[14]	[15]
05 13 28.26	-65 47 18.4	14.122	0.036	15.067	0.088	15.098	0.027	15.328	0.039	-0.031	0.092	2.06	k,A	
25	05 31 16.06	-70 53 43.0	19.020	0.090	18.960	0.065	18.784	0.063	18.985	0.096	0.176	0.091	7.68	...
	05 31 16.76	-70 53 44.2	20.102	0.122	19.662	0.081	19.547	0.115	19.246	0.110	0.115	0.141	8.86	...
26	05 31 17.35	-66 07 23.7	19.942	0.133	20.064	0.089	20.029	0.045	20.189	0.100	0.035	0.100	8.12	...
	05 31 19.21	-66 07 26.1	19.700	0.114	19.758	0.050	19.680	0.049	19.669	0.092	0.078	0.070	7.26	...
27	05 31 36.45	-65 18 20.6	20.586	0.223	19.857	0.061	19.744	0.052	19.746	0.088	0.113	0.080	5.13	...
	05 31 36.75	-65 18 23.1	20.649	0.233	20.006	0.274	20.040	0.062	20.002	0.139	-0.034	0.281	8.18	...
29	05 32 24.31	-65 35 01.1	19.771	0.044	19.576	0.046	19.703	0.097	0.195	0.064	9.96	n,A
	05 32 25.85	-65 35 01.3	20.727	0.178	19.536	0.037	18.336	0.026	17.173	0.054	1.200	0.045	8.44	n,A
30	05 32 31.92	-65 51 46.4	19.150	0.147	19.360	0.046	19.244	0.092	18.981	0.121	0.116	0.103	5.39	...
31	05 32 48.81	-66 22 14.1	20.506	0.247	20.178	0.063	19.859	0.094	20.08	0.169	0.319	0.113	5.91	...
	05 32 49.33	-66 22 19.6	19.343	0.089	19.204	0.091	19.062	0.101	19.667	0.325	0.142	0.136	6.42	...
	05 32 51.07	-66 22 17.0	17.846	0.046	18.066	0.090	18.243	0.103	18.297	0.042	-0.177	0.137	8.33	...
33	05 35 04.28	-67 00 14.9	18.128	0.050	18.444	0.066	18.53	0.114	18.585	0.062	-0.086	0.132	9.54	...
	05 35 06.78	-67 00 14.4	19.006	0.076	19.190	0.061	19.092	0.046	19.016	0.060	0.098	0.076	5.43	...
34	05 35 41.20	-66 51 51.9	17.939	0.230	18.412	0.161	18.311	0.087	17.745	0.134	0.101	0.183	0.06	...
	05 35 41.66	-66 51 48.6	17.606	0.041	18.363	0.137	17.926	0.045	-0.757	0.143	4.38	...
35	05 35 52.34	-65 30 35.3	21.877	0.147	21.387	0.115	0.490	0.187	9.16	...
	05 35 53.41	-65 30 43.6	21.007	0.303	20.918	0.082	20.447	0.074	19.814	0.106	0.471	0.110	9.86	...
	05 35 54.60	-65 30 29.4	20.027	0.189	20.430	0.085	19.849	0.048	18.816	0.064	0.581	0.098	6.79	...
	05 35 54.64	-65 30 37.7	17.915	0.054	18.026	0.105	16.952	0.101	15.720	0.102	1.074	0.146	6.40	n,A
	05 35 54.69	-65 30 31.5	21.440	0.165	21.156	0.146	0.284	0.220	6.11	...
37	05 39 39.90	-69 44 41.1	15.873	0.213	16.287	0.185	16.023	0.117	15.547	0.136	0.264	0.219	7.64	...
*	05 39 40.03	-69 44 33.4	11.745	0.033	12.295	0.035	12.080	0.054	11.493	0.180	0.215	0.064	6.54	...
38	05 41 26.58	-69 01 16.8	19.274	0.110	19.451	0.036	19.250	0.042	19.125	0.058	0.201	0.055	6.18	...
	05 41 26.80	-69 01 28.5	19.913	0.127	19.745	0.067	19.610	0.050	19.454	0.071	0.135	0.084	5.57	...
39	05 41 20.55	-69 36 31.6	20.113	0.256	19.884	0.292	0.229	0.388	9.01	...
	05 41 22.31	-69 36 38.8	20.957	0.206	20.247	0.088	20.084	0.095	20.022	0.121	0.163	0.129	9.82	...
	05 41 22.93	-69 36 33.3	17.122	0.045	17.399	0.033	17.326	0.036	17.243	0.059	0.073	0.049	5.74	n?,A
	05 41 21.78	-69 36 20.2	18.487	0.135	17.813	0.080	16.767	0.049	15.642	0.056	1.046	0.094	9.11	...

Table 3 – continued

Src ID	R.A. (h m s)	Decl. ($^{\circ}$ ' ")	U	errU	B	errB	V	errV (mag)	I	errI	B-V	err(B-V)	Offset (")	C/part
[1]	[2]	[3]	[4]	[5]	[6]	[7]	[8]	[9]	[10]	[11]	[12]	[13]	[14]	[15]
40	05 41 33.57	-68 25 52.2	20.065	0.129	18.948	0.077	19.064	0.076	18.240	0.059	-0.116	0.108	6.63	...
42	05 43 57.78	-65 39 46.33	20.280	0.051	19.357	0.065	18.260	0.045	0.923	0.083	5.82	n,A
	05 43 59.57	-65 39 53.0	20.445	0.154	20.171	0.055	19.956	0.050	19.707	0.084	0.215	0.074	9.76	n,A
43	05 44 05.13	-71 00 50.8	14.598	0.031	15.292	0.029	15.235	0.022	15.220	0.029	0.057	0.036	5.75	k
44	05 44 14.01	-66 33 48.4	20.865	0.069	20.705	0.067	20.337	0.123	0.160	0.096	9.01	...
	05 44 14.68	-66 33 42.9	21.123	0.074	20.935	0.089	20.463	0.113	0.188	0.116	8.61	...
	05 44 16.32	-66 33 41.4	20.966	0.071	20.685	0.076	0.281	0.104	9.93	...
	05 44 16.34	-66 33 51.4	22.719	0.339	21.504	0.127	20.583	0.172	1.215	0.362	5.23	...
	05 44 16.68	-66 33 56.2	20.853	0.242	19.898	0.049	19.203	0.041	18.059	0.055	0.695	0.064	9.38	...
	05 44 16.86	-66 33 45.4	18.886	0.101	18.678	0.026	18.536	0.029	18.422	0.058	0.142	0.039	9.32	...
45	05 46 49.39	-68 51 46.2	18.150	0.071	18.480	0.041	18.440	0.038	18.520	0.060	0.040	0.056	5.93	n,A

Notes – Similarly to Table 2, the most likely counterpart of each X-ray source is indicated in bold. Three dots indicate that an entry was not available in the MCPS catalog. Bright refers to stars with $V \lesssim 20$ mag and $B - V \lesssim 0.2$ mag. 2σ search radius corresponds to $10''$ from the X-ray source position. X-ray sources, which do not appear in this table, do not have any bright optical match within $5''$ to $10''$ from their position. Their most likely counterpart is found either within $5''$ from the X-ray position (Table 2) or at larger than $10''$ distances (especially for those X-ray sources with larger than $10''$ positional uncertainties; see Table 4). An input "n" in Column 15 indicates a newly identified counterpart from this work, a "k" a known in the literature counterpart, and an "A" those counterparts that are discussed in the Appendix A.

Additional identifications and notes for these sources follow below, which however by no means consist a complete list.

Src 8: [OGLE-CL]129 at $5.21''$ (R.A., Dec.) $_{J2000.0}=(05:07:38.63,-68:47:45.9)$ with age $\log(\text{age}) \sim 7.9$ (Pietrzyński & Udalski 2000a); AGN [Veron+2010]1.4418.1930 at $7.9''$ (R.A., Dec.) $_{J2000.0}=(05:07:36.5,-68:47:51)$ from the X-ray source position with $z=0.53$ and $V=19.81$ mag (Véron-Cetty & Véron 2010).

Src 14: [Massey2002]119691 with $V = 14.12$ mag, and $B - V = 0.02$ mag at $1.34''$ from X-ray source position; 2MASS J05202986-6931556 with $J = 14.372 \pm 0.059$ mag, $H = 14.211 \pm 0.070$ mag, $K = 14.276 \pm 0.099$ mag at $0.69''$ from the X-ray source position. This is the same counterpart as the one given by Edge et al. (2004), though the photometry listed there (which is taken from Coe et al. 2001) is a bit different (average OGLE magnitudes: $B = 14.39$ mag, and $V = 14.45$ mag, thus $B - V = -0.06$ mag).

Src 43: [OGLE-II]05440524-7100512 with (R.A., Dec.) $_{J2000.0}=(05:44:05.24,-71:00:51.2)$ is a Type-1/2 object (i.e. Type-1 star with luminosity jumps in its light curve) in the work of Sabogal et al. 2005, located at $5.31''$ from the X-ray source; [MACHO]15.10314.14 variable star $5.73''$ from X-ray position; 2MASS J05440522-7100507 at $5.31''$ from X-ray source.

★ Although this object (a known B-type supergiant; B3f(a) from Fariña et al. 2009) is the brightest match within the 2σ search radius around the well studied source LMC X-1, the known optical counterpart of this BH-HMXB (Cowley et al. 1995) is another object (i.e., the nearest and bluest match) within the 1σ search radius (shown in bold in Table 2).

Table 4. Additional bright ($V \lesssim 20$ mag and $B - V \lesssim 0.2$ mag) optical counterparts of HMXBs with positional uncertainty larger than $10''$

Src ID	R.A. (h m s)	Decl. ($^{\circ}$ ' ")	U	errU	B	errB	V	errV	I	errI	B-V	err(B-V)	Offset ($''$)	C/part
[1]	[2]	[3]	[4]	[5]	[6]	[7]	[8]	[9]	[10]	[11]	[12]	[13]	[14]	[15]
4	04 57 15.39	-66 12 22.7	15.452	0.027	15.633	0.030	15.630	0.021	15.459	0.022	0.003	0.037	22.10	n
15	05 23 16.94	-70 04 00.0	15.803	0.041	15.358	0.035	15.025	0.052	14.402	0.045	0.333	0.063	15.88	n,A
17	05 27 06.47	-70 04 40.2	18.370	0.075	18.692	0.054	18.580	0.122	18.826	0.078	0.112	0.133	21.08	...
	05 27 10.14	-70 04 53.4	19.211	0.084	18.782	0.052	18.626	0.074	18.372	0.061	0.156	0.090	13.23	n,A
	05 27 10.95	-70 04 45.2	18.656	0.081	18.661	0.054	18.381	0.060	18.068	0.077	0.280	0.081	21.48	...
19	05 29 22.81	-69 52 16.5	19.168	0.109	17.771	0.094	16.711	0.051	15.511	0.076	1.060	0.107	16.88	...
	05 29 22.97	-69 52 00.0	18.984	0.093	18.476	0.076	18.366	0.058	18.434	0.355	0.110	0.096	18.69	...
	05 29 22.99	-69 52 21.5	20.236	0.153	19.063	0.154	18.817	0.064	17.918	0.135	0.246	0.167	18.34	...
	05 29 23.18	-69 52 07.9	18.463	0.076	18.546	0.062	18.805	0.180	18.506	0.131	-0.259	0.190	14.38	...
	05 29 24.76	-69 51 59.3	20.326	0.209	19.385	0.109	18.357	0.096	17.153	0.093	1.028	0.145	13.07	...
	05 29 24.87	-69 52 24.7	20.247	0.153	18.798	0.122	17.907	0.296	1.449	0.196	14.73	...
	05 29 24.87	-69 52 29.3	20.271	0.186	19.355	0.114	18.635	0.115	17.624	0.079	0.720	0.162	19.07	...
	05 29 24.93	-69 52 19.7	16.389	0.193	16.490	0.083	16.508	0.044	16.608	0.094	-0.018	0.094	10.08	n,A
	05 29 25.83	-69 52 27.0	18.797	0.114	18.871	0.260	17.725	0.144	16.924	0.166	1.146	0.297	16.05	...
	05 29 26.62	-69 51 53.3	19.011	0.095	18.912	0.120	18.870	0.144	0.099	0.153	18.11	...
	05 29 26.88	-69 51 58.1	18.528	0.088	18.612	0.079	18.504	0.088	18.473	0.106	0.108	0.118	13.85	...
	05 29 26.96	-69 52 27.3	20.121	0.152	19.585	0.096	19.747	0.110	19.251	0.150	-0.162	0.146	17.16	...
	05 29 27.10	-69 52 23.2	20.038	0.167	18.257	0.072	16.916	0.053	15.213	0.053	1.341	0.089	13.67	...
	05 29 28.33	-69 52 12.1	19.875	0.168	18.834	0.099	18.431	0.073	17.396	0.147	0.403	0.123	12.60	...
	05 29 28.66	-69 52 05.8	18.907	0.097	18.417	0.042	18.514	0.041	18.323	0.091	-0.097	0.059	15.16	...
	05 29 28.82	-69 52 00.7	19.430	0.113	18.834	0.069	18.508	0.066	17.947	0.083	0.326	0.095	18.25	...
	05 29 29.04	-69 52 09.8	19.196	0.146	18.245	0.066	17.543	0.064	16.582	0.064	0.702	0.092	16.25	...
	05 29 28.20	-69 52 05.2	19.256	0.099	18.013	0.066	16.625	0.081	1.243	0.119	13.20	...
	05 29 28.33	-69 52 12.1	19.875	0.168	18.834	0.099	18.431	0.073	17.396	0.147	0.403	0.123	12.60	...
23	05 30 48.60	-66 06 35.5	18.270	0.129	18.082	0.052	0.188	0.139	21.72	n,A
	05 30 48.79	-66 06 35.5	17.879	0.089	17.719	0.051	18.165	0.029	17.811	0.107	-0.446	0.059	22.13	n,A
28	05 32 24.83	-71 06 56.0	18.060	0.046	18.354	0.032	18.354	0.034	18.413	0.051	0.000	0.047	37.48	n
29	05 32 20.71	-65 35 17.7	20.035	0.116	19.644	0.028	18.745	0.030	17.789	0.037	0.899	0.041	29.79	...
	05 32 20.90	-65 35 25.9	20.377	0.281	19.812	0.059	19.540	0.035	19.692	0.097	0.272	0.069	32.09	...

Table 4 – continued

Src ID	R.A. (h m s)	Decl. (° ' ")	U	errU	B	errB	V	errV (mag)	I	errI	B-V	err(B-V)	Offset (")	C/part
[1]	[2]	[3]	[4]	[5]	[6]	[7]	[8]	[9]	[10]	[11]	[12]	[13]	[14]	[15]
	05 32 21.98	-65 35 15.9	20.239	0.133	19.877	0.063	18.912	0.040	18.105	0.095	0.965	0.075	21.72	...
	05 32 23.53	-65 35 33.3	20.661	0.160	20.012	0.038	19.043	0.037	18.127	0.043	0.969	0.053	26.65	...
	05 32 24.24	-65 34 59.4	19.550	0.042	19.490	0.037	19.640	0.109	0.060	0.056	11.61	n,A
	05 32 27.65	-65 34 49.0	19.789	0.123	19.722	0.049	18.837	0.066	17.919	0.060	0.885	0.082	24.74	...
	05 32 27.72	-65 35 02.4	20.149	0.203	19.639	0.047	19.281	0.038	19.181	0.078	0.358	0.060	16.37	n,A
	05 32 28.33	-65 35 33.8	19.628	0.090	18.717	0.028	17.600	0.032	16.590	0.030	1.117	0.043	31.08	...
	05 32 28.99	-65 35 29.9	20.504	0.138	20.191	0.043	19.231	0.032	18.415	0.142	0.960	0.054	31.00	...
	05 32 29.19	-65 34 59.5	18.893	0.034	17.470	0.065	1.423	0.073	25.91	...
35	05 35 56.76	-65 30 22.8	17.558	0.048	17.825	0.031	17.882	0.027	18.060	0.051	-0.057	0.041	21.57	n,A
	05 35 51.28	-65 30 22.8	18.630	0.054	18.822	0.083	18.818	0.036	19.061	0.120	0.004	0.090	19.25	n,A
39	05 41 20.10	-69 36 22.9	11.307	0.067	11.790	0.093	11.790	0.051	11.910	0.130	0.000	0.106	12.52	k,A
45	05 46 44.77	-68 51 43.4	17.844	0.070	17.994	0.038	17.890	0.059	17.934	0.061	0.104	0.070	19.41	n,A
	05 46 44.97	-68 50 53.3	16.231	0.055	16.905	0.050	16.887	0.033	17.165	0.131	0.018	0.060	56.67	n,A
	05 46 54.37	-68 51 06.9	17.819	0.067	18.175	0.042	18.115	0.035	18.138	0.053	0.060	0.055	51.82	n,A

Notes – Similarly to Table 2, the most likely counterpart of each X-ray source is indicated in bold. Only X-ray sources with a probable optical counterpart in larger than 10" distances are shown in this table. For example, although HMXB #3 has an 11.1" positional uncertainty, it is not listed in this table, since its most likely optical counterpart is a match found using a search radius of 10" (i.e. listed in Table 3). Three dots indicate that an entry was not available in the MCPS catalog (see also general notes of Tables 2 and 3). Eleven sources have bright matches ($V \lesssim 20$ mag and $B - V \lesssim 0.2$ mag) in larger than 10" distances from the X-ray position. Two of those sources (HMXB#4 and #28 with 14.5" and 24.3" positional uncertainties, respectively) have an unambiguous counterpart even at those large distances. The remaining 9 sources have matches usually in both Tables 2 and 3.

Table 5. Final classification of sources listed as HMXBs in the literature

ID	Name	X-ray Source	Literature	XRB Classification	This Work	Notes
[1]	[2]		[3]		[4]	[5]
1	Swift J045106.8-694803, LXP187		HMXB/Be-XRB? (10), Be-XRB (70)	Be-XRB	...	
2	Swift J045558.9-702001		Be-XRB (72)	Be-XRB	...	
3*	RX J0456.9-6824		HMXB? (37,38)	Be-XRB?	...	
4*	RX J0457.2-6612		HMXB? (37,38)	Be-XRB?	...	
5	IGR J05007-7047 (23), CXOU J050046.0-704436 (20)		HMXB (15), Be-XRB? (24)	Be-XRB?	...	
6	RX J0501.6-7034, CAL 9, 2E 0501.8-7038, 1E 0501.8-7036		Be-XRB (62)	Be-XRB	...	
7	RX J0502.9-6626, CAL E, LXP4.10		Be-XRB (62)	Be-XRB	...	
8*	RX J0507.6-6847, RX J050736-6847.8		HMXB/Be-XRB? (36)	Be-XRB?	...	
9	LXP169, XMMU J050755.4-682505		eclipsing Be-XRB (73)	Be-XRB	we do not attempt to identify the eclipsing nature of this system	
10*	RX J0512.6-6717		HMXB? (38)	Be-XRB?	...	
11	Swift J0513.4-6547 (12), LXP27.3		HMXB (12), Be-XRB? (45), Be-XRB (76)	Be-XRB	...	
12	RX J0516.0-6916		HMXB? (25)	Be-XRB?	see Appendix A1	
13	XMMU J052016.0-692505		likely WD/Be-XRB (8)	Be-XRB	we do not attempt to classify the compact object	
14	RX J0520.5-6932, LXP8.04		Be-XRB (4)	Be-XRB	see Appendix A2	
15*	RX J0523.2-7004		HMXB (38)	Be-XRB?	see Appendix A3	
16*	RX J0524.2-6620		HMXB (38)	Be-XRB?	...	
17*	RX J0527.1-7005		HMXB (38)	not an HMXB	see Appendix A4	
18*	RX J0527.3-6552		HMXB? (37,38)	Be-XRB?	...	
19*	RX J0529.4-6952		HMXB (37,38)	Be-XRB?	see Appendix A5	
20	XMMU J052947.4-655639 (6), LXP69.2, RX J0529.8-6556 (5), RX J0529.7-6556		Be-XRB (5)	Be-XRB	...	

Table 5 – continued

ID	Name	X-ray Source	Literature	XRB Classification This Work	Notes
[1]	[2]		[3]	[4]	[5]
21	XMMU J053011.2-655122, LXP272, RX J0530.1-6551		Be-XRB? (6)	Be-XRB?	...
22	Swift J053041.9-665426 (58), LXP28.8		Be-XRB? (59), Be-XRB (26)	Be-XRB	...
23★	RX J0530.7-6606		HMXB (38)	Be-XRB?	see Appendix A6
24	RX J0531.2-6607, EXO 0531.1-6609, LXP13.7, XMMU J053113.3-660705, EXO 053109-6609.2 (46), XMMU J053113.1-660707, IRXS J053111.0-660657 (19), IGR J05305-6559 (69)		Be-XRB (47)	Be-XRB	see Appendix A7
25	XMMU J053115.4-705350		HMXB (48, 71)	SG-XRB?	see Appendix A8
26★	XMMU J053118.2-660730		HMXB? (48)	Be-XRB?	see Appendix A7
27	RX J0531.5-6518, IRXS J053137.1-651759 (19)		HMXB (49), BeXRB? (1)	Be-XRB?	...
28★	RX J0532.3-7107, CAL 50 (19), IRXS J053219.5-710806 (19)		HMXB? (37,38)	Be-XRB?	...
29★	RX J0532.4-6535, IRXS J053226.0-653505 (19)		HMXB? (49)	not an HMXB	see Appendix A9
30	RX J0532.5-6551, XMMUJ05322.4-655139, IRXS J053224.1-655112 (19)		SG-XRB (51)	SG-XRB	see Appendix A10
31	2A 0532-664, LMC X-4, LXP13.5, RX J0532.8-6622 (19), CAL 49, IRXS J053246.1-662203 (38), 4U 0532D66 (57), RASS 232 (49)		HMXB (79)	HMXB	see Appendix A11
32	Swift J053321.3-684121 (66)		HMXB? (66)	SG-XRB	...
33	RX J0535.0-6700		Be-XRB (1)	Be-XRB	...
34	1A 0535-668, RX J0535.6-6651, LXP0.07, CAL G (19), IRXS J053539.0-665158 (19)		Be-XRB (52)	Be-XRB	...

Table 5 – *continued*

ID	Name	X-ray Source	Literature	XRB Classification		Notes
				This Work	[4]	
[1]	[2]		[3]		[4]	[5]
35★	RX J0535.8-6530, IRXS J053555.0-653039 (19)		HMXB? (49)		not an HMXB	see Appendix A9
36	IH 0538-641, LMC X-3, XMMU J053856.7-640503 (19), IRXS J053855.6-640457 (19), IRXS J053855.5-640457 (19), RX J0538.9-6405, CAL 70 (19), 3A 0539-641, 4U 0538-64 (19),		BH-HMXB (18)	there is no MCPS coverage
37	3A 0540-697, LMC X-1, IRXS J053938.8-694515 (19)		BH-HMXB (53,54)	HMXB	...	we do not attempt to classify the compact object; counterpart compatible with having an OB spectral type
38	IGR J05414-6858 (13), LXP4.42		Be-XRB? (14), Be-XRB (61)	Be-XRB
39	RX J0541.4-6936		SG-XRB? (2)	SG-XRB	...	see Appendix A12
40	XMMU J054134.7-682550, LXP60.8		HMXB? (48), Be-XRB? (60)	Be-XRB?
41	RX J0541.5-6833, RX J0541.6-6832 (40)		HMXB? (2)	HMXB	...	see Appendix A13
42★	RX J0543.9-6539 (38)		HMXB? (37)	not an HMXB	...	see Appendix A14
43	ISAX J0544.1-7100, LXP96.1, RX J0544.1-7100 (38), AX J0548-704, AX J0544.1-7100 (40), 1WGA J0544.1-7100		Be-XRB (4)	Be-XRB
44	H 0544-665 (41)		Be-XRB (55,56)	Be-XRB
45★	RX J0546.8-6851, RX J0547.0-6852 (38), 2E 0547.2-6852, IRXS J054655.3-685142		HMXB? (38)	Be-XRB?	...	see Appendix A15

Notes – References given in parenthesis are similar to those listed in Table 1.

★ New counterparts for these X-ray sources are identified in the present work.

Table 6. The young X-ray source population of the LMC

XRB type	Total number of sources	
	Literature	This work
[1]	[2]	[3]
Be-XRBs	21	33
SG-XRBs	2	4
HMXBs (w/o further classification)	20	3
BH-HMXB	2	... •
HMXBs (all)	45	40
X-ray pulsars	14	14★

Notes – Each class includes confirmed and candidate systems. There is one source (LMC X-3) without MCPS coverage, thus we do not classify this system.

- With the present work we do not obtain info about the nature of the compact object, so we cannot classify any source as a BH-HMXB. For the one known BH-HMXB that there is MCPS coverage (LMC X-1; see Table 5), we only classify this X-ray source as an HMXB.

- ★ We did not perform any timing analysis, so the number of known X-ray pulsars is the one found in the literature.

Table 7. Compilation of metallicity values of B-type stars in the Magellanic Clouds

Galaxy	Source Name	R.A. (J2000.0) (h m s)	Decl. (° ' ")	Spectral Type	[Fe/H] (-dex)	Z/Z_{\odot}^{\dagger}	Z^{\ddagger}
[1]	[2]	[3]	[4]	[5]	[6]	[7]	[8]
LMC	N11-024 (6)	04 55 32.93 (6)	-66 25 27.7 (6)	B1 Ib (6)	-0.39 ± 0.16• (5)	0.41 ± 0.15	0.005 ± 0.002
	N11-017 (6)	04 56 17.57 (6)	-66 18 18.5 (6)	B2.5 Iab (6)	-0.30 ± 0.16• (5)	0.50 ± 0.18	0.007 ± 0.002
	N11-016 (6)	04 56 20.59 (6)	-66 27 14.0 (6)	B1 Ib (6)	-0.24 ± 0.28• (5)	0.58 ± 0.37	0.008 ± 0.005
	N11-002 (6)	04 56 23.51 (6)	-66 29 51.7 (6)	B3 Ia (6)	-0.16 ± 0.16• (5)	0.69 ± 0.25	0.009 ± 0.003
	N11-014 (6)	04 56 48.02 (6)	-66 20 09.8 (6)	B2 Iab (6)	-0.27 ± 0.17• (5)	0.54 ± 0.22	0.007 ± 0.003
	N11-012 (6)	04 56 51.15 (6)	-66 31 48.3 (6)	B1 Ia (6)	-0.40 ± 0.27• (5)	0.40 ± 0.25	0.005 ± 0.003
	N11-001 (6)	04 57 08.85 (6)	-66 23 25.1 (6)	B2 Ia (6)	-0.05 ± 0.17• (5)	0.89 ± 0.36	0.012 ± 0.005
	N11-009 (6)	04 57 17.68 (6)	-66 26 31.5 (6)	B3 Iab (6)	-0.26 ± 0.14• (5)	0.55 ± 0.17	0.007 ± 0.002
	N11-015 (6)	04 57 22.08 (6)	-66 24 27.5 (6)	B0.7 Ib (6)	-0.29 ± 0.26• (5)	0.51 ± 0.31	0.007 ± 0.004
	N11-110 (6)	04 57 37.11 (6)	-66 23 44.7 (6)	B1 III (6)	-0.38 ± 0.16• (5)	0.42 ± 0.16	0.006 ± 0.002
	N11-036 (6)	04 57 41.00 (6)	-66 29 56.4 (6)	B0.5 Ib (6)	-0.33 ± 0.23• (5)	0.47 ± 0.25	0.006 ± 0.003
	PS 34-16 (3)	05 04 32.5 (3)	-66 24 47 (3)	I dwarf	~ -0.17 ± 0.06 (3)	~ 0.68	~ 0.009
	NGC 1818/D1	05 04 32.5 (14)	-66 24 51.0 (14)	B1 V (14)	-0.16 ± 0.30 (1)	0.69 ± 0.48	0.009 ± 0.006
	NGC 2004/B15 (6)	05 29 11.46 (6)	-67 15 24.40 (6)	B1.5 II (6)	-0.45 ± 0.40 (1)	0.35 ± 0.33	0.005 ± 0.004
	NGC 2004/B30 (6)	05 30 11.03 (6)	-67 22 57.10 (6)	B0.2 Ib (6)	-0.42 ± 0.30 (1)	0.38 ± 0.26	0.005 ± 0.004
BRU 217 (1)	05 34 51.76 (11.7)	-69 22 44.7 (11.7)	B Ib (1), O/B0 (11)	-0.55 ± 0.30 (1)	0.28 ± 0.20	0.004 ± 0.003	
BRU 231 (1)	05 35 17.44 (11.7)	-69 19 54.2 (11.7)	B Ib (1), B1/2 (11)	-0.46 ± 0.30 (1)	0.35 ± 0.24	0.005 ± 0.003	
LH 10-3270 (20)	05 57 21.2 (20)	-66 25 01 (20)	B1 V (20)	-0.9 (16)	0.13	0.002	
SMC	AV 175 (1)	00 56 38.07 (12)	-72 36 35.3 (12)	B1 I (12)	-0.86 ± 0.40 (1)	0.14 ± 0.13	0.002 ± 0.002
	NGC346-11 (2)	00 57 29.50 (7)	-72 16 00.5 (7)	B9 II (6)	~ -0.7• (9)	~ 0.20	~ 0.003
	NGC346-039 (6)	00 57 47.42 (6)	-72 16 40.44 (6)	B0.7 V (6)	-0.56 ± 0.17• (5)	0.28 ± 0.11	0.004 ± 0.001
	AV 218 (1)	00 59 04.34 (12)	-72 19 40.8 (12)	B1 I (12)	-0.51 ± 0.30 (1)	0.31 ± 0.22	0.004 ± 0.003

Table 7 – continued

Galaxy	Source Name	R.A. (h m s)	Decl. (° ' ")	Spectral Type	[Fe/H] (-dex)	Z/Z_{\odot}^{\dagger}	Z^{\ddagger}
[1]	[2]	[3]	[4]	[5]	[6]	[7]	[8]
	NGC346-637 (2)	00 59 14.60> (10)	-72 12 01.45> (10)	B0 V (10)	$\sim -0.8^{\star}$ (9)	~ 0.16	~ 0.002
	NGC346-037 (6)	00 59 18.84 (6)	-72 06 29.27 (6)	B3 III (6)	$-0.67 \pm 0.21^{\bullet}$ (5)	0.21 ± 0.11	0.003 ± 0.001
	NGC346-021 (6)	00 59 19.58 (6)	-72 14 50.47 (6)	B1 III (6)	$-0.36 \pm 0.18^{\bullet}$ (5)	0.44 ± 0.19	0.006 ± 0.002
	NGC346-044 (6)	00 59 26.46 (6)	-72 13 11.78 (6)	B1 II (6)	$-0.51 \pm 0.18^{\bullet}$ (5)	0.31 ± 0.13	0.004 ± 0.002
	AV 304 (2,4)	01 02 21.47 (7)	-72 39 14.7 (7)	B0.5 V (8,4)	$\sim -0.8^{\star}$ (9)	~ 0.16	~ 0.002
					-0.79 ± 0.19 (4)	0.16 ± 0.07	0.002 ± 0.001
					-1.2 (16)	0.06	0.001
SMC	SK 194 (14)	01 45 03 (14)	-74 31 32 (14)	B9 Ia (15)	~ -1.35 (14)	~ 0.04	~ 0.001
Wing \boxplus	IDK-D2 (13)	02 06 59.06 (13)	-74 16 55.9 (13)	B2 (13)	$\sim -1.1^{\star}$ (9)	~ 0.08	~ 0.001
	DI 1239 (19)	02 30 40.81 (19)	-74 04 45.3 (19)	B1 (19)	-1.6 (16)	0.03	$\sim 4 \times 10^{-4}$
Magellanic	DI 1388 (18)	02 57 11.94 (18)	-72 52 54.61 (18)	B0 V (14), O8 (13)	-1.9 (16)	0.01	$\sim 10^{-4}$
Bridge \boxplus	DGIK 975 (18)	04 19 58.63 (18)	-73 52 25.80 (18)	B2 (17)	-1.7 (16)	0.02	$\sim 10^{-4}$

\dagger Using $Z/Z_{\odot} = 10^{[\text{Fe}/\text{H}]}$.

\ddagger With the solar chemical composition of [Asplund et al. \(2009\)](#), the mass fractions of H, He, and metals in the present-day photosphere become $X = 0.7381$, $Y = 0.2485$, and $Z = 0.0134$, i.e. the solar metallicity has been revised from the canonical 2% value first recommended in the literature in the 90's. In the present study we use the revised value ($Z_{\odot} = 0.0134$).

\bullet Defined as the difference between the weighted mean absolute abundances of [Trundle et al. \(2007\)](#) and the Fe abundance in the present-day solar photosphere (the latter is equal to 7.50 ± 0.04 from [Asplund et al. 2009](#)).

\star Heavy element depletion ($[\text{M}/\text{H}]$).

\triangleright Original equatorial B1950.0 coordinates were transformed to J2000.0 using NASA/IPAC Extragalactic Database (NED); <https://ned.ipac.caltech.edu/forms/calculator.html>).

\boxplus The SMC Wing is the area defined as $-75.5^{\circ} \leq \text{Decl} \leq -73.5^{\circ}$ and $1.6^{\text{h}} \leq \text{R.A.} \leq 2.6^{\text{h}}$, while for the Magellanic Bridge it is $\text{R.A.} \gtrsim 3^{\text{h}}$ (see Fig. 1 in [Lehner et al. 2008](#)).

References: (1) [Kom et al. \(2000\)](#); (2) [Rolleston et al. \(1993\)](#); (3) [Rolleston et al. \(2002\)](#); (4) [Peters & Adelman \(2006\)](#); (5) [Trundle et al. \(2007\)](#); (6) [Evans et al. \(2006\)](#); (7) [Skrutskie et al. \(2006\)](#); (8) [Crampton & Greasley \(1982\)](#); (9) [Rolleston \(1995\)](#); (10) [Massey et al. \(1989\)](#); (11) <ftp://ftp.lowell.edu/pub/bas/starcats/brunet.lmc> (version: 15 Feb 2008; originally in [Brunet et al. 1975](#)); (12) <ftp://ftp.lowell.edu/pub/bas/starcats/azv.dat> (version: 28 Aug 2008); (13) [Irwin et al. \(1990\)](#); (14) [Blair et al. \(2009\)](#); (15) [Ardeberg & Maurice \(1977\)](#); (16) [Dufton et al. \(2008\)](#); (17) [Ayres \(2010\)](#); (18) [Lehner \(2002\)](#); (19) [Rolleston et al. \(1999\)](#); (20) [Parker et al. \(1992\)](#).

Table 8. Compilation of age and metallicity values of young (< 100 Myr) star clusters in the Magellanic Clouds

Galaxy	Cluster	Age		[Fe/H]		Z/Z _⊙		Z		Ref.♦
		Value	Error	Value	Error	Value	Error	Value	Error	
[1]	[2]	[3]	[4]	[5]	[6]	[7]	[8]	[9]	[10]	[11]
		(Myr)		(-dex)						
LMC	LH47/48	2.00	...	-0.40	...	0.40	...	0.005	...	(1)
	NGC1850B	3.98	0.92	-0.12	0.03	0.76	0.05	0.010	0.001	(2)
	NGC1948	7.08	2.45	-0.40	...	0.40	...	0.005	...	(3)
	NGC1858	7.94	...	-0.40	...	0.40	...	0.005	...	(4)
	LH72	8.91	5.13	-0.60	...	0.25	...	0.003	...	(5)
	R136	10.00	...	-0.40	...	0.40	...	0.005	...	(6)
	LH52/53	10.00	...	-0.40	...	0.40	...	0.005	...	(7)
	NGC2027	11.48	3.70	-0.40	...	0.40	...	0.005	...	(8)
	NGC1955	15.49	5.35	-0.40	...	0.40	...	0.005	...	(8)
	NGC2004	15.49	5.35	~-0.40	...	0.40	...	0.005	...	(8)
	LH77	15.85	5.11	-0.40	...	0.40	...	0.005	...	(8)
	SL503	15.85	8.03	-0.40	...	0.40	...	0.005	...	(8)
	NGC1818	17.78	16.38	~-0.40	...	~0.40	...	~-0.005	...	(18,19)
	NGC2100	44.67	5.14	(18)
		<40	...	>-0.03	...	>0.93	...	>0.013	...	(13)
		15.85	...	-0.32	0.03	0.48	0.03	0.006	0.000	(17,16)
SL218	50	10	-0.40	0.15	0.40	0.14	0.005	0.002	0.002	(20)
NGC1711	50.12	5.77	-0.57	0.17	0.27	0.11	0.004	0.001	0.001	(10)
NGC1850A	50.12	11.54	-0.12	0.03	0.76	0.05	0.010	0.001	0.001	(2)
NGC1863	50	10	-0.40	0.15	0.40	0.14	0.005	0.002	0.002	(20)
BRHT4b	100	25	-0.40	0.15	0.40	0.14	0.005	0.002	0.002	(20)
NGC1838	100	25	-0.40	0.15	0.40	0.14	0.005	0.002	0.002	(20)
NGC1866	100	...	-0.43	0.18	0.37	0.15	0.005	0.002	0.002	(11)
NGC2136	100.00	23.03	-0.55	0.23	0.28	0.15	0.004	0.002	0.002	(10)
NGC2164	100	...	-0.20	0.20	0.63	0.29	0.008	0.004	0.004	(12)
NGC2214	100	...	-0.20	0.20	0.63	0.29	0.008	0.004	0.004	(12)

Table 8 – continued

Galaxy	Cluster	Age		[Fe/H]		Z/Z_{\odot}		Z		Ref.♣
		Value	Error	Value	Error	Value	Error	Value	Error	
[1]	[2]	[3]	[4]	[5]	[6]	[7]	[8]	[9]	[10]	[11]
SMC	L66	15	10	-0.70	...	0.20	...	0.003	...	(21,14)
	L51	15	10	-0.70	...	0.20	...	0.003	...	(21,14)
	L39	15	10	-0.70	...	0.20	...	0.003	...	(21,14)
	L72≡NGC376	25	10	-0.70	...	0.20	...	0.003	...	(22)
	L49≡NGC299	25	+6/-5	-0.70	...	0.20	...	0.003	...	(14)
	NGC 330	25	15	-0.82	0.10	0.15	0.03	0.002	0.000	(8)
		30	2	-0.82	0.11	0.15	0.04	0.002	0.001	(24,15)
		31.62	...	-0.22	...	0.60	...	0.008	...	(25)
		17.5♣	7.5♣	<-0.22	...	<0.60	...	<0.008	...	(26)
		29★	19★	(26)
	L63	45	...	-0.70	...	0.20	...	0.003	...	(14)
		110	+30/-20	-0.70	...	0.20	...	0.003	...	(14)
		50.12	<34.62	(23)
	HW8	50	20	-0.70	...	0.20	...	0.003	...	(21,14)
	L50≡NGC306	80	20	-0.70	...	0.20	...	0.003	...	(14)

Notes – The age and [Fe/H] values (Columns 3 and 5, respectively) are taken from the references listed in Column 11. The values of the remaining columns have been derived using $Z/Z_{\odot} = 10^{[\text{Fe}/\text{H}]}$, and $Z_{\odot} = 0.0134$ (Asplund et al. 2009). For few clusters, e.g., LMC systems NGC2100 and NGC1818, the values of age and [Fe/H] are taken from two different references. In these cases, we list both references in Column 11: the first one corresponds to the age and the second one to the [Fe/H] value.

♣, ★ In the original reference, Chiosi et al. (1995) give an age range (10–25 Myr and 10–48 Myr, respectively), while here we chose to list a mean age value along with its error (defined as half this age range).

♣ **References:** (1) Oey & Massey (1995); (2) Gilmozzi et al. (1994); (3) Will et al. (1996); (4) Vallenari et al. (1994); (5) Olsen et al. (1997); (6) Hunter et al. (1995); (7) Hill et al. (1995); (8) Da Costa & Hatzidimitriou (1998); (10) Dirsch et al. (2000); (11) Hilker et al. (1995); (12) Sagar & Richtler (1991); (13) Colucci et al. (2011); (14) Piatti et al. (2008); (15) Hill (1999); (16) Jasniewicz & Thevenin (1994); (17) Elson (1991); (18) Liu et al. (2009); (19) Kom et al. (2000); (20) Piatti et al. (2003); (21) Piatti et al. (2005); (22) Piatti et al. (2007); (23) Chiosi et al. (2006); (24) Sfrinanni et al. (2002); (25) Pietrzynski & Udalski (1999); (26) Chiosi et al. (1995)

Table 9. Formation efficiency for different XRB types

XRB type	N(XRBs)	Age (Myr)	Major Star-Formation Duration (yr)	Observed Mean Burst Rate ($10^{-6}M_{\odot}/\text{yr}/(\text{arcmin})^2$)	N(MCPS)	XRB Formation Efficiency (systems/ M_{\odot}/yr)	SFR required for production of 1 system ($10^{-3}M_{\odot}/\text{yr}$)	N(XRBs)/ M_{\star} ($10^{-2}M_{\odot}^{-1}$)
[1]	[2]	[3]	[4]	[5]	[6]	[7]	[8]	[9]
all HMXBs	40	6.3	>22	$333.9^{+32.2}_{-24.9}$	38	$21.9^{+4.1}_{-3.8}$	$45.7^{+8.5}_{-8.0}$	0.6 ± 0.1
	...	50.1^{\dagger}	>123	$84.6^{+9.6}_{-7.7}$
all HMXBs w/o WD or BH	38	6.3	>11	$318.7^{+31.0}_{-23.7}$	36	$23.0^{+4.4}_{-4.1}$	$43.5^{+8.2}_{-7.8}$	0.7 ± 0.1
	...	50.1^{\dagger}	108	$79.3^{+9.1}_{-7.3}$
confirmed Be-XRBs	16	12.6	20	$161.1^{+12.9}_{-10.6}$	16	$43.1^{+11.3}_{-11.2}$	$23.2^{+6.1}_{-6.0}$	0.3 ± 0.1
confirmed NS/Be-XRBs	15	12.6	16	$148.3^{+12.0}_{-9.7}$	15	$46.8^{+12.7}_{-12.5}$	$21.4^{+5.8}_{-5.7}$	0.3 ± 0.1
candidate Be-XRBs	17	6.3	>10	$121.6^{+19.4}_{-15.1}$	16	$60.7^{+17.6}_{-16.5}$	$16.5^{+4.8}_{-4.5}$	0.8 ± 0.2
	...	100^{\dagger}	133	$48.6^{+5.4}_{-4.4}$
X-ray pulsars	14	12.6	32	$113.3^{+11.5}_{-9.5}$	14	$61.3^{+17.5}_{-17.2}$	$16.3^{+4.7}_{-4.6}$	0.3 ± 0.1
SG-XRBs	4	6.3	>11	$81.4^{+12.6}_{-10.2}$	4	$85.3^{+44.7}_{-44.0}$	$11.7^{+6.1}_{-6.0}$	0.3 ± 0.2
BH-HMXB	1	6.3	>16	$15.1^{+5.6}_{-6.3}$	1	$458.4 (\leq 947.8)$	$2.2 (\leq 4.5)$	$0.5^{+0.6}_{-0.5}$
LMC WD/Be-XRB	1	25.1	29	$17.8^{+3.4}_{-3.2}$	1	$390.3 (\leq 788.0)$	2.6 ± 2.6	0.2 ± 0.2
SMC WD/Be-XRB	1	42.2	110 \ddagger	$28.6^{+43.6}_{-13.6}$	1	$242.7 (\leq 685.2)$	$4.1 (\leq 11.6)$	$0.0^{+0.1}_{-0.0}$

Notes – The duration of the major star-formation burst (Column 4) refers to the total duration of the star-formation episode and it includes the period before it reached its maximum SFR (see Figs. 4, 5). The number of MCPS subregions (Column 6; each $12' \times 12'$ [HZ09]) denotes the total area used for the derivation of the average star-formation history of regions with different XRB types (as these are given in Columns 1 and 2). The formation efficiencies presented here (Column 7) are derived as the ratio of the total number of XRBs for each class of objects to the maximum SFR (for more details see Section 5.2). M_{\star} is the total stellar mass produced on the specific SF burst episode. The errors in the N(XRBs)/ M_{\star} quantity (listed in Column 8) reflect the upper and lower limits of the SFR in Figs. 4, 5.

\dagger This peak is not associated with the particular XRB population (see Section 5.1). This non-symmetric SF burst was approximated by a Gaussian.

\ddagger Double-peak star-formation burst episode.

Table 10. Main-sequence lifetimes of OB-type stars

Spectral Class	M (M_{\odot})	t_{MS} (Myr)
[1]	[2]	[3]
O7.5 V	22.9	4.0
O8 V	20.8	5.1
O8.5 V	18.8	6.5
O9 V	17.1	8.3
O9.5 V	15.6	10.4
B0 V	14.6	12.3
B0.5 V	13.2	15.8
B1 V	11.0	24.9
B2 V	8.6	46.1
B3 V	6.1	108.8
B4 V	5.1	170.2
B5 V	4.4	246.2

Note – The spectral classes and masses are taken from Table 1.1 of Williams, Stephen J., "Optical Spectroscopy of Massive Binary Stars" (2011), Physics and Astronomy Dissertations, Paper 49, http://digitalarchive.gsu.edu/phy_astr_diss/49, while their main-sequence lifetimes are estimated using equation (1) reported in Section 5.5.

APPENDIX A: NOTES ON SPECIFIC SOURCES**A1 RX J0516.0-6916 (source ID # 12)**

The optical counterpart of this source has been spectroscopically classified by Cowley et al. (1997) as approximately a B1-type star. However, RX J0516.0-6916 has been listed in the literature as a candidate HMXB (i.e. HMXB? in Tables 1 and 5). Based on its B and V magnitudes and its position on the $V, B - V$ color-magnitude diagram shown in Fig. 1, we have identified here that this source may well be a Be-type star that when Cowley et al. observed it in 1997 did not show any emission (possibly observed during a disk-loss episode). We thus classify this source as a candidate Be-XRB.

A2 RX J0520.5-6932 (source ID # 14)

None of the optical matches listed within $5''$ from the X-ray source position (in Table 2) has been presented in the literature. Although most of the reported coordinates for the optical match of RX J0520.5-6932 are compatible with the identified matches in this work, their photometric magnitudes are totally different, especially the $B - V$ color. In particular, RX J0520.5-6932 has one bright, very blue match with $V = 16.004 \pm 0.471$ mag, and $B - V = -1.692 \pm 0.479$ mag. We note that there are very few sources spectroscopically classified with these B and V magnitudes (also note that this very blue match is outside the $B - V$ color range shown in Fig. 1). Although the identified counterpart has been spectroscopically classified as an O8-9e star (Schmidtke et al. 1994, Coe et al. 2001), thus bright, blue, magnitudes are expected, perhaps the deblending photometric algorithm used in the MCPS survey resulted in erroneous B and/or V magnitudes in this case, given the very contradictory values present in the literature (also, in the MCPS catalog in particular, the errors in the B and V magnitudes for this object is of the order of 0.5 mag). As noted in Table 3, there is a blue source (ID 119691 in the catalog of Massey 2002) with $V = 14.12$ mag, and $B - V = 0.02$ mag at $1.34''$ from the X-ray source position. This is also source 66519 in LMC field (SC) 6 from the OGLE-II survey (Udalski et al. 2000) with $V = 14.461$ mag and $B - V = -0.054$ mag. In the latest OGLE-III catalog (Ulaczyk et al. 2012) there are 2 sources in Field 100.1 both within only $\sim 1''$, of the X-ray position: source 5424 at $1.0''$ with $I = 14.362$ mag, and $V = 14.449$ mag, and source 138 at $1.1''$ with $I = 14.358$ mag, and $V = 14.446$ mag. Thus, most probably the MCPS, but also prior works, have blended together multiple point sources, resulting in erroneous B and/or V magnitudes. This source has been classified in the past as a Be-XRB and given the uncertainty of its photometric properties we decided not to revise its classification.

A3 RX J0523.2-7004 (source ID # 15)

This source has two equally probable matches (based on their similar chance coincidence probabilities; Fig. 3), thus we cannot propose either as its optical counterpart. They are located at $15.88''$ and $3.62''$ from the X-ray source position (90% error radius $9.9''$), and they are both bright ($V \sim 15$ mag; the nearest one is redder by ~ 0.5 mag). Based on their photometric properties, we classify this source as a candidate Be-XRB.

A4 RX J0527.1-7005 (source ID # 17)

Based on the brightness of the identified matches for source RX J0527.1-7005, which has a positional uncertainty of $11.9''$, we

propose as the most likely counterpart the source at $4.91''$ with $V = 15.308 \pm 0.050$ mag and $B - V = 1.208 \pm 0.066$ mag (see Table 2). This optical match is perhaps too red for an HMXB (as previously classified; Haberl & Pietsch 1999a), although few Be and B[e] III-V sources have been found by Reid & Parker (2012) to have even redder $B - V$ colors (see Fig. 1). Nevertheless, following a conservative approach we opted here to exclude this source from the list of HMXBs in the LMC. We also note that outside the 1σ search radius (i.e. at $13.23''$) there is another optical match with $V = 18.626 \pm 0.074$ mag and $B - V = 0.156 \pm 0.090$ mag (from Table 4), which falls at the faint end of the Be-stars locus in the $V, B - V$ color-magnitude diagram (see Fig. 1).

A5 RX J0529.4-6952 (source ID # 19)

Within its r_{90} ($\sim 9.8''$), this source has two equally probable matches (based on their similar chance coincidence probabilities; Fig. 3). We propose as the most likely counterpart the brightest one, located at $10.08''$ from the X-ray source position. This match falls well within the locus of Be stars, thus we classify this source as a candidate Be-XRB.

A6 RX J0530.7-6606 (source ID # 23)

This X-ray source has a positional uncertainty of $11.4''$ (see Table 1), and we have identified two optical sources (in Table 4) as equally likely matches due their similar chance coincidence probabilities (Fig. 3), photometric properties (i.e. position on the $V, B - V$ color-magnitude diagram) and offsets from the X-ray position. Nevertheless, we choose as the most probable match the one that falls nearer to the locus of Be stars in Fig. 1 (i.e. the one with an offset of $21.72''$, while the one at $22.13''$ is too blue and it is presented in this color-magnitude diagram as a less probable match) and we classify this source as a candidate Be-XRB.

A7 RX J0531.2-6607 (source ID # 24) and XMMU J053118.2-660730 (source ID # 26): Two different X-ray sources

We treat sources with IDs # 24 and # 26, which have been both detected by *XMM-Newton* (for more details see Table 1), as two different sources since they are $\sim 38''$ away from each other. For RX J0531.2-6607 we find an OB counterpart within $5.71''$ from the X-ray position, in agreement with previous studies (Negueruela & Coe 2002 assigned a B0.7Ve spectral type to this counterpart, so we retain its classification as a Be-XRB system). Similarly, we find a bright OB star within $3.21''$ from source with ID # 26, which has $V = 16.873 \pm 0.023$ mag and $B - V = -0.069 \pm 0.031$ mag (see Table 2). Based on this new identification, we classify XMMU J053118.2-660730 as a candidate Be-XRB (Shtykovskiy & Gilfanov 2005 list this as an uncertain HMXB).

A8 XMMU J053115.4-705350 (source ID # 25): a new candidate supergiant XRB

This source has been classified by Shtykovskiy & Gilfanov (2005) as a likely HMXB candidate with $R = 13.6$ mag and $V - R = 0.1$ mag. Here, we identify its counterpart as the MCPS source with $V = 14.051 \pm 0.025$ mag and $B - V = -0.042 \pm 0.043$ mag located at $1.64''$ from the X-ray position (Table 2; we note that this is a unique match within a search radius of $5''$). Reid & Parker (2012)

assign a B0 Ie spectral type to this source (object [RP2006]444 in their catalog) and list it as an HMXB. We go one step further and classify this source as a new candidate SG-XRB given its luminosity class. Although the optical counterpart is a B-type emission-line object (i.e. a Be-type star), thus XMMU J053115.4-705350 could be classified as a Be-XRB, on the other hand, being a supergiant contradicts the definition of Be stars, which explicitly excludes luminosity class I-II objects.

A9 RX J0532.4-6535 (source ID # 29) and RX J0535.8-6530 (source ID # 35)

These are two sources for which all identified brighter than $V \sim 20$ mag optical matches have similarly large chance coincidence probabilities (Fig. 3). Following the same conservative approach as for source RX J0527.1-7005 (source ID # 17), we chose to exclude both of them from the list of HMXBs in the LMC. Nevertheless, we note that these sources have other faint matches that lie along the main sequence (see Tables 3 and 4), and in particular the ones for source RX J0535.8-6530 lie on the faint end of the Be-star locus (see Fig. 1).

Moreover, we note that RX J0532.4-6535 is erroneously listed in Liu et al. (2005) (but not in their Tables 1 and 2) as a supergiant system, citing for this classification Haberl & Pietsch (1999b). However, Haberl & Pietsch (1999b) classify RX J0532.4-6535 as an uncertain HMXB and based on its low variability they suggest that this source is an X Per type HMXB detected during the persistent quiescent state. Even if we look for an OB counterpart out to $\sim 35''$ (about twice the r_{90} listed above) from the X-ray position, we find none.

A10 RX J0532.5-6551 (source ID # 30): one of the few identified LMC supergiant XRBs

RX J0532.5-6551 has been detected by Haberl et al. (1995) (this is also ROSAT PSPC source # 184 with (R.A., Dec.)_{J2000.0} = (05:32:32.1,-65:51:42) and $r_{90} = 3.3''$ in Haberl & Pietsch 1999b). Based on the optical magnitude of the associated source Sk-65 66, Haberl et al. (1995) suggested that this may be a supergiant system. Later, Negueruela & Coe (2002) classified source Sk-65 66 as a B0 II type star and confirmed that RX J0532.5-6551 was the first wind-fed SG-XRB in the LMC. Independently, Jaxon et al. (2001) derived a B0.5 II spectral type for Sk-65 66 (with (R.A., Dec.)_{J2000.0} = (05:32:32.6,-65:51:42) and $B = 12.9$ mag, $V = 13.1$ mag). In the MCPS catalog, this counterpart has $B = 12.474 \pm 0.138$ mag and $V = 13.048 \pm 0.076$ mag and it has a $3.85''$ offset from the X-ray position, thus we adopt the classification of this system as a SG-XRB.

A11 LMC X-4 (source ID # 31)

The counterpart of this well-studied X-ray source presented here is the same as the one reported in the literature, i.e. a very bright blue object with $B \simeq V \sim 14$ mag (the MCPS source listed in Table 2 has $B - V = -0.227 \pm 0.041$ mag). The striking difference between this study and earlier works though is the reported U magnitude. The MCPS catalog lists this source with a U magnitude equal to 15.449 ± 0.070 mag, resulting in $U - B$ color of 1.509 ± 0.076 mag. This is significantly redder than any previous reports, although significant variability has also been reported (e.g., Pakull & Olander

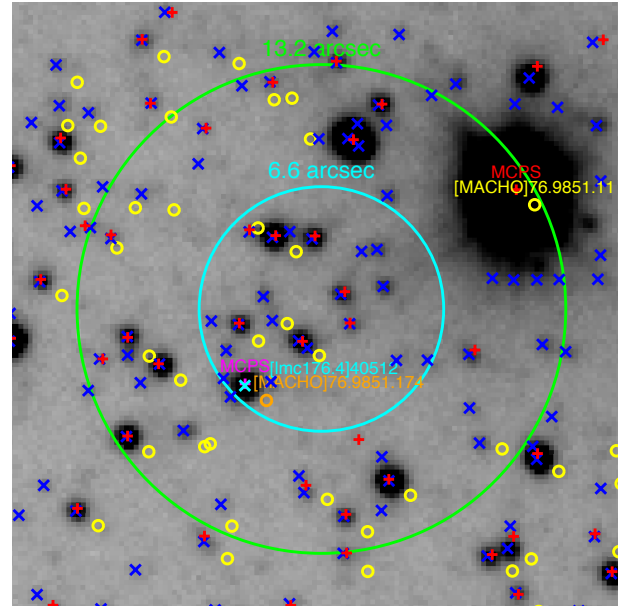


Figure A1. Finding chart of RX J0541.4-6936 (source ID # 39; $\sim 30''$ in each side with North up and East on the left) from the OGLE-III V -band image (Field ID 176.4; the WCS was tied to 2MASS). OGLE-III, MCPS and MACHO sources are shown with blue "x" points, red crosses and yellow circle points, respectively. The 1σ ($6.6''$) and 2σ ($13.2''$) positional uncertainties around source RX J0541.4-6936 are shown in cyan and green circles, respectively. In the literature, the proposed counterpart of this source is MACHO object 76.9851.11 (a supergiant star). In this work, we have also identified a closer Be-star like match: its OGLE-III position is shown with a cyan "x" point (marked by field and source ID), while this is also MACHO object 76.9851.174 (shown with an orange circle point). For a detailed discussion see Appendix A12.

1976, Blanco & Hiltner 1977, Chevalier & Ilovaisky 1977, Ilovaisky et al. 1984). Given the spectral type of the donor star of this RLOF-fed X-ray pulsar (O8 III; Negueruela & Coe 2002), we classify this system as an HMXB.

A12 RX J0541.4-6936 (source ID # 39)

Liu et al. (2005) list this source as a B2 type SG-XRB following Sasaki et al. (2000). However, Sasaki et al. (2000) only classify RX J0541.4-6936 (ROSAT HRI source 328 with (R.A., Dec.)_{J2000.0} = (05:41:22.2,-69:36:29) and $r_{90} = 6.6''$) as a candidate HMXB and associate it with a source from Sanduleak 1970. This object is source Sk -69 271 ((R.A., Dec.)_{J2000.0} = (05:41:20.14,-69:36:23.0)) \equiv CPD-69 500 at $12.33''$ from the X-ray source position, which has photometric parameters typical of OB supergiants ($V = 11.790 \pm 0.051$ mag and $B - V = 0.000 \pm 0.106$ mag from the MCPS catalog). Recently, Fariña et al. (2009) classified source Sk -69 271 as a B4 III-I type star (with (R.A., Dec.)_{J2000.0} = (05:41:20.04,-69:36:22.4) and $V = 11.80$ mag). RX J0541.4-6936 is also listed in the XMM-Newton Serendipitous Source Catalogue 2XMMi-DR3 as 2XMM J054123.0-693633 (source ID 53010).

Although there are several other sources within its error circle (Fig. A1), some of which fall in the locus of B-type stars, the chance coincidence probability for the initially proposed counterpart is much lower than that for the other candidate sources, and therefore we adopt the previously reported classification.

A13 RX J0541.5-6833 = RX J0541.6-6832 (source ID # 41)

This source has photometric properties compatible with OB III-V stars (see Fig. 1). In addition, its most likely counterpart has been classified as a B0 III star (Massey 2002), thus we only classify this source as an HMXB and not as a (candidate) Be-XRB.

A14 RX J0543.9-6539 (source ID # 42)

This source has a positional uncertainty (r_{90}) of $8.6''$, and within a search radius of $10''$ there are 3 matches from the MCPS catalog. Based on their very large chance coincidence probabilities (Fig. 3), and similarly to X-ray sources with IDs #23, #29, and #35, we exclude this source from the list of HMXBs in the LMC.

A15 RX J0546.8-6851 (source ID # 45)

The adopted optical counterpart of this source is located at $56.67''$ from the X-ray source position ($r_{90} \sim 48.7''$; Table 1). It is well within the locus of Be stars, thus we classify this source as a candidate Be-XRB system. We also note there are 3 additional fainter matches located at $5.93''$, $19.41''$, and $51.82''$ from the X-ray source position.

This paper has been typeset from a $\text{\TeX}/\text{\LaTeX}$ file prepared by the author.